chemosensors

MDPI

Article

Design and Synthesis of Arylboronic Acid Chemosensors for the Fluorescent-Thin Layer Chromatography (f-TLC) Detection of Mycolactone

Gideon Atinga Akolgo [1], Benjamin M. Partridge [2], Timothy D. Craggs [2], Kingsley Bampoe Asiedu [3] and Richard Kwamla Amewu [1,*]

[1] Department of Chemistry, University of Ghana, Legon-Accra P.O. Box LG56, Ghana; gaakolgo001@st.ug.edu.gh
[2] School of Physical and Mathematical Sciences, Dainton Building, University of Sheffield, Sheffield S3 7HF, UK; t.craggs@sheffield.ac.uk (T.D.C.)
[3] Department of Neglected Tropical Diseases, World Health Organization, 1211 Geneva, Switzerland; asieduk@who.int
* Correspondence: ramewu@ug.edu.gh

Abstract

Fluorescent chemosensors are increasingly becoming relevant in recognition chemistry due to their sensitivity, selectivity, fast response time, real-time detection capability, and low cost. Boronic acids have been reported for the recognition of mycolactone, the cytotoxin responsible for tissue damage in Buruli ulcer disease. A library of fluorescent arylboronic acid chemosensors with various signaling moieties with certain beneficial photophysical characteristics (i.e., aminoacridine, aminoquinoline, azo, BODIPY, coumarin, fluorescein, and rhodamine variants) and a recognition moiety (i.e., boronic acid unit) were rationally designed and synthesised using combinatorial approaches, purified, and fully characterised using a set of complementary spectrometric and spectroscopic techniques such as NMR, LC-MS, FT-IR, and X-ray crystallography. In addition, a complete set of basic photophysical quantities such as absorption maxima ($\lambda_{abs}{}^{max}$), emission maxima ($\lambda_{em}{}^{max}$), Stokes shift ($\Delta\lambda$), molar extinction coefficient (ε), fluorescence quantum yield (Φ_F), and brightness were determined using UV-vis absorption and fluorescence emission spectroscopy techniques. The synthesised arylboronic acid chemosensors were investigated as chemosensors for mycolactone detection using the fluorescent-thin layer chromatography (f-TLC) method. Compound 7 (with a coumarin core) emerged the best ($\lambda_{abs}{}^{max}$ = 456 nm, $\lambda_{em}{}^{max}$ = 590 nm, $\Delta\lambda$ = 134 nm, ε = 52,816 $M^{-1}cm^{-1}$, Φ_F = 0.78, and brightness = 41,197 $M^{-1}cm^{-1}$).

Keywords: mycolactone; Buruli ulcer; boronic acid; chemosensor; diagnosis; molecular recognition; mycolactone; *Mycobacterium ulcerans*

Received: 27 February 2025
Revised: 27 March 2025
Accepted: 7 April 2025
Published: 9 July 2025

Citation: Akolgo, G.A.; Partridge, B.M.; Craggs, T.D.; Asiedu, K.B.; Amewu, R.K. Design and Synthesis of Arylboronic Acid Chemosensors for the Fluorescent-Thin Layer Chromatography (f-TLC) Detection of Mycolactone. *Chemosensors* **2025**, *13*, 244. https://doi.org/10.3390/chemosensors13070244

1. Introduction

Over the years, researchers, inspired by certain biological processes in nature, looked for new concepts that allow for the selective molecular recognition of target molecules that play important roles in complex chemical processes in various disciplines such as medicine, biology, agriculture, biomedicine, environment, and social sciences [1]. Molecular recognition is achieved by the utility of chemosensors. Chemosensors are molecules of abiotic origin that signal the presence of matter or energy. A fluorescent chemosensor, therefore, is a compound that interacts with an analyte in such a way as to produce a

detectable fluorescent signal [2]. Fluorescent chemosensors have been of particular interest in supramolecular chemistry because of their ability to recognise guest species as well as their high selectivity, sensitivity, and simplicity [3,4]. Generally, a fluorescent chemosensor is composed of a recognition moiety that interacts with an analyte of interest and relays the recognition event through a signalling unit. Thus, the engineering of an appropriate fluorescent chemosensor with the right recognition and signalling moieties can result in favourable interactions with specific analytes.

A boronic acid motif can be explored as a recognition unit in the design of chemosensors to exploit the 1,3-diol moieties on the structure of the analyte. This is because boronic acids and their derivatives have been known for decades to form five- or six-membered cyclic boronate esters with both *cis*-1,2- and 1,3-diols that are present on biologically relevant molecules through covalent bonding [5–10]. The phenomenon of the complexation of boronic acids with polyols dates to over 70 years but remains an area of interest. The first reported use of boronic acids as recognition units for *cis*-1,2 or 1,3-diol-containing compounds was published by Lorand and Edwards in 1959 [11]. They demonstrated the complexation equilibria of aqueous benzeneboronate ion with several polyols and compared the association constants to that of borate. Following the early seminal work of Lorand and Edwards, boronic acids have greatly evolved into an area of research for molecular recognition, thus gaining significant interest in the design of many fluorescent chemosensors. This is because of their selective binding behaviour for a considerable number of biological molecules possessing polyhydroxy motifs, their high stability, environmental friendliness, general low toxicity, and their relatively inexpensive nature. The first fluorescent boronic-acid-based sensor was developed later in 1992 by Yoon and Czarnik for saccharide sensing [12]. Since then, boronic acids have attracted considerable interest in molecular recognition, in which the boronic acid functionality has increasingly become a very important recognition moiety in the design and synthesis of molecular recognition chemosensors, taking advantage of this unique intrinsic affinity for *cis*-1,2 and/or 1,3-diols. The selective binding behaviour of the boronic acid unit has been explored for the detection of diol-containing analytes based on the "lock-and-key" concept of enzyme-substrate recognition [1]. The unique properties of boronic acid functionality have positioned it as an invaluable receptor and have shown great promise for the specific recognition and detection of various species in real-world situations [13]. They have become popular as sensors for various biological polyol molecules including monosaccharides and in particular glucose [14], catecholamines [15], and dopamine. Others include various polysaccharides, glycoproteins, and glycated haemoglobin [16–21], ionic compounds [22–24], anions such as cyanides and fluoride [9,25–27], water traces in solvents [28,29], and hydrogen peroxide (H_2O_2) [30,31]. Furthermore, boronic acids have also been employed as biochemical tools for a variety of applications, including but not limited to enzyme inhibitors [32], cell delivery methods [33], whole-body diagnostic imaging [34], and tumour cell imaging [35,36].

The pathogenesis of *Mycobacterium ulcerans* disease is widely dependent on the activity of a unique toxin called mycolactone [37]. Mycolactone **1**, plays a significant role in the virulence, pathogenicity, and cytotoxicity of Buruli ulcer (BU) disease. It has immunosuppressive properties and is responsible for the tissue damage seen in BU [38,39]. Structurally, mycolactone A/B is a polyketide macrolide toxin composed of a 12-membered macrocyclic lactone core (C1–C11) with two laterally attached side chains; a C-linked northern side chain (C12–C20) with two hydroxyl groups in 1,3-diol positions at C17 and C19; and an esterified C5-O-linked highly polyunsaturated acyl southern side chain (C1′–C16′) possessing a conjugated pentaenoic acid ester chromophore and three hydroxyl groups, two of which are in 1,3-diol positions at C13′ and C15′ [40,41] (Figure 1).

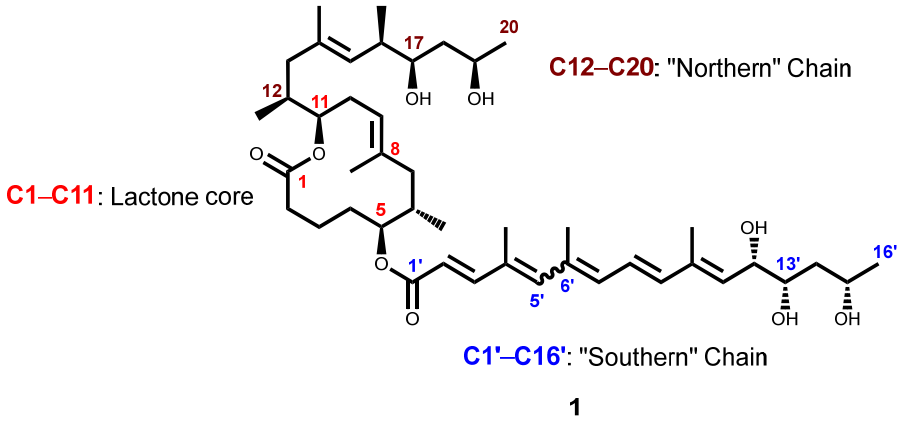

Figure 1. Structure of mycolactone A/B. Reproduced with permission from Akolgo et al., *BMC Infectious Diseases*, published by Springer Nature, 2023 [42].

The secretion of mycolactone is a distinguishing feature of *M. ulcerans* amongst other human mycobacteria. According to Hong et al., mycolactone A/B appears to be biosynthetically limited to *M. ulcerans*, uniformly distributed inside the infected tissue, and demonstrated to diffuse beyond the sites of primary infection. For these reasons, mycolactone-specific detection is crucial for the diagnosis of BU [43]. Histopathological studies have shown that in tissues, mycolactone is widely distributed compared to the causative organism [44]. Consequently, the detection of its presence in biological samples is necessary for the diagnosis of the disease. Based on these findings, Kishi and colleagues developed a sensitive and practical flourescent-thin layer chromatographine (f-TLC) technique for detecting the toxin. The diagnostic method utilises the derivatisation of diol motifs of mycolactone A/B using a 2-naphthylboronic acid that forms six-membered cyclic boronate esters, which can be detected on a TLC plate as an adduct (Figure 2). Accordingly, the 2-naphthylboronic acid and mycolactone work as an acceptor–donor FRET pair. The boronic acid unit reacts selectively with 1,3-diol(s) moieties of mycolactone to form boronate esters, significantly enhancing fluorescent intensity. The proposed general mechanism involves the FRET process, where a donor, in this case the pentaenoate chromophore of mycolactone, is excited at a defined wavelength (365 nm), and the energy is transferred, via non-radiative dipole–dipole interactions, to a properly selected acceptor (the 2-naphthylboronic acid), which emits through radiative relaxation. The free 2-naphthylboronic acid with the lowest ($n - p^*$) excited singlet state (S1) has the lower absorptivity and so it is weakly fluorescent. On the other hand, the hybridisation of boron atoms plays a secondary role in affecting fluorescence intensity. Therefore, binding with mycolactone at the right temperature results in the formation of the cyclic boronate, in which the hybridisation of boron atom changes from sp^2 to sp^3, has the lowest ($p - p^*$)-excited singlet state, and results in a large enhancement of fluorescence emission (Figure 2).

This idea led to research into alternative commercially available boronic acids, and it was discovered that 9,9-Diphenyl-9H-fluoren-4-yl)boronic acid (BA18) could be a viable substitute for 2-naphthylboronic acid (BA) [45]. The f-TLC method holds great promise because it is relatively cheap, simple to use, and rapid. [42,46,47]. Although the method has been successfully evaluated using clinical samples [48,49], it is hampered by the fact that it is non-quantitative. There are also concerns about interferences from other co-extracted and co-eluted lipids which make reading the results of the method subjective [48]. There is a need to improve upon the low detection and quantification rates as well as discriminate the mycolactone from other autofluorescent co-extracted human tissues. This study aimed to address these principal challenges associated with the f-TLC technique for the diagnosis of Buruli ulcers. To the best of our knowledge, no chemosensor has been

designed for the molecular recognition of mycolactone. Considering the broad application of boron-based fluorescence sensors, our goal was to incorporate the boronic acid motif into various fluorescent dyes as chemosensors for mycolactone detection. Considering the unique structure of mycolactone, we hypothesised that boronate ester formation between the diol moieties of mycolactone and a boronic acid binding site attached to a fluorescent molecule would allow for signal transduction that could be exploited for mycolactone detection. Therefore, we employed various fluorescent dyes (fluorophores) such as 9-aminoacridine, 8-aminoquinoline, azo, BODIPYs, coumarins, fluorescein, and rhodamine dyes, which are all amenable to boronic acid tethering to design, synthesise, and characterise various fluorescent arylboronic acid dye chemosensors. These are already well-known fluorophores with excellent photophysical properties including large excitation and emission maxima, extinction coefficient, high fluorescence quantum yield (Φ), large Stokes shift, high brightness, adequate solubility, good thermal and photostability, and sufficient chemical stability [50–52] (Figure 3). Secondly, these dyes are commercially available and can be coupled to diverse functional groups.

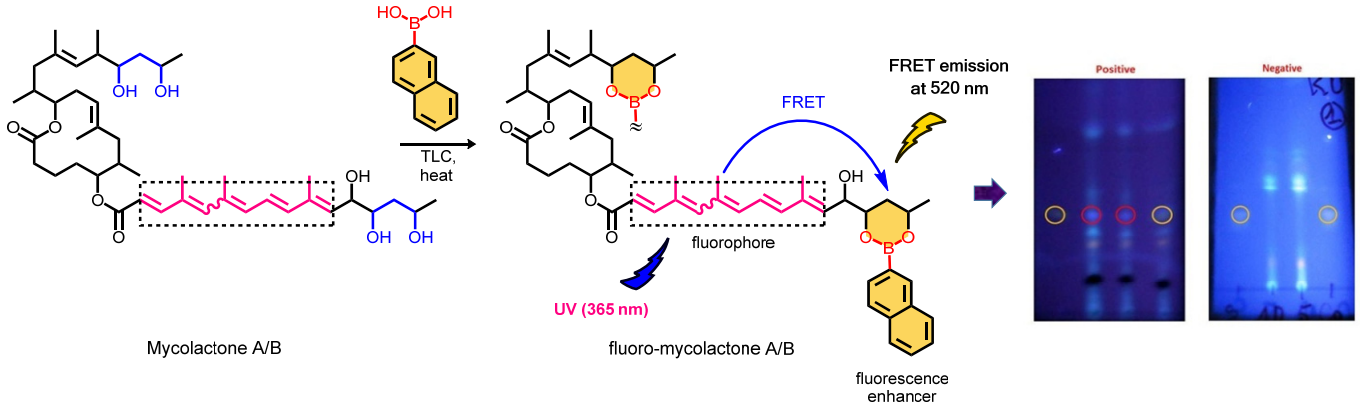

Figure 2. A schematic representation of the proposed mechanism of fluorescence of mycolactone and 2-naphthylboronic acid, as observed on TLC.

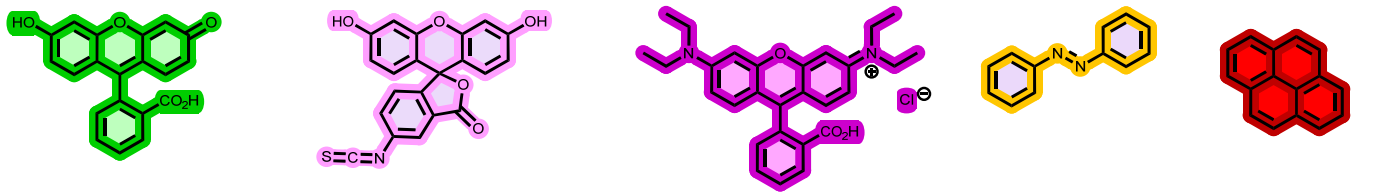

Fluorescein
$\lambda_{max\ abs}$ = 495 nm
$\lambda_{max\ em}$ = 520 nm
ε = 8.3×10^4 M^{-1}cm^{-1}
Φ_F = 0.79 (EtOH)

Fluorescein isothiocyanate (FITC)
$\lambda_{max\ abs}$ = 495 nm
$\lambda_{max\ em}$ = 525 nm
ε = 7.5×10^4 M^{-1}cm^{-1}
Φ_F = 0.92

Rhodamine B
$\lambda_{max\ abs}$ = 545 nm
$\lambda_{max\ em}$ = 566 nm
ε = 1.06×10^5 M^{-1}cm^{-1}
Φ_F = 0.70 (EtOH)

Azobenzene
$\lambda_{max\ abs}$ = 319 nm
$\lambda_{max\ em}$ = NA
ε = 2.24×10^4 M^{-1}cm^{-1}
Φ_F = NA

Pyrene
$\lambda_{max\ abs}$ = 241 nm
$\lambda_{max\ em}$ = NA
ε = 8.17×10^4 M^{-1}cm^{-1}
Φ_F = NA

Unbelliferone
$\lambda_{max\ abs}$ = 360 nm
$\lambda_{max\ em}$ = 450 nm
ε = 1.7×10^4 M^{-1}cm^{-1}
Φ_F = 0.63

Aminoquinoline
$\lambda_{max\ abs}$ = NA
$\lambda_{max\ em}$ = NA
ε = NA
Φ_F = NA

Aminoacridine
$\lambda_{max\ abs}$ = 360 nm
$\lambda_{max\ em}$ = 450 nm
ε = 1.7×10^4 M^{-1}cm^{-1}
Φ_F = 0.63

BODIPY 505/515
$\lambda_{max\ abs}$ = 505
$\lambda_{max\ em}$ = 515
ε = 9.4×10^4 M^{-1}cm^{-1}
Φ_F = (MeOH)

BODIPY 493/503
$\lambda_{max\ abs}$ = 493
$\lambda_{max\ em}$ = 503
ε = 1.06×10^5 M^{-1}cm^{-1}
Φ_F = 0.90

Resazurin
$\lambda_{max\ abs}$ = 568 nm
$\lambda_{max\ em}$ = 582 nm
ε = NA
Φ_F = 0.90

Figure 3. Structures of common fluorescent dyes.

2. Materials and Methods

2.1. Reagents and Instruments

Standard laboratory apparatus and glassware were used for all reactions. Unless otherwise specified, all solvents and reagents were used as supplied by commercial vendors without further purification. All air-sensitive reactions were conducted in oven-dried apparatus under nitrogen atmosphere. Aluminium-backed Merck silica gel 60 F_{254} plates pre-coated with silica were used for thin-layer chromatography (TLC). Plates were visualised using either ultraviolet light of 254 nm or 365 nm or by dipping the plates into solutions of vanillin, ninhydrin, or potassium permanganate followed by heating. All column chromatography was performed under 'flash' conditions using silica gel mesh 40–63. Fourier transform infrared (FT-IR) spectra were recorded on a Perkin Elmer 100 FT-IR instrument on the neat compounds. The spectrum was processed in the software and displayed. The relevant and characteristic absorptions were reported in wavenumbers (cm^{-1}), with the intensities of the bands recorded as broad (b), strong (s), medium (m), and weak (w). NMR spectroscopy was carried out using Brüker Avance III 400 and 500 MHz spectrometers. ^{1}H NMR spectra, ^{13}C NMR spectra, and ^{11}B NMR were obtained at the indicated 101, 126, 128, 377, 400, and 500 MHz as dilute solutions in various deuterated solvents at room temperature. All spectra were recorded in deuterated dimethyl sulfoxide (DMSO-d_6) or deuterated chloroform ($CDCl_3$) obtained from Sigma Aldrich. Chemical shifts (δ) are reported in parts per million (ppm) relative to the following residual solvent peaks (δ_H: $CHCl_3$ = 7.26 ppm, DMSO-d_6 = 2.50 ppm) or the solvent itself (δ_C: $CDCl_3$ = 77.0 ppm, DMSO-d_6 = 39.52 ppm). For ^{11}B NMR, $BF_3{\cdot}OEt_2$ (δ = 0 ppm) was used as an external standard. Coupling constants (*J*) were measured in hertz (Hz). Multiplicities are reported as singlet (s), broad singlet (br s), doublet (d), doublet triplet (dt), triplet doublet (td), doublet doublet of doublets of doublets (ddd), quartet (q), broad quartet (br q), or multiplet (m). High-resolution mass spectra were recorded using a 1260 Infinity LC (Agilent Technologies), coupled to a Quadrupole–Time of Flight tandem mass spectrometer 6530 Infinity Q-ToF detector (Agilent Technologies) by a Jet Stream ESI interface (Agilent Technologies). High-resolution MS spectra were acquired in the positive mode in the 100–2400 m/z range. Single crystal X-ray Diffraction (SCXRD) data were collected on a Bruker D8 VENTURE diffractometer (Bruker AXS, Karlsruhe, Germany), equipped with a PHOTON 100 CMOS detector with graphite-monochromatised Cu-Kα radiation (λ = 1.54178 Å) or a Bruker X8 Apex-II diffractometer, equipped with an Apex-II CCD area detector diffractometer (Bruker, Karlsruhe, Germany) with graphite-monochromatised Mo-Kα radiation (λ = 0.71073 Å). A suitable crystal was mounted in Fomblin oil on a MiTeGen MicroLoop and cooled in a stream of cold N_2 to 100 K. Data were corrected for absorption using empirical methods (SADABS) [53–55] based upon symmetry-equivalent reflections combined with measurements at different azimuthal angles. All crystal structures were solved and refined against F^2 values using ShelXT [56] for the solution and ShelXL [57] for refinement, accessed via the Olex2 program [58]. All non-hydrogen atoms were refined with anisotropic displacement parameters. All hydrogen atoms were added at calculated positions and refined with a riding model and isotropic displacement parameters fixed in magnitude relative to the attached carbon atoms. Details regarding the structures and a summary table of crystallographic and data collection parameters are provided in Electronic Supplementary Information (Table S1).

2.2. Synthesis and Characterisation

Synthesis of 4-(4,4,5,5-tetramethyl-1,3,2-dioxaborolan-2-yl)benzaldehyde **2**: Using a variation of the procedure of Miyaura et al. [59], a mixture of 4-bromobenzaldehyde (1.0 g, 5.4 mmol, 1.0 equiv.), B_2pin_2 (1.65 g, 6.5 mmol, 1.2 equiv.), KOAc (1.59 g, 16.2 mmol,

3.0 equiv.), and $PdCl_2$(dppf) (119 mg, 0.162 mmol) in dry 1,4-dioxane (20 mL) in an oven-dried two-necked round-bottom flask was degassed for 5–10 min using N_2 gas and stirred at 80 °C for 16 h (overnight). Upon completion (as monitored by TLC), the reaction mixture was allowed to cool, filtered through a plug of celite, washed with EtOAc (200 mL), extracted twice with water (2 × 50 mL), and then with brine. The organic layer was dried with anhydrous $MgSO_4$, filtered, and concentrated in vacuo. The crude product was purified on silica gel using DCM (100%) to obtain product **2** as a white solid (872 mg, 70% yield). ^{1}H NMR (400 MHz, $CDCl_3$) δ_H 10.02 (s, 1H, H1), 7.94 (d, *J* = 8.2 Hz, 2H, H5), 7.83 (d, *J* = 8.2 Hz, 2H, H4), 1.33 (s, 12H, H8). ^{13}C NMR (101 MHz, $CDCl_3$) δ_C 192.9 (C2), 138.4 (C3), 135.6 (C4), 129.0 (C5), 84.7 (C7), 25.2 (C8) (C6 bonded to B not observed due to broadening). LC-MS: retention time: 9.4 min; ESI-QTOF HRMS (*m*/*z*): for $[C_{13}H_{18}BO_3]^+$ $[M + H]^+$: exact mass calcd.: 233.1349; found: 233.1358; for $[C_{13}H_{17}BO_3Na]^+$ $[M + Na]^+$: exact mass calcd.: 255.1168; found: 255.1172.

1-(4-(4,4,5,5-tetramethyl-1,3,2-dioxaborolan-2-yl)phenyl)ethan-1-one **3**: This title compound was prepared as described above for **2** using 4-bromoacetophenone (5.0 g, 25.1 mmol, 1.0 equiv.), and B_2pin_2 (7.65 g, 30.1 mmol, 1.2 equiv.), KOAc (7.39 g, 75.3 mmol, 3.0 equiv.), $PdCl_2$(dppf) (551 mg, 0.75 mmol) in 1,4-dioxane (20 mL). The crude product was purified on silica gel using hexane/ethyl acetate = 50:1 (*V*:*V*) to obtain product **3** as a white solid (6.15 g, 96% yield). ^{1}H NMR (500 MHz, $CDCl_3$) δ_H 7.90 (d, *J* = 6.3 Hz, 2H, H4), 7.87 (d, *J* = 6.3 Hz, 2H, H5), 2.58 (s, 3H, H1), 1.33 (s, 12H, H8). ^{13}C NMR (126 MHz, $CDCl_3$) δ_C 198.7 (C2), 139.3 (C3), 135.2 (C5), 127.6 (C4), 84.5 (C7), 27.0 (C1), 25.2 (C8) (C6 bonded to B not observed due to broadening).

2.3. Categories of Fluorescent Arylboronic Acid Chemosensor Dyes

2.3.1. Coumarin Dyes

Synthesis of 7-(diethylamino)-2H-chromen-2-one **4**: A mixture of 4-(diethylamino) salicylaldehyde (6.0 g, 28.69 mmol) and diethyl malonate (10.84 g, 67.75 mmol) in 90 mL anhydrous ethanol was treated with 3 mL of piperidine and then refluxed for 13 h. After removing the solvent, 120 mL of mixed solution (concentrated HCl:glacial acetic acid = 1:1 (*V*:*V*)) was added to the crude product and refluxed for another 7 h. After cooling the reaction solution to room temperature, it was transferred into 300 mL of water and the pH was adjusted to 5 using NaOH. The solid was filtered and purified over silica gel (hexane: ethyl acetate = 9:1 (*V*:*V*) to give a beige solid **4** (yield: 85%). ^{1}H NMR (500 MHz, $CDCl_3$) δ_H 7.53 (d, *J* = 9.3 Hz, 1H, H9), 7.23 (d, *J* = 8.7 Hz, 1H, H5), 6.56 (dd, *J* = 8.8, 2.5 Hz, 1H, H4), 6.46 (d, *J* = 2.5 Hz, 1H, H6), 6.01 (d, *J* = 9.3 Hz, 1H, H10), 3.40 (q, *J* = 7.2 Hz, 4H, H2), 1.20 (t, *J* = 7.2 Hz, 6H, H1). ^{13}C NMR (126 MHz, $CDCl_3$) δ_C 162.4 (C11), 156.7 (C3), 150.7 (C7), 143.8 (C9), 128.8 (C5), 109.0 (C10), 108.7 (C8), 108.3 (C4), 97.4 (C6), 44.8 (C2), 12.4 (C1).

Synthesis of 7-(diethylamino)-2-oxo-2H-chromene-3-carbaldehyde **5**: Under N_2, anhydrous DMF (4.20 g, 57.5 mmol, 4.4 mL, 12.5 equiv.) was dropped into phosphoryl chloride ($POCl_3$) (1.76 g, 11.5 mmol, 1.1 mL, 2.5 equiv.) with stirring for 6 h in an ice bath. The solution of 7-(diethylamino)-*2H*-chromen-2-one **4** (1.00 g, 4.6 mmol, 1.0 equiv.) in anhydrous 1,2-dichloroethane (50 mL) was added to the above solution, and the mixture was stirred at 60 °C for 12 h. After completing the process, the mixture was poured into ice water and neutralised with NaOH solution (20%) to pH 7. The formed precipitate was filtered off and washed three times with water. The residue was chromatographed on silica, eluting with ethyl acetate/hexane (1:1, *V*:*V*) to form **5** as an orange-red solid product (yield: 79%). ^{1}H NMR (500 MHz, $CDCl_3$) δ_H 10.10 (s, 1H, H13), 8.23 (s, 1H, H9), 7.39 (d, *J* = 9.0 Hz, 1H, H5), 6.63 (dd, *J* = 9.0, 2.5 Hz, 1H, H4), 6.47 (d, *J* = 2.5 Hz, 1H, H6), 3.46 (q, *J* = 7.2 Hz, 4H, H2), 1.24 (t, *J* = 7.1 Hz, 6H, H1). ^{13}C NMR (126 MHz, $CDCl_3$) δ_C 188.0 (C12), 162.0 (C11), 159.0

(C3), 153.6 (C7), 145.5 (C9), 132.6 (C5), 114.5 (C10), 110.3 (C8), 108.4 (C4), 97.3 (C6), 45.4 (C2), 12.6 (C1). FTIR (cm^{-1}): υ (C–H st) 2879, υ (C=O st, carboxyl) 1709, υ (C=C st) 1609.

Synthesis of (E)-7-(diethylamino)-3-(3-oxo-3-(4-(4,4,5,5-tetramethyl-1,3,2-dioxaborolan-2-yl)phenyl)prop-1-en-1-yl)-2H-chromen-2-one **6**: compound **5** (0.50 g, 2.0 mmol, 1.0 equiv.) and 1-(4-(4,4,5,5-tetramethyl-1,3,2-dioxaborolan-2-yl)phenyl)ethan-1-one **3** (0.98 g, 4.0 mmol, 2.0 equiv.) were added to 20 mL of the mixed solvent (CH_2Cl_2/anhydrous CH_3CH_2OH = 1:1 (*V*:*V*)), then 10 drops of pyrrolidine was dropped into the above solution. The mixture was stirred at room temperature for 4 d, and the solvent was removed under reduced pressure. The residue was added to 40 mL of hexane/ethyl acetate (*V*:*V*=1:1) to yield red precipitations. The precipitates were collected on a filter funnel to give compound **6** as a bright red solid (yield: 51%). ^{1}H NMR (500 MHz, DMSO-d_6) δ_H 8.48 (s, 1H, H9), 8.03 (d, *J* = 3.2 Hz, 1H, H18), 8.00 (d, *J* = 4.4 Hz, 2H, H17), 7.85 (d, *J* = 7.7 Hz, 2H, H16), 7.67 (d, *J* = 15.4 Hz, 1H, H12), 7.50 (d, *J* = 8.9 Hz, 1H, H5), 6.80 (dd, J = 9.0, 2.4 Hz, 1H, H4), 6.60 (d, *J* = 2.3 Hz, 1H, H6), 3.48 (q, *J* = 7.1 Hz, 4H, H2), 1.32 (s, 12H, H20), 1.15 (t, *J* = 7.0 Hz, 6H, H1). ^{13}C NMR (126 MHz, DMSO-d_6) δ_C 189.1 (C14), 160.0 (C11), 156.5 (C3), 152.0 (C7), 146.0 (C12), 140.0 (C9), 139.9 (C15), 134.8 (C17), 130.7 (C5), 127.4 (C16), 120.7 (C10), 113.1 (C13), 110.0 (C8), 108.4 (C4), 96.3 (C6), 84.1 (C19), 44.3 (C2), 24.7 (C20), 12.4 (C1) (C18 bonded to B not observed due to broadening).

(E)-(4-(3-(7-(diethylamino)-2-oxo-2H-chromen-3-yl)acryloyl)phenyl)boronic acid **7**: Deprotection of pinacol boronate esters was performed according to the procedure by Akgun [60]. (*E*)-7-(diethylamino)-3-(3-oxo-3-(4-(4,4,5,5-tetramethyl-1,3,2-dioxaborolan-2-yl)phenyl)prop-1-en-1-yl)-*2H*-chromen-2-one **6** (150 mg, 0.36 mmol, 1.0 equiv.) was dissolved in THF: water (4:1 mL) (4:1 *V*:*V*). Then sodium periodate (231 mg, 1.08 mmol, 3.0 equiv.) was added to the solution and stirred at room temperature for 30 min under an ambient atmosphere. Finally, the reaction mixture was stirred for 24 h at room temperature after adding HCl (0.2 mL, 1 N). The mixture was then concentrated in vacuo. After that, it was dissolved in EtOAc (30 mL) and washed with water (8 mL) and brine (8 mL). The organic layer was dried using $MgSO_4$, filtered, and concentrated in vacuo to obtain pure (*E*)-(4-(3-(7-(diethylamino)-2-oxo-*2H*-chromen-3-yl)acryloyl)phenyl)boronic acid **7** (yield: 90%). ^{1}H NMR (400 MHz, DMSO-d_6) δ_H 8.47 (s, 1H, H9), 8.29 (s, 2H, H19), 8.06 (d, *J* = 19.8 Hz, 1H, H5), 8.00–7.95 (m, 4H, H16, H17), 7.66 (d, *J* = 15.4 Hz, 1H, H12), 7.48 (d, *J* = 9.0 Hz, 1H, H13), 6.78 (dd, *J* = 9.0, 2.4 Hz, 1H, H4), 6.59 (d, *J* = 2.4 Hz, 1H, H6), 3.47 (q, *J* = 7.0 Hz, 4H, H2), 1.14 (t, *J* = 7.0 Hz, 6H, H1). ^{13}C NMR (101 MHz, DMSO-d_6) δ_C 189.2 (C14), 160.0 (C11), 156.5 (C3, 151.9 (C7), 145.5 (C12), 139.4 (C9), 139.0 (C15), 134.4 (C17), 130.7 (C5), 127.0 (C16), 120.9 (C10), 113.2 (C13), 109.9 (C8), 108.4 (C4), 96.3 (C6), 44.3 (C2), 12.4 (C1) (C18 bonded to B not observed due to broadening). ^{11}B NMR (128 MHz, DMSO-d_6) δ_B 28.4. LC-MS: retention time: 8.8 min; ESI-QTOF HRMS (*m*/*z*): for $[C_{22}H_{23}BNO_5]^+$ $[M + H]^+$: exact mass calcd.: 392.1669; found: 392.1680. FTIR (cm^{-1}): υ (O–H st) 3378, υ (C–H st) 2974, υ (C=O st, carboxyl) 1719, υ (C=C st) 1560.

(4-(((4-methyl-2-oxo-2H-chromen-7-yl)oxy)methyl)phenyl)boronic acid **22**: 4-Bromomethylphenylboronic acid (297 mg, 1.0 mmol) and 4-methylumbelliferone (4-MU) (194 mg, 1.1 mmol) were dissolved in 5 mL dry dimethylformamide (DMF). Cesium chloride (360 mg, 1.1 mmol) was then added and stirred for 1.5 h at 70 °C. After cooling the mixture to room temperature, it was extracted using CH_2Cl_2 and deionised water. The organic layer was collected, dried over anhydrous magnesium sulphate, and concentrated. The crude material was purified using a silica column (hexane: ethyl acetate = 5:3) to afford **22** as a white solid (298 mg, 76%). ^{1}H NMR (400 MHz, DMSO-d_6) δ_H 8.06 (s, 2H, H16), 7.81 (d, *J* = 7.8 Hz, 2H, H14), 7.67 (d, *J* = 8.6 Hz, 1H, H9), 7.42 (d, *J* = 8.0 Hz, 2H, H13), 7.06–7.01 (m, 2H, H6, H7), 6.20 (d, *J* = 1.4 Hz, 1H, H2), 5.23 (s, 2H, H11), 2.38 (d, *J* = 1.3 Hz, 3H, H4). ^{13}C NMR (101 MHz, DMSO-d_6) δ_C 161.3 (C8), 160.1 (C1), 154.7 (C10), 153.4 (C3),

138.0 (C12), 134.3 (C14), 126.7 (C13), 126.5 (C6), 113.3 (C5), 112.7 (C2), 111.2 (C7), 101.7 (C9), 69.8 (C11), 18.1 (C4) (C15 bonded to B not observed due to broadening). ^{11}B NMR (128 MHz, DMSO-d_6) δ_B 28.9. LC-MS: retention time: 7.5 min; ESI-QTOF HRMS (m/z): for $[C_{17}H_{16}BO_5]^+$ [M + H]$^+$: exact mass calcd.: 311.1091; found: 311.1096. FTIR (cm^{-1}): υ(N–H st) 3328, υ (O–H st) 3224, υ (C–H st) 2938, υ (C=O st, carboxyl) 1691, υ (C=C st) 1604.

2.3.2. 9-Aminoacridine Dyes

Synthesis of N-(acridin-9-yl)-2-chloroacetamide **23**: Chloroacetyl chloride (1.15 g, 10.2 mmol, 0.8 mL, 2.0 equiv.) in THF (20 mL) was added dropwise while stirring to a mixture of 9-aminoacridine (1.00 g, 4.0 mmol, 1.0 equiv.) and TEA (1.03 g, 10.2 mmol, 1.4 mL, 2.0 equiv.) in THF at 0–5 °C. The reaction mixture was then stirred for 4 h. The solvent was evaporated under reduced pressure. The residue was washed with water to remove TEA.HCl before being dried and recrystallised from ethanol to obtain **23** (yield: 59%). ^{1}H NMR (400 MHz, DMSO-d_6) δ_H 12.19 (s, 1H, H9), 8.48 (d, 4H, H3), 8.23 (dd, J = 9.0, 6.5 Hz, 2H, H1), 7.87 (dd, 2H, H2), 4.84 (s, 2H, H11). ^{13}C NMR (101 MHz, DMSO-d_6) δ_C 166.6 (C10), 141.5 (C6, C8), 135.8 (C5, C7), 126.9 (C3), 125.9 (C1), 121.4 (C2), 43.2 (C11). LC-MS: retention time: 4.7 min; ESI-QTOF HRMS (m/z): for $[C_{15}H_{12}ClN_2O]^+$ [M + H]$^+$: exact mass calcd.: 271.0638; found: 271.0750.

(4-(((2-(acridin-9-ylamino)-2-oxoethyl)amino)methyl)phenyl)boronic acid **24**: *N*-(acridin-9-yl)-2-chloroacetamide **23** (536 mg, 1.98 mmol, 1.1 equiv.), (4-(aminomethyl)phenyl)boronic acid (270 mg, 1.80 mmol, 1.0 equiv.), and triethylamine (TEA, 0.5 mL, 3.60 mmol, 2.0 equiv.) were dissolved in acetonitrile (MeCN, 30 mL), stirred, and refluxed for 1 d. The oily residue was dissolved in methylene chloride and washed five times with 10 mL of water. The organic layer was dried over anhydrous Na_2SO_4. The solvent was removed under reduced pressure to obtain the crude product, which was purified by silica gel column chromatography (Hexanes: EtOAc-9:1) (yield: 22%). ^{1}H NMR (400 MHz, DMSO-d_6) δ_H 9.56 (s, 1H, H8), 9.24 (s, 1H, H11), 7.91 (s, 2H, H17), 7.58 (d, J = 7.9 Hz, 2H, H14), 7.49 (dd, J = 7.9, 1.5 Hz, 2H, H2), 7.28 (ddd, J = 8.3, 5.8, 1.5 Hz, 2H, H3), 7.02–6.95 (m, 4H, H1, H4), 6.90 (d, J = 7.7 Hz, 2H, H15), 3.23 (s, 2H, H12), 2.95 (s, 2H, H10). ^{13}C NMR (101 MHz, DMSO-d_6) δ_C 171.4 (C9), 140.3 (C5), 138.6 (C7), 134.0 (C13), 128.7 (C15), 128.0 (C3), 126.6 (C14), 119.5 (C1), 119.1 (C2), 114.9 (C6), 114.1 (C4), 53.3 (C12), 52.1 (C10) (C16 bonded to B not observed due to broadening). ^{11}B NMR (128 MHz, DMSO-d_6) δ_B 29.18. LC-MS: retention time: 0.5 min; ESI-QTOF HRMS (m/z): for $[C_{22}H_{21}BN_3O_3]^+$ [M + H]$^+$: exact mass calcd.: 386.1676; found: 386.1683. FTIR (cm^{-1}): υ (N–H st) 3328, υ (C-H st, carboxyl) 2976, υ (C=O st, amide) 1673, υ (C=C st and C=N st) 1613–1477.

2.3.3. 8-Aminoquinoline Dyes

Synthesis of 2-(tert-butoxycarbonylamino)acetic acid **25**: Based on the procedure adopted from Ear et al. [61], Glycine (10.0 g, 133.2 mmol, 1.0 equiv.) was dissolved in a dioxane–water (1:1) (200 mL) mixture. Triethylamine (18.5 mL, 133.2 mmol, 1.0 equiv.) and di-*tert*-butyl dicarbonate (Boc_2O, 31.98 g, 146.5 mmol, 1.1 equiv.) were added and the mixture was stirred for 2 h at room temperature. After evaporation of the volatiles, they were redissolved in water/diethyl ether (150 mL/250 mL) for extraction. The aqueous phase was recovered, and the pH was adjusted to 2 with a 2 M solution of HCl. The mixture was extracted with ethyl acetate (2 × 150 mL), dried over $MgSO_4$, and concentrated in vacuo, to yield white crystalline product **25**, yield (15.08 g, 65% yield). The data were consistent with the literature [61]. ^{1}H NMR (400 MHz, DMSO-d$_6$) δ_H 7.05 (t, J = 6.2 Hz, 1H, H4), 3.57 (d, J = 6.2 Hz, 2H, H5), 1.38 (s, 9H, H1). ^{13}C NMR (101 MHz, DMSO-d$_6$) δ_C 171.8 (C6), 155.9 (C3), 78.1 (C2), 41.8 (C5), 28.2 (C1). LC-MS: retention time: 4.7 min; ESI-QTOF HRMS (m/z): for $[C_{14}H_{17}BNO_2]^+$ [M + H]$^+$: exact mass calcd.: 198.0742; found: 198.0756.

Synthesis of tert-butyl (2-oxo-2-(quinolin-8-ylamino)ethyl)carbamate **26**: A mixture of 8-aminoquinoline (2.56 g, 17.7 mmol, 1.0 equiv.), DMAP (108 mg, 5 mol%), and *Boc*-Gly-OH, **25** (1.22 g, 6.94 mmol, 2.0 equiv.) in dichloromethane (100 mL) was stirred in an ice bath (~0 °C) for 30 min, followed by an addition of EDC·HCl (1.33 g, 6.94 mmol, 2.0 equiv.). The reaction mixture was stirred at 0 °C for 2 h and stirred overnight at room temperature. The crude was extracted with NH_4Cl (aq.) (100 mL). The organic layer was dried over $MgSO_4$, filtered, and concentrated under a vacuum. The crude product was purified through silica gel column chromatography using hexane/ethyl acetate (3:2) as an eluent to afford tert-butyl (2-oxo-2-(quinolin-8-ylamino)ethyl)carbamate **26** as a white solid (4.95 g, 93% yield). The data were consistent with the literature [62]. ^{1}H NMR (500 MHz, $CDCl_3$) δ_H 10.26 (s, 1H, H10), 8.74 (d, *J* = 4.2 Hz, 1H, H1), 8.70 (dd, *J* = 6.3, 2.7 Hz, 1H, H3), 8.10 (d, *J* = 8.3 Hz, 1H, H7), 7.48 (d, *J* = 8.4 Hz, 1H, H5), 7.46 (s, 1H, H2), 7.40 (dd, *J* = 8.3, 4.2 Hz, 1H, H6), 5.51 (s, 1H, H13), 4.11 (d, *J* = 5.9 Hz, 2H, H12), 1.50 (s, 9H, H16). ^{13}C NMR (126 MHz, $CDCl_3$) δ_C 168.1 (C11), 156.1 (C14), 148.3 (C1), 138.4 (C9), 136.4 (C8), 133.9 (C3), 128.0 (C4), 127.3 (C6), 122.0 (C2), 121.7 (C5), 116.8 (C7), 80.3 (C15), 45.4 (C12), 28.4 (C16). LC-MS: retention time: 8.0 min; ESI-QTOF HRMS (*m*/*z*): for $[C_{16}H_{20}N_3O_3]^+$ $[M + H]^+$: exact mass calcd.: 302.1505; found: 302.1523.

Boc deprotection of tert-butyl (2-oxo-2-(quinolin-8-ylamino)ethyl)carbamate **27**: Based on the procedure by Ear et al., *tert*-butyl (2-oxo-2-(quinolin-8-ylamino)ethyl)carbamate **26** (3.00 g, 9.96 mmol, 1.0 equiv.) was dissolved in CH_2CI_2 (150 mL) and HCI-dioxane (4 M solution, 20 mL) was added and the mixture was stirred at rt overnight. The reaction was monitored by TLC. After completion of the reaction, the solvents were removed in vacuo to obtain the hydrochloride salt of the amine. The residue was dissolved in diethyl ether and extracted with NaOH (2 M) and Et_2O. The organic layer was dried over $MgSO_4$ and the solvent was evaporated under reduced pressure to obtain the product 2-amino-*N*-(quinolin-8-yl)acetamide **27** (1.68 g, 84% yield). ^{1}H NMR (500 MHz, $CDCl_3$) δ_H 11.25 (s, 1H, H10), 8.85 (d, 1H, H1), 8.82 (dd, 1H, H3), 8.14 (d, 1H, H7), 7.56–7.47 (m, 2H, H2, H5), 7.43 (dd, *J* = 8.3, 4.2 Hz, 1H, H6), 3.64 (s, 2H, H13), 1.81 (s, 2H, H12). ^{13}C NMR (126 MHz, $CDCl_3$) δ_C 171.9 (C11), 148.9 (C1), 139.3 (C9), 136.6 (C8), 134.6 (C3), 128.4 (C4), 127.7 (C6), 122.1 (C2), 121.9 (C5), 116.9 (C7), 46.5 (C12). LC-MS: retention time: 1.1 min; ESI-QTOF HRMS (*m*/*z*): for $[C_{11}H_{12}N_3O]^+$ $[M + H]^+$: exact mass calcd.: 202.0980; found: 202.0997; for $[C_{11}H_{11}N_3ONa]^+$ $[M + Na]^+$: exact mass calcd.: 224.0800; found: 224.0804.

Synthesis of N-(quinolin-8-yl)-2-((4-(4,4,5,5-tetramethyl-1,3,2-dioxaborolan-2-yl)benzyl) amino)acetamide **28**: 2-amino-*N*-(quinolin-8-yl)acetamide **27** (0.82 g, 4.07 mmol, 1.2 equiv.) and 4-(4,4,5,5-tetramethyl-1,3,2-dioxaborolan-2-yl)benzaldehyde **2** (0.79 g, 3.39 mmol, 1.0 equiv.) were dissolved in 1, 2-dichloroethane (50 mL). The reaction mixture was then charged with sodium triacetoxyborohydride (1.08 g, 1.5 equiv.). The reaction was then stirred under nitrogen for 1 h. After an hour, additional sodium triacetoxyborohydride (0.75 g, 1.0 equiv.) was added to the reaction and the mixture was stirred for a further 1 h. The reaction mixture was then quenched with saturated $NaHCO_3$ solution (100 mL). The aqueous phase was extracted with CH_2Cl_2 (2 × 100 mL), and the combined organics dried over anhydrous $MgSO_4$ and concentrated to dryness in vacuo to afford *N*-(quinolin-8-yl)-2-((4-(4,4,5,5-tetramethyl-1,3,2-dioxaborolan-2-yl)benzyl)amino)acetamide **28** as a white solid (0.75 g, 53% yield). ^{1}H NMR (400 MHz, $CDCl_3$) δ_H 11.61 (s, 1H, H10), 8.92 (dd, *J* = 4.2, 1.7 Hz, 1H, H1), 8.82 (dd, *J* = 7.0, 2.0 Hz, 1H, H3), 8.17 (d, *J* = 8.2 Hz, 1H, H7), 7.83 (d, *J* = 7.4 Hz, 2H, H17), 7.62 (d, *J* = 7.8 Hz, 2H, H16), 7.59–7.49 (m, 2H, H2, H5), 7.48 (dd, *J* = 8.3, 4.3 Hz, 1H, H6), 3.94 (s, 2H, H14), 3.61 (s, 2H, H12), 1.36 (s, 12H, H20). ^{13}C NMR (101 MHz, $CDCl_3$) δ_C 170.4 (C11), 148.6 (C1), 142.8 (C9), 139.1 (C15), 136.3 (C8), 135.2 (C17), 134.5 (C3), 128.2 (C4), 128.0 (C16), 127.5 (C6), 121.8 (C2), 121.7 (C5), 116.6 (C7), 83.9 (C19), 54.4 (C14), 53.4 (C12), 25.0 (C20) (C18 bonded to B not observed due to broadening).

^{11}B NMR (128 MHz, $CDCl_3$) δ_B 31.6. LC-MS: retention time: 6.9 min; ESI-QTOF HRMS (m/z): for $[C_{24}H_{29}BN_3O_3]^+$ [M + H]$^+$: exact mass calcd.: 418.2302; found: 418.2320; for $[C_{24}H_{28}BN_3O_3Na]^+$ [M + Na]$^+$: exact mass calcd.: 440.2121; found: 440.2123.

(4-(((2-oxo-2-(quinolin-8-ylamino)ethyl)amino)methyl)phenyl)boronic acid **29**: Deprotection of pinacol boronate esters was performed according to the procedure by Akgun [60]. The title compound was prepared as described above for **7**. *N*-(quinolin-8-yl)-2-((4-(4,4,5,5-tetramethyl-1,3,2-dioxaborolan-2-yl)benzyl)amino)acetamide **28** (150 mg, 0.36 mmol, 1.0 equiv.) was dissolved in THF: water (4:1 mL) (4:1 *V*:*V*). Then, sodium periodate (231 mg, 1.08 mmol, 3.0 equiv.) was added to the solution and stirred at room temperature for 30 min under an ambient atmosphere. Lastly, the reaction mixture was stirred for 24 h at room temperature after adding HCl (0.2 mL, 1 N). The mixture was then concentrated in vacuo. After that, it was dissolved in EtOAc (30 mL) and washed with water (8 mL), and brine (8 mL). The organic layer was dried using $MgSO_4$, filtered, and concentrated in vacuo to obtain pure (4-(((2-oxo-2-(quinolin-8-ylamino)ethyl)amino)methyl)phenyl)boronic acid **29** as a white solid (yield: 76%). ^{1}H NMR (400 MHz, DMSO-d_6) δ_H 11.62 (s, 1H, H10), 8.98 (dd, *J* = 4.2, 1.7 Hz, 1H, H1), 8.71 (dd, *J* = 7.6, 1.4 Hz, 1H, H3), 8.43 (dd, *J* = 8.3, 1.7 Hz, 1H, H7), 8.00 (s, 2H, H19), 7.78 (d, *J* = 8.0 Hz, 2H, H17), 7.69 – 7.68 (m, 1H, H13), 7.66 (dd, *J* = 2.7, 1.4 Hz, 1H, H6), 7.62 – 7.57 (m, 2H, H2, H6), 7.53 (d, *J* = 7.9 Hz, 2H, H16), 3.82 (s, 2H, H14), 3.40 (s, 2H, H12). ^{13}C NMR (101 MHz, DMSO-d_6) δ_C 170.5 (C11), 149.0 (C1), 138.1 (C9), 136.6 (C15), 134.2 (C8), 134.1 (C17), 133.9 (C3), 127.9 (C4), 127.4 (C16), 127.1 (C6), 122.3 (C2), 121.7 (C5), 115.4 (C7), 53.2 (C14), 52.6 (C12). ^{11}B NMR (128 MHz, DMSO-d_6) δ_B 29.09. LC-MS: retention time: 5.2 min; ESI-QTOF HRMS (m/z): for $[C_{18}H_{19}BN_3O_3]^+$ [M + H]$^+$: exact mass calcd.: 336.1519; found: 336.1524. FTIR (cm^{-1}): υ (O–H st) 3265, υ (C–H st) 2829, υ (C=O st, amide) 1669, υ (C=C st and C=N st) 1604–1524.

2.3.4. Fluorescein Dyes

Synthesis of fluorescein methyl ester **34**: To fluorescein (1.0 g, 3.1 mmol) methanol solution (10 mL) in a 50 mL round-bottom flask was added concentrated sulfuric acid (98%) (1 mL). The solution was refluxed and stirred for 4 h. After cooling, excess methanol was removed under reduced pressure and excess water was added to the residue. The red solid formed was washed with water several times and filtered in a vacuum until almost free from fluorescence. After drying in a vacuum, the crude product was redissolved and columned using CH_2Cl_2: methanol (10:1) to obtain red solid fluorescein methyl ester **34** (93% yield). ^{1}H NMR (400 MHz, DMSO-d_6) δ_H 8.31 (dd, *J* = 7.8, 1.3 Hz, 1H, H18), 7.96 (td, *J* = 7.5, 1.4 Hz, 1H, H16), 7.88 (td, *J* = 7.7, 1.4 Hz, 1H, H17), 7.55 (dd, *J* = 7.5, 1.4 Hz, 1H, H15), 7.31 (d, *J* = 9.2 Hz, 2H, H6, H10), 7.24 (d, *J* = 2.2 Hz, 2H, H2, H12), 7.10 (dd, *J* = 9.2, 2.2 Hz, 2H, H3, H13), 3.57 (s, 3H, H21). ^{13}C NMR (101 MHz, DMSO-d_6) δ_C 171.5, 165.0, 158.1, 133.3, 133.1, 132.3, 130.9, 130.3, 129.1, 120.7, 116.0, 102.5, 52.6. LC-MS: retention time: 6.8 min; ESI-QTOF HRMS (m/z): for $[C_{21}H_{15}O_5]^+$ [M + H]$^+$: exact mass calcd.: 347.0920; found: 347.0934.

Synthesis of fluorescein hydrazide **35**: Fluorescein methyl ester **34** (0.40 g) and hydrazine hydrate (0.24 g, 4.8 mmol) were added to methanol (5 mL), refluxed, and stirred for 6 h. After collecting by filtration, the light brown precipitate was washed with a small amount of methanol and water and dried in a vacuum to obtain the crude product. The crude material was pre-adsorbed onto silica and purified by column chromatography using CH_2Cl_2: MeOH (10:1) to obtain pure straw-yellow fluorescein hydrazide **35** (96% yield). ^{1}H NMR (400 MHz, DMSO-d_6) δ_H 9.80 (s, 2H, H22), 7.77 (ddd, *J* = 5.2, 2.4, 0.8 Hz, 1H, H18), 7.50–7.47 (m, 2H, H16, H17), 7.00–6.98 (m, 1H, H15), 6.59 (d, *J* = 2.3 Hz, 2H, H6, H10), 6.45 (dd, *J* = 8.6, 2.4 Hz, 2H, H2, H12), 6.40 (d, *J* = 8.6 Hz, 2H, H3, H13), 4.38 (s, 2H, H21). ^{13}C NMR (101 MHz, DMSO-d_6) δ_C 165.5, 158.2, 152.4, 151.5, 132.6, 129.3, 128.4, 128.0, 123.4,

122.4, 112.0, 110.0, 102.4, 64.6. LC-MS: retention time: 6.5 min; ESI-QTOF HRMS (*m*/*z*): for $[C_{20}H_{15}N_2O_4]^+$ $[M + H]^+$: exact mass calcd.: 347.1032; found: 347.1028.

(E)-(4-(((3′,6′-dihydroxy-3-oxospiro[isoindoline-1,9′-xanthen]-2-yl)imino)methyl)phenyl)boronic acid **36**: 4-formylphenylboronic acid (0.391 mL, 1.77 mmol) was dissolved in 20 mL of a mixture of ethanol/toluene (90:10) and then **35** (0.200 g, 0.578 mmol) was added. A Dean-Stark trap was fixed to the reaction vessel and filled with 10 mL of the same solvent mixture for the azeotropic removal of water. The reaction was then allowed to stir for 16 h at 100 °C, at which time TLC showed that the starting material had fully reacted. The solvent was removed under vacuum, and the product was recrystallised to obtain the product **36** (64% yield). ^{1}H NMR (400 MHz, DMSO-d_6) δ_H 9.92 (s, 2H, H27), 8.96 (s, 1H, H21), 8.10 (s, 2H, H26), 7.92 (d, *J* = 7.3 Hz, 1H, H18), 7.75 (d, *J* = 7.9 Hz, 2H, H24), 7.68–7.55 (m, 2H, H16, H17), 7.38 (d, *J* = 8.0 Hz, 2H, H23), 7.14 (d, *J* = 7.4 Hz, 1H, H15), 6.67 (d, *J* = 2.2 Hz, 2H, H6, H10), 6.51 (d, *J* = 8.6 Hz, 2H, H2, H12), 6.46 (dd, *J* = 8.6, 2.3 Hz, 2H, H). ^{13}C NMR (101 MHz, DMSO-d_6) δ_C 163.7, 158.6, 152.2, 150.5, 148.9, 135.8, 134.5, 134.1, 129.1, 128.9, 128.0, 125.7, 123.8, 123.2, 112.4, 110.1, 102.5, 65.3. ^{11}B NMR (128 MHz, DMSO-d_6) δ_B 28.1. LC-MS: retention time: 7.4 min; ESI-QTOF HRMS (*m*/*z*): for $[C_{27}H_{20}BN_2O_6]^+$ $[M + H]^+$: exact mass calcd.: 479.1414; found: 479.1412. FTIR (cm^{-1}): υ (O–H st) 3287, υ (C=O st, amide) 1668, υ (C=C st and C=N st) 1600–1318.

3-(3-(3′,6′-Dihydroxy-3-oxo-3H-spiro[isobenzofuran-1,9′-xanthene]-5-yl)thioureido)phenylboronic acid **37**: 3-Aminobenzeneboronic acid (0.35 g, 2.57 mmol) was added to a solution of fluorescein isothiocyanate isomer I (1.00 g, 2.57 mmol) in DMF (5 mL). The reaction mixture was stirred at room temperature for 12 h and then poured into methanol (10 mL). The solvents were removed in vacuo; the residue was then dissolved in the minimum amount of fresh methanol. Chloroform was added and product **37** was obtained as a bright orange precipitate (920 mg, 68% yield). LC-MS: retention time: 7.0 min; ESI-QTOF HRMS (*m*/*z*): for $[C_{27}H_{20}BN_2O_7S]^+$ $[M + H]^+$: exact mass calcd.: 527.1084; found: 527.1123.

2.3.5. Rhodamine Dyes

Synthesis of rhodamine B hydrazide **38**: To 0.4 g of rhodamine B (I) dissolved in 15 mL of methanol, an excessive hydrazine hydrate (0.5 mL) was added and then the reaction solution was refluxed till the pink colour disappeared. After that, the cooled reaction solution was poured into distilled water and extracted with ethyl acetate (6 × 25 mL). The combined extracts were dried with sodium sulphate anhydrous and filtered, and the solvent was evaporated to obtain rhodamine B hydrazide **38** in 68% yield. ^{1}H NMR (400 MHz, DMSO-d_6) δ_H 7.79–7.73 (m, 1H, H12), 7.50–7.43 (m, 2H, H10, H11), 7.01–6.95 (m, 1H, H9), 6.37 (t, *J* = 1.4 Hz, 2H, H2), 6.33 (d, *J* = 1.4 Hz, 4H, H3, H6), 4.26 (s, 2H, H15), 3.31 (q, 8H, H16), 1.08 (t, *J* = 7.0 Hz, 12H, H17). ^{13}C NMR (101 MHz, DMSO-d_6) δ_C 165.3 (C14), 153.0 (C5), 151.9 (C1), 148.1 (C8), 132.4 (C10), 129.6 (C13), 128.1 (C11), 127.7 (C3), 123.5 (C9), 122.1 (C12), 107.8 (C4), 105.5 (C2), 97.4 (C6), 64.8 (C7), 43.7 (C16), 12.5 (C17). LC-MS: retention time: 8.6 min; ESI-QTOF HRMS (*m*/*z*): for $[C_{28}H_{33}N_4O_2]^+$ $[M + H]^+$: exact mass calcd.: 457.2604; found: 457.2596.

(E)-(4-(((2-(3′,6′-bis(diethylamino)-3-oxospiro[isoindoline-1,9′-xanthen]-2-yl)ethyl)imino)methyl) phenyl)boronic acid **39**: 4-formylphenylboronic acid (0.391 mL, 1.77 mmol) was dissolved in 20 mL of a mixture of ethanol/toluene (90:10) and then **38** (0.200 g, 0.578 mmol) was added. A Dean–Stark trap was fixed to the reaction vessel and filled with 10 mL of the same solvent mixture for the azeotropic removal of water. The reaction was then allowed to stir for 16 h at 100 °C, at which time TLC showed that the starting material **38** had fully reacted. The solvent was removed under vacuum, and the product was recrystallised to obtain product **39** (73% yield). ^{1}H NMR (400 MHz, $CDCl_3$) δ_H 8.07 (d, *J* = 7.8 Hz, 1H, H12), 8.00 (d, *J* = 6.4 Hz, 1H, H10), 7.74 (d, *J* = 7.8 Hz, 1H, H11), 7.65 – 7.62 (m, 3H, H9, H20),

7.56 – 7.53 (d, *J* = 7.1 Hz, 2H, H18), 7.47 (d, *J* = 7.1 Hz, 2H, H17), 7.14 – 7.09 (m, 1H, H15), 6.52 (dd, *J* = 8.9, 6.5 Hz, 2H, H2), 6.46 (dd, *J* = 14.9, 2.6 Hz, 2H, H3), 6.24 (ddd, *J* = 9.1, 7.2, 2.6 Hz, 2H, H6), 3.31 (q, *J* = 9.0, 8.1 Hz, 8H, H16), 1.15 (t, *J* = 6.6 Hz, 12H, H17). ^{13}C NMR (101 MHz, $CDCl_3$) δ_C 165.3, 153.4, 153.2, 152.0, 149.1, 149.1, 147.1, 137.5, 135.63, 134.0, 133.6, 133.4, 128.4, 128.1, 127.0, 124.0, 123.6, 108.2, 106.0, 98.0, 58.6, 44.5, 12.7. ^{11}B NMR (128 MHz, $CDCl_3$) δ_B 29.9. LC-MS: retention time: 10.2 min; ESI-QTOF HRMS (*m*/*z*): for $[C_{35}H_{38}BN_4O_4]^+$ $[M + H]^+$: exact mass calcd.: 589.2986; found: 589.2994. FTIR (cm^{-1}): υ (O–H st) 3310, υ (C–H st) 2893, υ (C=O st, amide) 1696, υ (C=C st and C=N st) 1614–1306.

2.3.6. BODIPY Dyes

Synthesis of protected BODIPY dye **42**: A mixture of a protected 4-formylphenylboronic acid **2** (1.50 g, 6.5 mmol, 1.0 equiv.) and 2,4-dimethyl-*1H*-pyrrole (1.24 g, 13.0 mmol, 2.0 equiv.) was dissolved in anhydrous DCM (40 mL) under nitrogen. TFA (0.4 mL) was added to the mixture and stirred at room temperature for 3 h. The consumption of the aldehyde was monitored by TLC. A solution of *p*-chloranil in DCM (1.92 g, 7.8 mmol, 1.2 equiv.) was added at 0 °C and stirred for 30 min. TEA (3.95 g, 5.4 mL, 39.0 mmol, 6.0 equiv.) was added at 0 °C and stirred for a further 30 min. Following dropwise addition of $BF_3{\cdot}OEt_2$ (9.23 g, 8.0 mL, 65.0 mmol, 10.0 equiv.) to the reaction mixture, it was stirred for 12 h at room temperature. The crude product was obtained by evaporating the mixture under reduced pressure. The crude product was purified by silica gel column using hexane/ethyl acetate (1:0 → 9:1) to obtain the desired product **42** in 47% yield. ^{1}H NMR (500 MHz, $CDCl_3$) δ_H 7.90 (d, *J* = 7.5 Hz, 2H, H10), 7.29 (d, *J* = 7.5 Hz, 2H, H9), 5.97 (s, 2H, H3), 2.55 (s, 6H, H6), 1.38 (s, 12H, H13), 1.36 (s, 6H, H7). ^{13}C NMR (126 MHz, $CDCl_3$) δ_C 155.6 (C4), 143.4 (C1), 141.8 (C2), 138.0 (C8), 135.5 (C10), 131.4 (C5), 127.5 (C9), 121.3 (C3), 84.3 (C12), 29.8 (C7), 25.1 (C13), 14.7 (C6) (C11 bonded to B not observed due to broadening). LC-MS: retention time: 12.4 min; ESI-QTOF HRMS (*m*/*z*): for $[C_{25}H_{31}B_2F_2N_2O_2]^+$ $[M + H]^+$: exact mass calcd.: 451.2540; found: 451.2555.

Deprotection of protected BODIPY dye **42** *to obtain* **45**: Deprotection of pinacol boronate esters was performed according to the procedure by Akgun [60]. BODIPY dye **42** (150 mg, 0.36 mmol, 1.0 equiv.) was dissolved in THF: water (4:1 mL) (4:1 *V*:*V*). Then sodium periodate (231 mg, 1.08 mmol, 3.0 equiv.) was added to the solution and stirred at room temperature for 30 min under an ambient atmosphere. Lastly, HCl (0.2 mL, 1 N) was added to the reaction mixture, which was stirred for 24 h at room temperature. The reaction mixture was concentrated in vacuo. Then it was dissolved in EtOAc (30 mL) and washed with water (1 × 8 mL), and brine (1 × 8 mL). The organic fraction was dried ($MgSO_4$), and the solids were removed by gravity filtration. The crude product was preabsorbed onto 5 mL of silica and dried under vacuum. Flash chromatography (1:3 hexanes/EtOAc) provided a pure deprotected BODIPY dye **45** (89% yield) as a reddish-orange powder after solvent removal. ^{1}H NMR (400 MHz, DMSO-d_6) δ_H 8.25 (s, 2H, H12), 7.96 (d, *J* = 7.9 Hz, 2H, H10), 7.33 (d, *J* = 7.9 Hz, 2H, H9), 6.17 (s, 2H, H3), 2.44 (s, 6H, H6), 1.32 (s, 6H, H7). ^{13}C NMR (101 MHz, DMSO-d_6) δ_C 154.8, 150.9, 142.8, 142.2, 135.7, 134.9, 130.6, 129.2, 126.7, 121.4, 113.8, 101.6, 14.3, 14.0. LC-MS: retention time: 9.0 min; ESI-QTOF HRMS (*m*/*z*): for $[C_{19}H_{21}B_2F_2N_2O_2]^+$ $[M + H]^+$: exact mass calcd.: 369.1757; found: 369.1763. FTIR (cm^{-1}): υ (O–H st) 3201, υ(C–H st) 2916, υ(C=C st and C=N st) 1545–1454.

2.3.7. Azo Dyes

Synthesis of (2-((m-tolylamino)methyl)phenyl)boronic acid **46**: 2-formylbenzeneboronic acid (3.00 g, 20.1 mmol, 1.0 equiv.) and m-toluidine (2.7 mL, 24.1 mmol, 1.1 equiv.) were dissolved in 1, 2-dichloroethane (50 mL). The reaction mixture was then charged with sodium triacetoxyborohydride (6.39 g, 1.5 equiv.). The reaction was then stirred under

nitrogen for 1 h. After an hour, additional sodium triacetoxyborohydride (4.26 g, 1.0 equiv.) was added to the reaction and stirred further for another 1 h. The reaction mixture was then quenched with saturated $NaHCO_3$ solution (100 mL). The aqueous phase was extracted with CH_2Cl_2 (2 × 100 mL), and the combined organics dried over anhydrous $MgSO_4$ and concentrated to dryness in vacuo to afford (2-((m-tolylamino)methyl)phenyl)boronic acid **46** as a cream-coloured solid (3.64 g, 75% yield). The material was used without further purification. ^{1}H NMR (400 MHz, $CDCl_3$) δ_H 7.74 (dd, *J* = 7.6, 1.5 Hz, 1H, H5), 7.45 (m, 2H, H2, H12), 7.38–7.32 (m, 3H, H6, H16), 7.02–6.97 (m, 2H, H1, H11), 6.66 (m, 2H, H10, H14), 6.52 (s, 1H, H8), 4.36 (s, 2H, H7), 2.14 (s, 3H, H15). LC-MS: retention time: 6.4 min; ESI-QTOF HRMS (*m*/*z*): for $[C_{14}H_{17}BNO_2]^+$ [M + H]$^+$: exact mass calcd.: 242.1352; found: 242.1354.

(E)-(2-(((3-methyl-4-((4-nitrophenyl)diazenyl)phenyl)amino)methyl)phenyl)boronic acid **47a**: 4-nitroaniline (504 mg, 3.64 mmol, 1.1 equiv.) was mixed in water (2 mL), methanol (2 mL), and hydrochloric acid (2 mL, 5.0 M) and then cooled to 0–5 °C on an ice-bath. A chilled solution of sodium nitrite (186 mg, 2.69 mmol, 1.3 equiv.) was added dropwise. Excess nitrite was destroyed by the addition of sulfamic acid after stirring for 5 min. (2-((m-tolylamino)methyl)phenyl)boronic acid (500 mg, 2.07 mmol, 1.0 equiv.) was dissolved in methanol (3 mL) and dilute hydrochloric acid (2 mL, 1 M), then added dropwise to the reaction mixture, which quickly turned red. Sodium acetate was added to raise the pH of the solution to 4 and this was then left to stir at 0–5 °C for 3 h. Sodium hydroxide (2 M) was slowly added to raise the pH to 7. The resulting precipitate was collected by suction filtration and dried in a desiccator overnight to afford product **47a** as a dark red solid (44% yield). ^{1}H NMR (400 MHz, DMSO-d_6) δ_H 9.86 (s, 1H), 8.39 (d, *J* = 8.9 Hz, 2H), 8.33 (d, *J* = 8.9 Hz, 1H), 8.18 (s, 1H), 8.01 (d, *J* = 8.9 Hz, 2H), 7.92–7.85 (m, 2H), 7.75 (d, *J* = 9.1 Hz, 1H), 7.58–7.53 (m, 1H), 7.47 (s, 2H, 2H), 7.37–7.30 (m, 1H), 4.63 (s, 2H), 2.73 (s, 3H, 3H). ^{13}C NMR (101 MHz, DMSO-d_6) δ_C 156.8, 156.1, 153.6, 150.5, 148.3, 147.5, 146.5, 144.1, 142.6, 141.6, 141.5, 133.7, 130.4, 130.3, 129.0, 125.0, 123.0, 122.5, 122.4, 118.7, 116.3, 116.1, 52.7, 17.7. ^{11}B NMR (128 MHz, DMSO-d_6) δ_B 32.0. LC-MS: retention time: 9.9 min; ESI-QTOF HRMS (*m*/*z*): for $[C_{20}H_{20}BN_4O_4]^+$ [M + H]$^+$: exact mass calcd.: 391.1578; found: 391.1587.

(E)-4-((4-((2-boronobenzyl)amino)-2-methylphenyl)diazenyl)benzoic acid **47b**: The above procedure was repeated using 4-aminobenzoic acid (0.11 g, 0.83 mmol) instead of 4-nitroaniline. All other reagents were used in the same mole ratios to afford **47b** as an orange-red solid (62% yield). ^{1}H NMR (400 MHz, DMSO-d_6) δ_H 13.09 (s, 1H), 9.79 (s, 1H), 8.15–8.08 (m, 2H), 8.05 (dd, *J* = 8.6, 1.9 Hz, 1H), 7.90 (dd, *J* = 8.0, 6.3 Hz, 3H), 7.79 (dd, *J* = 8.5, 1.7 Hz, 1H), 7.72 (d, *J* = 9.1 Hz, 1H), 7.68 (dd, *J* = 9.1, 2.3 Hz, 1H), 7.56 (d, *J* = 2.4 Hz, 1H), 7.48 (s, 2H), 7.35 (dd, *J* = 7.8, 4.3 Hz, 1H), 4.64 (s, 2H), 2.73 (s, 3H). ^{13}C NMR (101 MHz, DMSO-d_6) δ_C 166.9, 155.1, 149.8, 148.4, 144.0, 140.6, 131.6, 130.6, 130.5, 130.4, 130.2, 122.5, 122.2, 118.8, 116.1, 116.0, 52.7, 48.6, 30.4, 17.7. ^{11}B NMR (128 MHz, DMSO-d_6) δ_B 30.4. LC-MS: retention time: 8.2 min; ESI-QTOF HRMS (*m*/*z*): for $[C_{21}H_{21}BN_3O_4]^+$ [M + H]$^+$: exact mass calcd.: 390.1625; found: 390.1634. FTIR (cm^{-1}): υ(O–H st) 3442, υ(C–H st) 2925, υ(C=O st, carboxyl) 1677, υ(C=C st and C=N st) 1677–1600.

(E)-3-((4-((2-boronobenzyl)amino)-2-methylphenyl)diazenyl)benzoic acid **47c**: The previous experiment was repeated using 3-aminobenzoic acid (499 mg, 3.64 mmol) instead of *p*-anisidine. All other reagents were used in the same mole ratios to afford **47c** as a red solid (25% yield). ^{1}H NMR (400 MHz, DMSO-d_6) δ_H 13.20 (s, 1H), 9.77 (s, 1H), 8.34 (t, *J* = 1.8 Hz, 1H), 8.25–8.16 (m, 1H), 8.10–8.03 (m, 3H), 7.89 (d, *J* = 7.3 Hz, 1H), 7.72 (d, *J* = 9.1 Hz, 2H), 7.70–7.66 (m, 2H), 7.56 (d, *J* = 2.4 Hz, 1H), 7.48 (s, 2H), 4.64 (s, 2H), 2.73 (s, 3H). LC-MS: retention time: 8.5 min; ESI-QTOF HRMS (*m*/*z*): for $[C_{21}H_{21}BN_3O_4]^+$ [M + H]$^+$: exact mass calcd.: 390.1625; found: 390.1630.

(E)-(2-(((4-((4-methoxyphenyl)diazenyl)-3-methylphenyl)amino)methyl)phenyl)boronic acid **47d**: The previous experiment was repeated using *p*-anisidine (0.61 g, 4.98 mmol, 6 equiv.) instead of 4-aminobenzoic acid. Purification was performed by washing the product (in dichloromethane) with 10% sodium hydrogen carbonate solution (w/w) to remove residual acetic acid, to yield **47d** as an orange-brown solid (56% yield). ^{1}H NMR (400 MHz, DMSO-d_6) δ_H 9.67 (s, 1H), 7.89 (d, J = 7.3 Hz, 1H), 7.84 (d, J = 8.9 Hz, 2H), 7.74–7.71 (m, 1H), 7.65–7.62 (m, 2H), 7.53 (d, J = 2.0 Hz, 1H), 7.48–7.45 (m, 2H), 7.34 (ddt, J = 9.2, 6.6, 3.2 Hz, 1H), 7.10 (d, J = 9.0 Hz, 2H), 7.08–7.02 (m, 1H), 4.61 (s, 2H), 3.85 (s, 3H), 2.69 (s, 3H). ^{13}C NMR (101 MHz, DMSO-d_6) δ_C 161.1, 148.4, 148.3, 146.9, 143.8, 138.9, 130.3, 130.0, 126.6, 126.4, 124.0, 123.4, 123.4, 122.5, 118.8, 115.9, 115.7, 114.5, 114.3, 55.5, 52.7, 17.7. ^{11}B NMR (128 MHz, DMSO-d_6) δ_B 29.9. LC-MS: retention time: 9.8 min; ESI-QTOF HRMS (m/z): for $[C_{21}H_{23}BN_3O_3]^+$ $[M + H]^+$: exact mass calcd.: 376.1832; found: 376.1836.

2.3.8. Sudan I Dyes Boronic Acid

Synthesis of Sudan I dyes boronic acid **48**: To a heated solution (50 °C) of Sudan I (347 mg, 1.39 mmol, 1.2 equiv.) in acetone (20 mL), potassium carbonate, K_2CO_3 (128 mg, 0.93 mmol, 0.80 equiv.), and 4-(bromomethyl)phenylboronic acid (250 mg, 1.16 mmol, 1.0 equiv.) were added. After 4 h of stirring and heating, additional potassium carbonate, K_2CO_3 (128 mg, 0.93 mmol, 0.80 equiv.) was added, and the suspension was stirred overnight. Finally, the reaction mixture was diluted with EtOAc and the organic layer was washed with 1 M hydrochloric acid (2 × 10 mL) and brine (20 mL), dried over Na_2SO_4, and concentrated in vacuo. The resulting solid was further purified using silica gel chromatography affording a pure Sudan I dye boronic acid **48** product. LC-MS: retention time: 9.7 min; ESI-QTOF HRMS (m/z): for $[C_{23}H_{19}BN_2O_3]^+$ $[M + H]^+$: exact mass calcd.: 383.2260; found: 383.1572.

2.4. Measurements of Photophysical Properties of Synthesised Compounds

Photophysical quantities such as absorption maxima ($\lambda_{abs}{}^{max}$), emission maxima ($\lambda_{em}{}^{max}$), Stokes shift ($\Delta\lambda$), molar extinction coefficient (ε), fluorescence quantum yield (Φ_F), and brightness were determined from absorption and emission data. Photophysical measurements were performed at ambient temperature (25 °C). UV-vis absorption spectra were recorded on a Shimadzu UV-1800 spectrophotometer between 200 and 800 nm using quartz cuvettes of 1 cm optical path length. The molar extinction coefficients (ε) of the different arylboronic acid dyes were determined at the respective maximum absorption wavelength using the Beer–Lambert law:

$$A = \varepsilon cl \quad (1)$$

where A is absorbance; ε is the extinction coefficient for the dye; c is the sample concentration; l is the pathlength of the sample cuvette. Fluorescence spectra of the synthesised compounds were acquired using a Shimadzu RF-6000 spectrofluorometer (Shimadzu, Kyoto, Japan). Emission spectra were recorded at room temperature with excitation wavelengths set at the $\lambda_{abs}{}^{max}$ of the respective dyes and emission range 250–800 nm. The excitation and emission slit widths were set at 5 nm. Fluorescence quantum yields were determined by the relative comparison procedure [63,64], using either rhodamine B (Φ_F = 0.70 in ethanol) [65] or quinine sulphate (Φ_F = 0.51 in 0.05 M H_2SO_4) [4,66]. Five different solutions with increasing concentrations of each of the synthesised compounds and the reference standards (rhodamine B or quinine sulphate) were prepared in different solutions and the absorbance of each solution was determined to be between 0.01–0.1 in 1 cm optical path length cuvette using a Shimadzu UV-1800 Spectrophotometer. Fluorescence spectra and the integrated fluorescence intensities for varying concentrations of solutions were measured using a Shimadzu RF-6000 spectrofluorometer. For each solution, graphs of the integrated fluores-

cence intensities as a function of the solution absorption were plotted in each case for both the synthesised dye and the reference standard (either rhodamine B or quinine sulphate). The resulting data points were fitted with linear plots and the slopes were calculated. The quantum yield (Φ_F) is calculated using the slope of the line determined from the plot of the absorbance against the integrated fluorescence intensities. In this case, the quantum yield of the unknown sample can be calculated using the following equation:

$$\Phi_{F,S} = \Phi_{F,R}\left(\frac{m_S}{m_R}\right)\left(\frac{\eta_S^2}{\eta_R^2}\right) \quad (2)$$

where m is the slope of the line obtained from the plot of the integrated fluorescence intensity vs. absorbance, η is the refractive index of solvent, and the subscripts $_R$ and $_S$ refer to the reference and unknown sample, respectively; Φ_S and Φ_R are the fluorescence quantum yield of the sample and that of the standard, respectively. The quantum yields were corrected for the differing refractive index of the solvent used for the sample and reference. Refractive indices (25 °C) were taken to be 1.3326, 1.3593, and 1.4793 for water, ethanol, and DMSO, respectively [67]. In instances where the same solvent was used for both the reference and unknown sample as a solvent, (η_S^2/η_R^2) will be 1, so the fluorescence quantum yield of the unknown (Φ_S) was obtained directly from the quotient of the two slopes.

3. Results and Discussion

3.1. Synthesis of Various Arylboronic Acid Chemosensor Fluorescent Dyes

3.1.1. Synthesis of the Building Blocks Through Miyaura Borylation

The syntheses of the various boronic ester building blocks were accomplished via a palladium-catalysed Miyaura borylation of aryl halides with a diboron reagent such as bis(pinacolato)diboron (B_2pin_2). Potassium acetate (KOAc) was employed as the base, and the reaction was carried out in 1,4-dioxane at 80 °C for 16 h [59,68,69]. The various pinacol-protected boronate esters were readily purified by silica gel chromatography to obtain analytically pure and white crystalline pinacol boronate ester solids with yields ranging from 70% to 96% (Scheme 1). They were characterised by ^{1}H and ^{13}C NMR, FTIR, and HRMS, and the data are provided in the Materials and Methods section with the corresponding spectra available in the Electronic Supplementary Information (Figures S1–S5). Interestingly, these boronate ester solids are indefinitely bench-stable under air compared to their corresponding boronic acids.

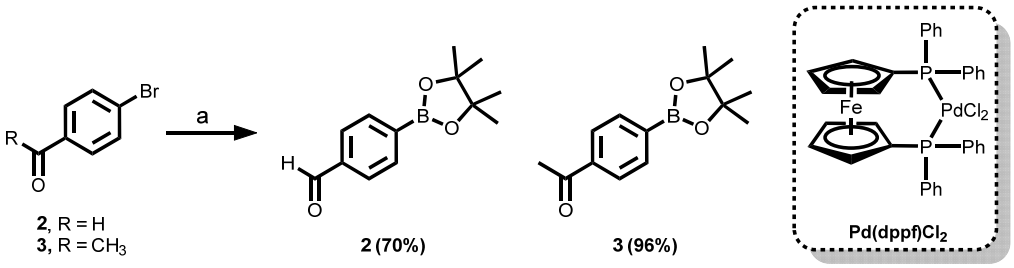

Scheme 1. Palladium-catalysed Miyaura borylation of aryl halides utilising bis(pinacolato)diboron. Reagents and conditions: (a) bis(pinacolato)diboron, KOAc, Pd(dppf)Cl_2, 1,4-dioxane, 80 °C, 16 h.

3.1.2. Coumarin-Tagged Boronic Acids

Coumarin and its derivatives are widely used as fluorescent probes because of their excellent chromogenic and fluorogenic properties such as high fluorescence quantum yields, large Stokes shifts, excellent photostability, and thermal stability [70–76]. Based on this knowledge, two coumarin-tagged boronic acids were designed and synthesised

(Schemes 2 and 3). The synthesis of the target compound **7** was achieved in four chemical steps as shown in Scheme 2. Characterisation was carried out by ^{1}H and ^{13}C NMR, FTIR, and HRMS, and the data are provided in the Materials and Methods section and the corresponding spectra are available in the Electronic Supplementary Information (Figures S6–S18). The first step of the synthesis was via a Knoevenagel condensation reaction of 4-(diethylamino)-2-hydroxybenzaldehyde with diethyl malonate in the presence of piperidine, cyclised, and then decarboxylated to afford 7-(diethylamino)-2*H*-chromen-2-one **4** in good yield (85%). Subsequently, compound **4** was subjected to Vilsmeier–Haack formylation in the presence of 1,2-dichloroethane (DCE) to produce 7-(diethylamino)coumarin-3-carbaldehyde **5** in 79% [76].

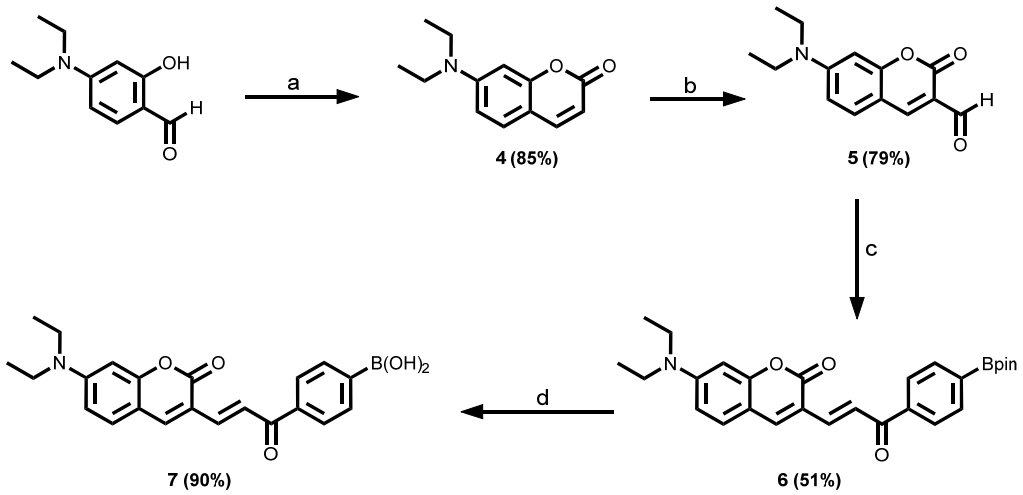

Scheme 2. Synthesis routes of coumarin-tagged boronic acid **7**. Reagents and conditions: (a) diethyl malonate, piperidine, EtOH, reflux, 13 h (**4**, 85%); (b) DMF/$POCl_3$, 1,2-dichloroethane, 0 °C → 60 °C, 12 h (**5**, 79%); (c) **3**, CH_2Cl_2/anhydrous CH_3CH_2OH=1:1 (*V*:*V*), pyrrolidine, room temperature, 4 d (**6**, 51%); (d) $NaIO_4$, THF/H_2O (4:1), room temperature, 30 min (**7**, 90%).

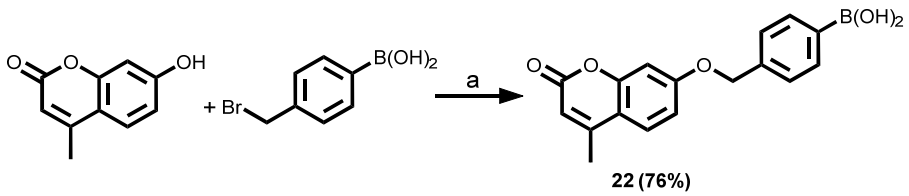

Scheme 3. Synthetic route to arylboronic acid dye 22. Reagents and conditions: (a) K_2CO_3, DMF, 70 °C, reflux, 1.5 h (22, 76%).

The formylation was deemed successful by the confirmation of the distinctive and unmistakable singlet at δ_H = 10.10 ppm observed in the ^{1}H NMR spectrum, which integrated for a single proton. This is characteristic of aldehydic protons [77].

Next, a base-catalysed Claisen–Schmidt condensation of 7-(diethylamino)coumarin-3-carbaldehyde **5** with 1-(4-(4,4,5,5-tetramethyl-1,3,2-dioxaborolan-2-yl)phenyl)ethan-1-one **3** building block using a catalytic amount of pyrrolidine in CH_2Cl_2/EtOH afforded the chalcone molecule **6** (yield = 51%) with extended conjugations [78]. Afterwards, the chalcone **6** which had the pinacol-protecting group was subjected to an oxidative hydrolysis deprotection protocol with aqueous sodium periodate ($NaIO_4$). This led to the smooth formation of the corresponding boronic acid **7** with excellent yield (up to 90%) [8,79]. ^{1}H NMR analysis of the product showed that the desired final compound was prepared following the disappearance of the Bpin peak at δ_H = 1.32 ppm (see Supplementary Materials Figure S14).

Another coumarin fluorescent dye arylboronic acid was synthesised from 7-hydroxycoumarin (umbelliferone). Unbelliferone is a known fluorophore with a high

quantum yield [80,81]. The coumarin-tagged boronic acid derivative in Scheme 3 was synthesised according to the procedure reported by Palanisamy et al. via a one-step alkylation reaction of 4-methylumbelliferone with 4-bromomethylphenylboronic acid in the presence of anhydrous potassium carbonate in dry DMF at 70 °C [82] to afford **22** in 76% yield after purification. The product was fully characterised by ^{1}H and ^{13}C NMR, and HRMS data are provided in the Materials and Methods section and the corresponding spectra are available in the Electronic Supplementary Information (Figures S19–S23).

3.1.3. 9-Aminoacridine-Tagged Boronic Acid Dyes

In another development, 9-aminoacridine-tagged boronic acid dyes were prepared. 9-Aminoacridine is a quinoline derivative that contains a tacrine-like moiety (Figure 4). Acridine and its derivatives are important quinoline structural derivatives that are generally planar tricyclic aromatic molecules which fluoresce at shorter wavelength regions [83,84]. Acridine-based fluorescence chemosensors have recently been synthesised and employed by Wang et al. for the selective detection of Fe^{3+} and Ni^{2+} ions [85].

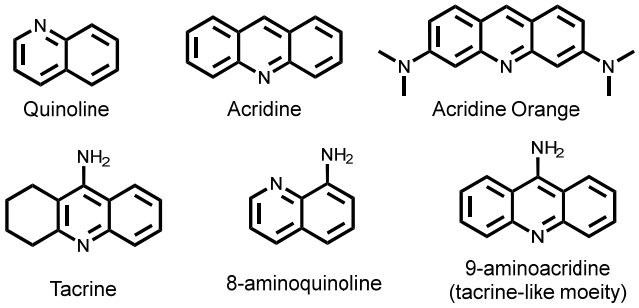

Figure 4. Structures of quinoline and quinoline derivatives.

Harnessing the advantages of the acridine moiety, a new arylboronic acid fluorescent chemosensor was prepared by coupling an aminoacridine fluorophore to a (4-(aminomethyl)phenyl)boronic acid via a chloroacetyl chloride linker in three steps (Scheme 4). *N*-(acridin-9-yl)-2-chloroacetamide **23** was prepared by reacting a commercially available 9-aminoacridine with chloroacetyl chloride according to chloroacetylation reaction procedures described in the literature [86–88]. This step was carried out in the presence of a catalytic amount of triethylamine (Et_3N). Chloroacetyl chloride plays a key role in synthetic and biological chemistry as a bifunctional linker for alcohols and amines [89]. Thus, it was employed to prepare the *N*-(acridin-9-yl)-2-chloroacetamide **23** as a suitable building block for the next step. The reaction was run overnight under room temperature, and the isolated yield was 59%. (4-(Aminomethyl)phenyl)boronic acid was then alkylated with the *N*-(9-acridinyl)-2-chloroacetamide using triethylamine as a catalyst under reflux in acetonitrile (CH_3CN) for 24 h to provide the target compound (4-(((2-(acridin-9-ylamino)-2-oxoethyl)amino)methyl)phenyl)boronic acid **24** in 22% yield.

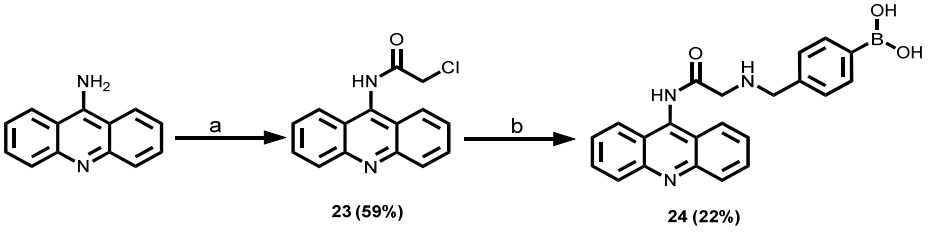

Scheme 4. Synthetic route to (4-(((2-(acridin-9-ylamino)-2-oxoethyl)amino)methyl)phenyl)boronic acid **24**. Reagents and conditions: (a) chloroacetyl chloride, Et_3N, THF, 0 °C to room temperature, overnight (**23**, 59%); (b) (4-(aminomethyl)phenyl)boronic acid, Et_3N, CH_3CN, reflux, 24 h (**24**, 22%).

3.1.4. 8-Aminoquinoline-Tagged Boronic Acid Dyes

8-aminoquinoline contains a quinoline moiety which is a well-known fluorophore unit [90]. Quinolines are particularly desirable because of their good coordination properties and their ability to form hydrogen bonds as a result of the presence of nitrogen in the ring as well as their small molecular size [90,91]. Furthermore, they are well known for their good metal affinity and hence are becoming leading candidates in the design of fluorescent probes for metals such as zinc and their applications in more complex biological research [90]. More importantly, the chemistry of quinoline is also well established and a plethora of synthetic methods are available to functionalise the core moiety [90]. With these advantages, attempts were made to synthesise an aminoquinoline-tagged boronic acid **29**. The synthesis was achieved in five steps as depicted in Scheme 5. The first step involves *Boc*-protection of glycine by reacting with *di-tert*-butyl dicarbonate (Boc_2O) under basic conditions to afford *Boc*-Gly-OH under 2 h. This was followed by amide coupling between the carboxylic acid functionality of the *N-Boc*-protected glycine **25** and 8-aminoquinoline in CH_2Cl_2 in the presence of EDC.HCl/DMAP as the activation/amide coupling agent.

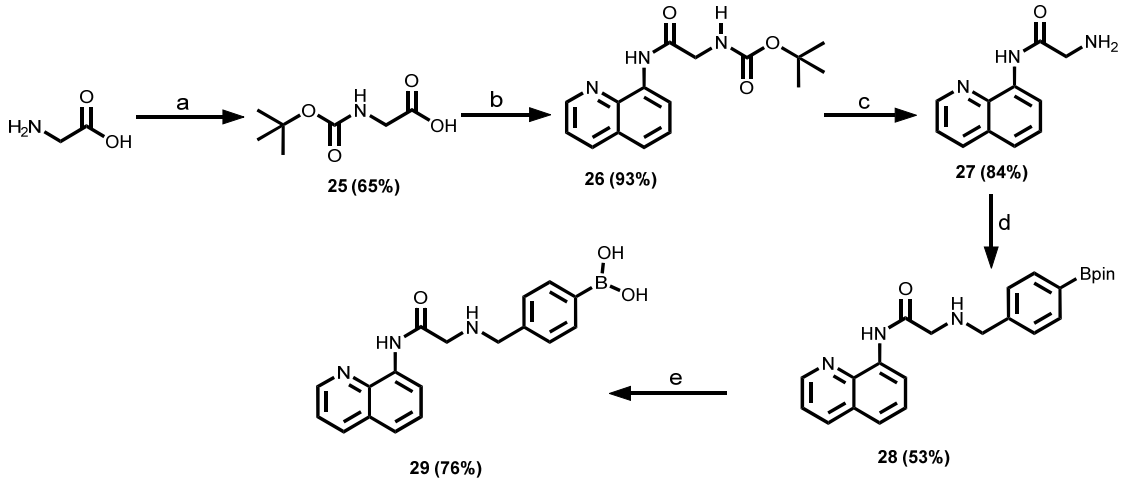

Scheme 5. Synthetic route to (4-(((2-oxo-2-(quinolin-8-ylamino)ethyl)amino)methyl)phenyl)boronic acid **18.** Reagents and conditions: (a) $(Boc)_2O$, Et_3N, 1,4-dioxane/H_2O (1:1), room temperature, 2 h (**6**, 65%); (b) 8-aminoquinoline, EDC.HCl, DMAP, CH_2Cl_2, room temperature, overnight (**15**, 93%); (c) HCl/dioxane (6 N), CH_2Cl_2, room temperature, overnight (**16**, 84%); (d) **2**, $NaBH(OAc)_3$, 1,2-dichloroethane, room temperature, 2 h (**28**, 53%); (e) $NaIO_4$, THF/H_2O (4:1), room temperature, 30 min (**29**, 76%).

The next step was to obtain the free amine through deprotection of the *N-Boc* group by using the traditional approach based on TFA-induced cleavage as reported previously [92] or with HCl (6 M) in dioxane at room temperature [93]. Both methods gave the desired products in excellent yields. The resultant free base was characterised by NMR and used in the next step without further purification. After the successful deprotection of the *N-Boc* group to obtain the free amine **27**, it was then coupled to the aldehyde functionality of the pinacol-protected 4-formylphenylboronic acid **2** building block that was previously synthesised under reductive amination conditions to give the aminomethyl derivative **28.** Sodium triacetoxyborohydride ($NaBH(OAc)_3$) was chosen as the reducing agent over others such as sodium cyanoborohydride ($NaBH_3CN$) and the less bulky hydride reagent $NaBH_4$ because of its high efficiency in reductive amination reactions with unreactive amines, leading to faster, better yields, and with fewer side products. Secondly, $NaBH(OAc)_3$ has been reported to be more selective for direct reductive aminations of ketones and aldehydes relative to the sodium cyanoborohydride alternative [94]. The other advantage of triacetoxyborohydride is the avoidance of the production of toxic by-products such as NaCN and

HCN that are usually associated with the use of $NaBH_3CN$ [27]. 1,2-dichloroethane (DCE) was preferred as a reaction solvent even though other similar amination reactions have been carried out in other solvents such as tetrahydrofuran (THF) and acetonitrile (CH_3CN). The final step was the deprotection of the boronate ester **28** using the optimised procedure of $NaIO_4$ to afford (4-(((2-oxo-2-(quinolin-8-ylamino)ethyl)amino)methyl)phenyl)boronic acid **29** in 76% yield.

3.1.5. Fluorescein-Tagged Boronic Acid Dyes

The synthesis of fluorescein-tagged boronic acid **36** was performed following the procedure in Scheme 6. First, esterification of cyclic fluorescein was carried out in the presence of a catalytic amount of concentrated sulfuric acid in methanol to afford fluorescein methyl ester **34** in an excellent yield (93%). The fluorescein methyl ester intermediate **34** was first characterised by X-ray crystallography (the crystallographic data are shown in Table S1). Then the ester was refluxed for 6 h with an excess amount of hydrazine hydrate in methanol via hydrazinolysis to produce the desired fluorescein hydrazide **35** with a yield of 96% [95]. An alternative method for the preparation of fluorescein hydrazide **35** (in 89% yield) involved the direct hydrazinolysis of the cyclic fluorescein using excess hydrazine hydrate under reflux in methanol for 12 h. Finally, through a Schiff base reaction, the fluorescein hydrazide **35** was coupled to 4-formylphenylboronic acid to form the fluorescein-tagged arylboronic acid chemosensor **36** in 64% yield.

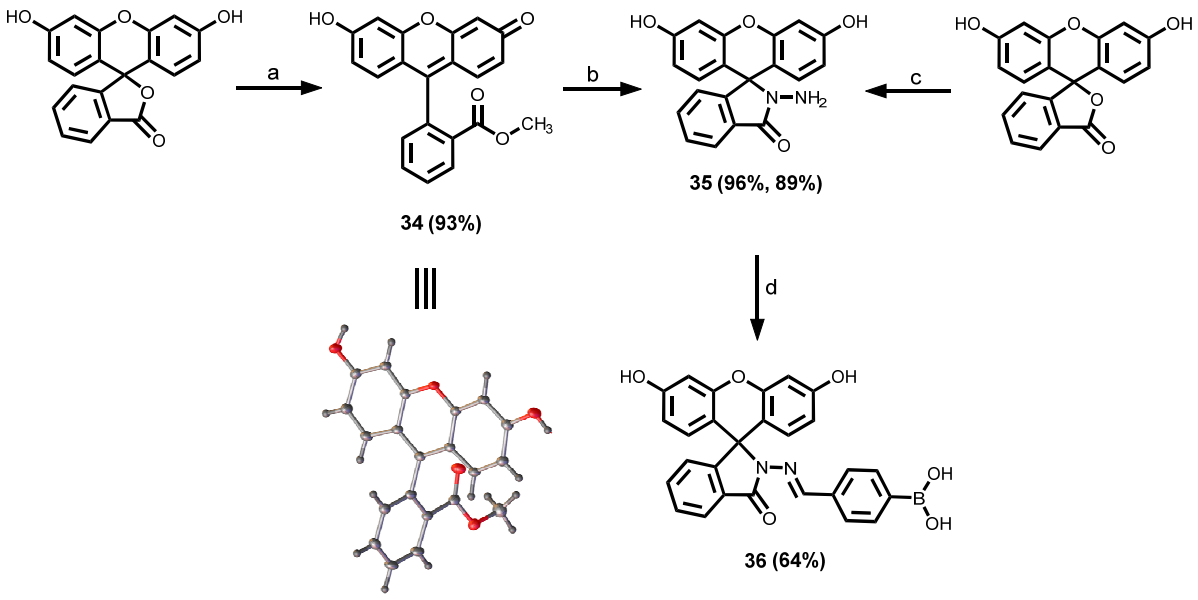

Scheme 6. Synthetic route to *(E)*-(4-(((3′,6′-dihydroxy-3-oxospiro[isoindoline-1,9′-xanthen]-2-yl)imino)methyl)phenyl)boronic acid. Reagents and conditions: (a) $MeOH/H_2SO_4$, reflux, 6 h (**34**, 93%); (b) $NH_2NH_2{\bullet}H_2O/MeOH$, reflux, 6 h (**35**, 96%); (c) $NH_2NH_2{\bullet}H_2O/MeOH$, reflux, 12 h (**35**, 89%); (d) 4-formylphenylboronic acid, EtOH, reflux, 5 h (**36**, 64%).

A second fluorescein boronic acid was synthesised via a one-step reaction of fluorescein isothiocyanate isomer I and 3-aminobenzeneboronic acid (Scheme 7). The fluorescein isothiocyanate contains an electrophilic carbon atom that readily reacted with nucleophile (amine), using dimethylformamide (DMF) as the solvent to form thiourea compound **37** in 68% yield [96,97].

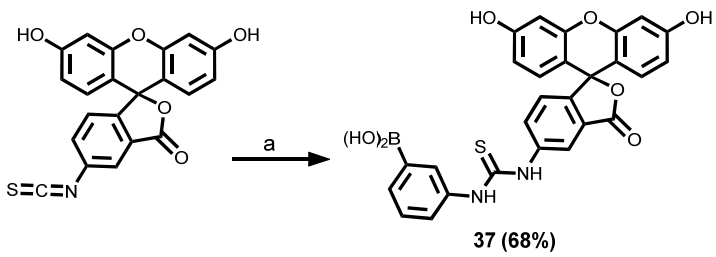

Scheme 7. Synthesis of (3-(3-(3′,6′-dihydroxy-3-oxo-3H-spiro[isobenzofuran-1,9′-xanthen]-5-yl)thioureido)phenyl)boronic acid. Reagents and conditions: (a) 3-aminobenzeneboronic acid, DMF, room temperature, 12 h (**37**, 68%).

3.1.6. Rhodamine-Tagged Boronic Acid Dye

Rhodamine dye fluorophores are part of the family of xanthenes along with fluorescein and eosin dyes [98]. The structures of xanthene chromophore and rhodamine dyes are shown in Figure 5. The carboxylic acid group of rhodamine dyes undergo intramolecular cyclisation. The ring-opened form is highly fluorescent, whereas the spirocyclic spirolactone form is essentially nonfluorescent [98,99].

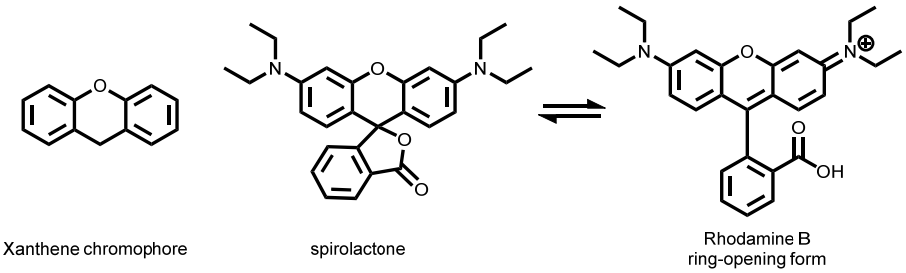

Figure 5. Molecular structure of Xanthene and Rhodamine B dye.

Rhodamine dyes and their derivatives have also been used extensively, in particular as chemosensors either in vitro or in vivo in the detection of metals including Hg(II) [100–102], peroxynitrite [51], Cu(II) [103], Fe(III) [104], Cr(III) [104]. Rhodamine derivatives are also employed as molecular switches [105]. Rhodamine B was chosen as the fluorescent dye for use in this study due to the high fluorescence quantum efficiency, high molar extinction coefficients, and low cost. A rhodamine-tagged boronic acid **39** was readily synthesised from rhodamine B by a two-step reaction (Scheme 8), where rhodamine B was treated with excess hydrazine in methanol to give rhodamine B hydrazide **38** in 68% yield. The hydrazide was further converted to the designed product **39** in 73% yield through a Schiff base reaction using 4-formylphenylboronic acid.

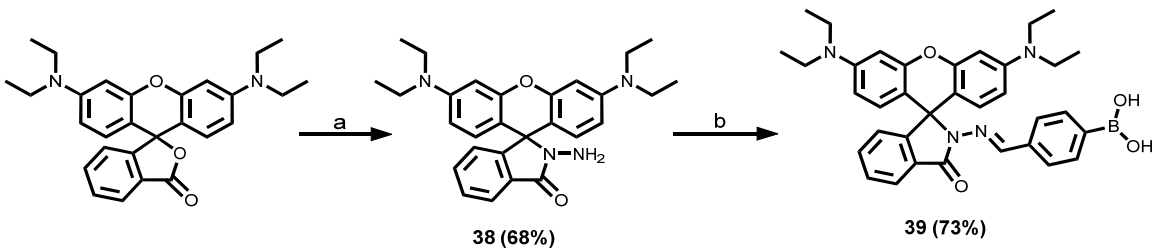

Scheme 8. Synthesis of (E)-(4-(((3′,6′-bis(diethylamino)-3-oxospiro[isoindoline-1,9′-xanthen]-2-yl)imino)methyl)phenyl)boronic acid **39**. Reagents and conditions: (a) $NH_2NH_2 \bullet H_2O$/MeOH, reflux, 6 h (**38**, 68%); (b) 4-formylphenylboronic acid, EtOH, reflux, 5 h (**39**, 73%).

3.1.7. BODIPY-Tagged Boronic Acid Dyes

4,4-difluoro-4-bora-3a-4a-diaza-s-indacene (simply known as BODIPY, difluoroboron dipyrromethene) and its derivatives are fluorescent organic dye molecules that were first discovered by Treibs and Kreuzer in 1968 [106] (Figure 6). Since then, several BODIPY and their derivatives have become the most popular dye molecules among the multitude of fluorescent dyes available with widespread applications in various areas, including tunable laser dyes, biological labelling [107–109], as fluorescent switches, fluorophores in sensors and labels, and light-harvesting systems in electroluminescent devices [110–112]. The interest in BODIPY chromophores can be attributed to their favourable physicochemical characteristics and desirable photophysical properties [113,114], such as high fluorescence quantum yields, relatively large molar absorption coefficients, narrow emission bandwidths, and tunable fluorescent properties, as well as relatively high thermal and photochemical stabilities [115–118]. These molecules generally have excitation/emission wavelength in the visible region with stable excited states. Other advantages include ease of modification of BODIPY chemically for the synthetic accessibility of various derivatives and good solubility in common solvents [119]. As a result, a significant number of BODIPY derivatives have since been synthesised and characterised [115,116]. Also, there is an abundance of literature that supports the synthetic versatility of the BODIPY chromophore which allows for far-reaching structural modifications, resulting in the alteration of the electronic, optical, and chemical properties of the dye [120].

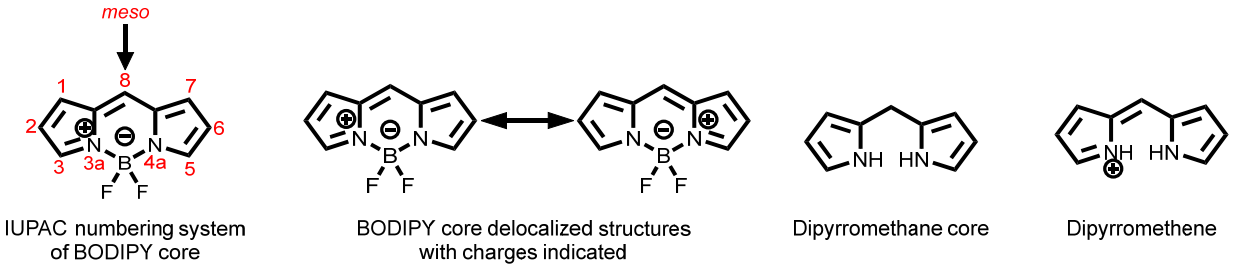

Figure 6. Representation of the BODIPY framework showing the IUPAC numbering system, delocalised structures, dipyrromethene, and dipyrromethene cores.

Thus, a procedure for the introduction of an arylboronic acid unit onto a BODIPY core was developed to take advantage of the desirable photophysical properties outlined above. Two approaches were employed to synthesise the boron dipyrromethene (BODIPY)-tagged boronic acid dye **45** (Scheme 9). The first route involved the use of the pinacol-protected 4-formylphenylboronic acid **2,** whereas in the second route, 4-formylphenylboronic acid was attempted directly without protecting it to reduce the number of steps, especially in instances where purification and hydrolysis of the boronate proved challenging. The synthesis began with an acid-catalysed condensation between two equivalents of 2,4-dimethylpyrrole and a suitable electrophile such as pinacol-protected 4-formylphenylboronic acid **2** to form a dipyrromethane intermediate **40**, followed by the addition of a few drops of trifluoroacetic acid (TFA). The complete consumption of the aldehyde was monitored by TLC. The dipyrromethane intermediate **40** was unstable and was therefore not isolated but converted directly to a dipyrromethene **41** in an oxidation step carried out using 2,3,5,6-tetrachloro-p-benzoquinone (*p*-chloranil) as an oxidant [121]. The dipyrromethene **41** was subsequently subjected to a boron trifluoride etherate ($BF_3 \cdot Et_2O$) complexation reaction catalysed by triethylamine (Et_3N) to afford the borondifluoride complex **42** in 47% yield [122,123]. The last step involved the deprotection of the boronate ester **42,** in the case where the protected boronate aldehyde was used, to obtain the BODIPY dye **45** as a red crystalline solid (89% yield).

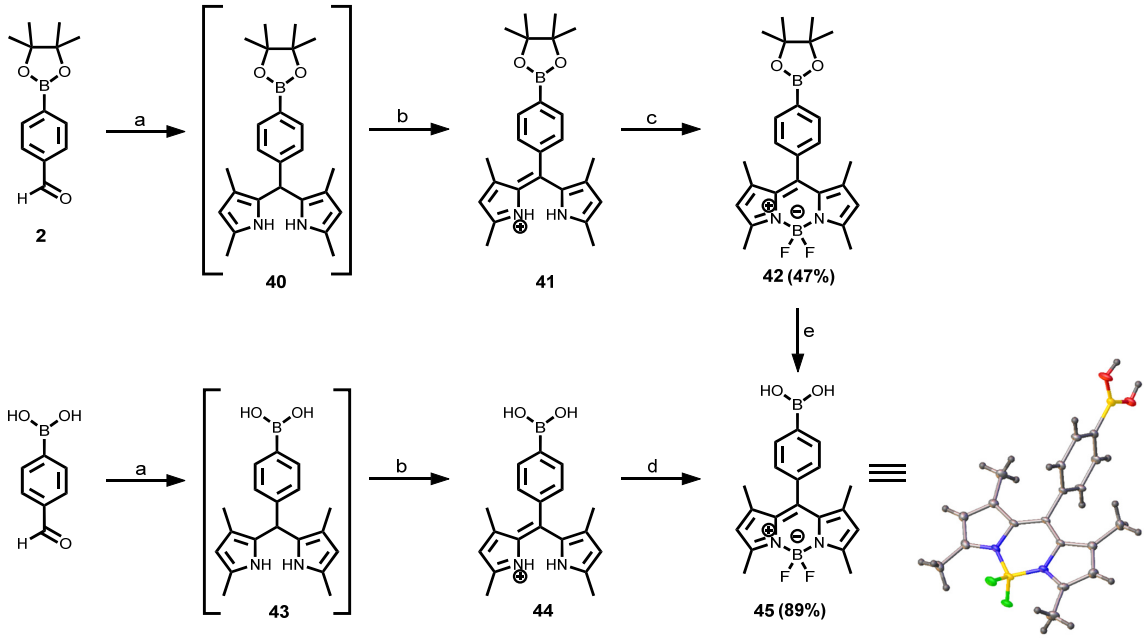

Scheme 9. Synthesis of BODIPY-tagged boronic acid **45** via two routes. Reagents and conditions: (a) 2,4-dimethylpyrrole, CH_2Cl_2, 0 °C to room temperature, 3 h; (b) *p*-chloranil, CH_2Cl_2, 0 °C to room temperature, 30 min; (c) Et_3N, BF_3•OEt_2, CH_2Cl_2, 0 °C to room temperature, 12 h (**42,** 47%); (d) Et_3N, BF_3•OEt_2, CH_2Cl_2, 0 °C to room temperature, 12 h (**45,** 89%); (e) $NaIO_4$, THF/H_2O (4:1), room temperature, 30 min (**45**, 89%).

A single-crystal diffraction analysis was measured for crystals of **45,** and the Oak Ridge thermal ellipsoid plot (ORTEP) diagram is displayed in Figure 7 and the crystallographic data are shown in Supplementary Materials (Table S1). The crystal structure of BODIPY **45** reveals that the molecule is virtually planar. This is corroborated by the following structure refinement data. The boron atom has a slightly distorted tetrahedral coordination with the two fluorine atoms being perpendicularly oriented with respect to the dipyrrin plane. The B1–N1 and B1–N2 bond lengths are 1.536(2) Å and 1.534(2) Å respectively. Likewise, the B1–F1 and B1–F2 bond lengths are 1.412(2) Å and 1.407(2) Å respectively. The bond distances of the two B–N and two B–F are virtually identical, which is an indication that **45** possess single B–N and B–F bonds. Also, the average N1–B1–N2 and F1–B1–F2 angles are 107.75(12) ° and 106.82(12)°, respectively. This also presupposes that there is an expected delocalisation of the positive charge.

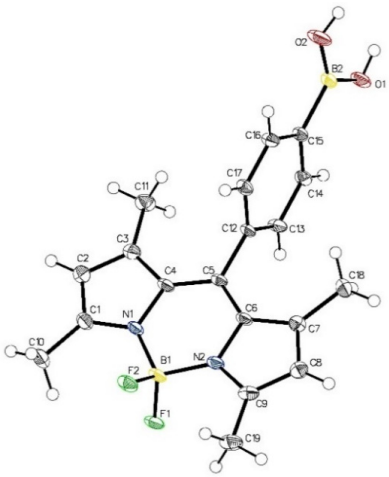

Figure 7. ORTEP representation of the compound **45** investigated by X-ray structure analysis; atomic labelling shown with 30% probability displacement ellipsoids.

3.1.8. Azo-Tagged Boronic Acid Dyes

Boronic acid azo dyes were used in the 1940s for investigations into the treatment of cancer by boron neutron capture therapy (BNCT) [124]. However, in 1991, a boronic acid azo dye synthesised from 4-aminophenylboronic acid was found to be sensitive to a selection of saccharides [125]. Subsequently, various conjugates of azo dyes have been developed as saccharide and sugar sensors [126–128]. A variety of azo-tagged boronic acid dyes in which subtle modifications are made to the electronic configuration of the azo chromophore by varying the substituent groups on the azo aromatic ring were synthesised as depicted in Scheme 10. The first step involved the synthesis of (2-((m-tolylamino)methyl)phenyl)boronic acid **46** by reductive amination, followed by diazotisation of various anilines containing electron-withdrawing groups such as *p*-NO_2, *p*-COOH, *p*-OCH_3, and *m*-COOH in the presence of an aqueous solution of sodium nitrite ($NaNO_2$) in concentrated HCl medium at 0 °C to form the corresponding diazonium salts. The destruction of excess sodium nitrite after the diazotisation reaction step was required because nitrites are toxic and can be harmful to the environment. This was achieved by using a common nitrous acid scavenger such as sulfamic acid (H_3NSO_3) that reacts with nitrous acid (HNO_2) to form stable and non-toxic compounds [129,130]. The diazonium salts that were formed in the previous step were not isolated but coupled in situ with (2-((*m*-tolylamino)methyl)phenyl)boronic acid **46** in a basic medium (NaOH) to give the respective target products, which were fully characterised by ^{1}H NMR, ^{13}C NMR, and HR-LCMS spectroscopic and spectrometric analysis. It is worth noting that the pH of the reaction mixture plays a significant role in the coupling reaction and therefore a careful balance must be struck between the equilibria governing the coupling component and the diazo component. The coupling reactions of the various aniline diazonium salts with the (2-((*m*-tolylamino)methyl)phenyl)boronic acid **46** occur predominantly para to the electron-donating anilinic nitrogen because of steric effects. This was directed by incorporating a methyl group *meta* to the anilinic nitrogen in the amine coupling agent, and it resulted in the exclusive para coupling products. This approach allowed for the synthesis of target compounds (**47a–d**) and avoided the potentially difficult separation of isomers [131].

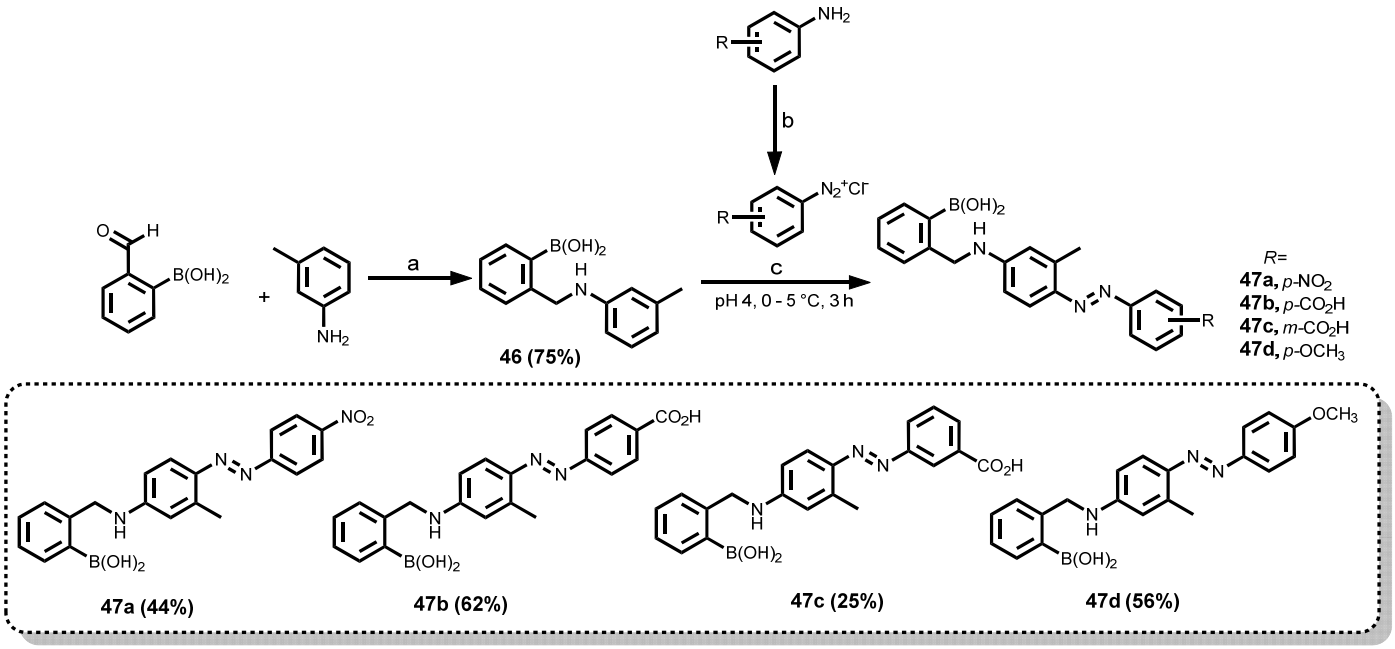

Scheme 10. Synthetic route to (E)-(2-(((3-methyl-4-(phenyldiazenyl)phenyl)amino)methyl)phenyl) boronic acid derivatives. Reagents and conditions: (a) $NaBH(OAc)_3$, 1,2-dichloroethane, room temperature, 2 h (**46**, 75%); (b) $NaNO_2$/conc HCl, 0 °C to 5 °C; (c) pH 4, 0 °C to 5 °C, 3 h.

3.1.9. Sudan I Boronic Acid Dye

Another azo boronic acid derivative was synthesised from Sudan I dye according to the one-step procedure in Scheme 11. Sudan I was reacted with 4-bromomethylphenylboronic acid in the presence of anhydrous potassium carbonate in dry acetone at 50 °C to afford **48**. The product was characterised by HRMS.

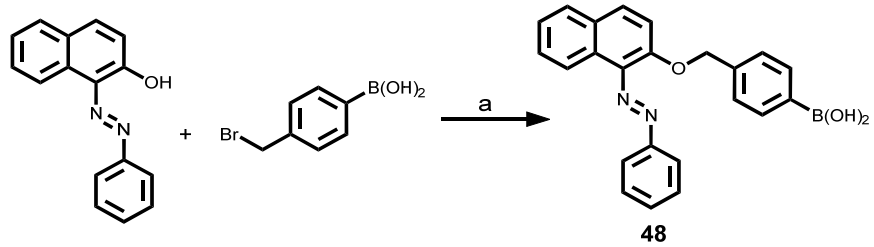

Scheme 11. Preparation of Sudan I boronic acid dye **48**. Reagents and conditions: (a) K_2CO_3, acetone, reflux, 50 °C, overnight.

3.2. Photophysical Properties of the Different Arylboronic Acid Chemosensor Dyes

A complete set of basic photophysical quantities such as absorption maxima ($\lambda_{abs}{}^{max}$), emission maxima ($\lambda_{em}{}^{max}$), Stokes shift ($\Delta\lambda$), molar extinction coefficient (ε), fluorescence quantum yield (Φ_F), and brightness of twelve (12) synthesised arylboronic acid chemosensors and two (2) commercially available boronic acids (2-naphthylboronic acid (BA) and 9,9-diphenyl-9H-fluoren-4-ylboronic acid (BA18)) were determined in different solvents including ethanol, dimethyl sulfoxide, and methanol through absorption and emission spectroscopy techniques. The data are summarised in Figure 8 and Table 1.

The UV-vis absorption spectra of the different synthesised compounds are depicted in Figure 9 (see also the Supplementary Materials). The absorption maxima wavelengths are recorded in Table 1. The UV–vis spectroscopy was also used to obtain the experimental extinction coefficient (ε). It was observed that the synthesised compounds were characterised by ε ranging from very low values for **22** (ε = 248 ±16 $M^{-1}cm^{-1}$ at 403 nm) to the largest for **7** (ε = 52,800 ± 1481 $M^{-1}cm^{-1}$ at 456 nm).

Table 1. Photophysical properties of synthesised fluorescent arylboronic acid dyes.

Dye	MW [$gmol^{-1}$]	Solvent	$\lambda_{abs}{}^{max}$ [nm]	$\lambda_{em}{}^{max}$ [nm]	Stokes Shift ($\Delta\lambda$) [nm]	ε [$M^{-1}cm^{-1}$]	Quantum Yield (Φ_F)	Brightness [$M^{-1}cm^{-1}$]
7	391.2	EtOH	456	590	134	52,816.1	0.78	41,196.6
22	310.1	DMSO	403	448	45	247.6	0.24	59.4
24	385.2	MeOH	248.5	429	180.5	ND		ND
29	335.2	DMSO	318	405	87	6468.8	0.031	200.5
36	478.3	EtOH	301	347	46	21,486.3		ND
37	526.3	EtOH	480	525	45	9368.7	0.47	4403.3
39	588.5	EtOH	540	569	29	296.5	0.48	142.3
45	368.0	EtOH	496	508	12	29,259.1	0.70	20,481.4
47a	390.2	EtOH	464	-	-	21,695.7		ND
47b	389.2	EtOH	416	-	-	20,550.8		ND
47c	389.2	EtOH	398	-	-	27,245.4		ND
48	382.2	MeOH	335	384	49	ND		ND
BA	172.0	MeOH	275	328	53	ND		ND
BA18	362.2	MeOH	270	333	63	ND		ND

Maximum absorption wavelength ($\lambda_{abs}{}^{max}$); maximum emission wavelength ($\lambda_{em}{}^{max}$); Stokes shift ($\Delta\lambda$): calculated as the difference between $\lambda_{abs}{}^{max}$ and $\lambda_{em}{}^{max}$; molar extinction coefficient (ε); fluorescence quantum yield (Φ_F): calculated by compared to fluorescence reference standards with known quantum yield values such as Rhodamine B (Φ_F = 0.70 in EtOH), Quinine sulphate (Φ_F = 0.51 in 0.1 M H_2SO_4); and brightness: this parameter was calculated using the following formula: brightness = extinction coefficient (ε) × fluorescence quantum yield (Φ_F); ND = not determined.

Compound 7
$\lambda_{max\ abs}$ = 456 nm
$\lambda_{max\ em}$ = 590 nm
$\Delta\lambda$ = **134 nm**
ε = **52816 $M^{-1}cm^{-1}$**
Φ = **0.79** (EtOH)
Brightness = **41197 $M^{-1}cm^{-1}$**

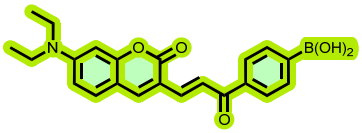

Compound 22
$\lambda_{max\ abs}$ = 403 nm
$\lambda_{max\ em}$ = 448 nm
$\Delta\lambda$ = 45 nm
ε = 247.6 $M^{-1}cm^{-1}$
Φ = 0.24 (DMSO)
Brightness = 59.4 $M^{-1}cm^{-1}$

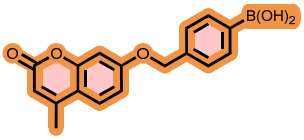

Compound 24
$\lambda_{max\ abs}$ = 248.5 nm
$\lambda_{max\ em}$ = 429 nm
$\Delta\lambda$ = 180.5 nm
ε = ND
Φ = ND
Brightness = ND

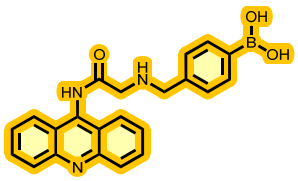

Compound 29
$\lambda_{max\ abs}$ = 318 nm
$\lambda_{max\ em}$ = 405 nm
$\Delta\lambda$ = 87 nm
ε = 6469 $M^{-1}cm^{-1}$
Φ = 0.031 (DMSO)
Brightness = 200.5 $M^{-1}cm^{-1}$

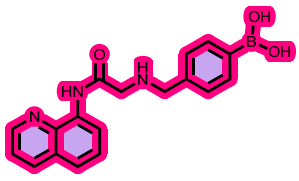

Compound 36
$\lambda_{max\ abs}$ = 301 nm
$\lambda_{max\ em}$ = 347 nm
$\Delta\lambda$ = 46 nm
ε = 21486.3 $M^{-1}cm^{-1}$
Φ = ND
Brightness = ND

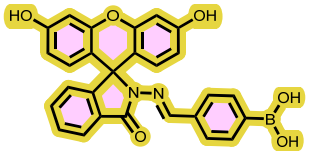

Compound 37
$\lambda_{max\ abs}$ = 301 nm
$\lambda_{max\ em}$ = 347 nm
$\Delta\lambda$ = 46 nm
ε = 21486.3 $M^{-1}cm^{-1}$
Φ = 0.47 (EtOH)
Brightness = ND

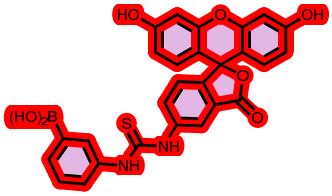

Compound 39
$\lambda_{max\ abs}$ = 540 nm
$\lambda_{max\ em}$ = 569 nm
$\Delta\lambda$ = 29 nm
ε = 296.5 $M^{-1}cm^{-1}$
Φ = 0.48 (EtOH)
Brightness = 142.3 $M^{-1}cm^{-1}$

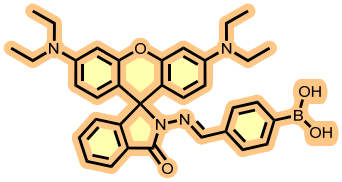

Compound 45
$\lambda_{max\ abs}$ = 496 nm
$\lambda_{max\ em}$ = 508 nm
$\Delta\lambda$ = 12 nm
ε = 29259 $M^{-1}cm^{-1}$
Φ = 0.70 (EtOH)
Brightness = 20481 $M^{-1}cm^{-1}$

Compound 47a
$\lambda_{max\ abs}$ = 464 nm
$\lambda_{max\ em}$ = ND
$\Delta\lambda$ = ND
ε = 21696 $M^{-1}cm^{-1}$
Φ = ND
Brightness = ND

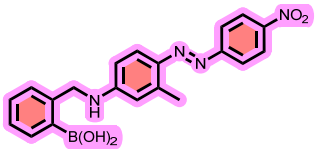

Compound 47b
$\lambda_{max\ abs}$ =416 nm
$\lambda_{max\ em}$ = ND
$\Delta\lambda$ = ND
ε = 20551 $M^{-1}cm^{-1}$
Φ = ND
Brightness = ND

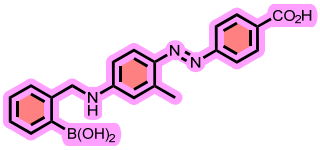

Compound 47c
$\lambda_{max\ abs}$ =398 nm
$\lambda_{max\ em}$ = ND
$\Delta\lambda$ = ND
ε = 27245 $M^{-1}cm^{-1}$
Φ = ND
Brightness = ND

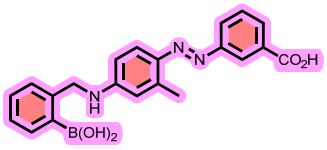

Compound 48
$\lambda_{max\ abs}$ = 496 nm
$\lambda_{max\ em}$ = 384 nm
$\Delta\lambda$ = 49 nm
ε = ND
Φ = ND
Brightness = ND

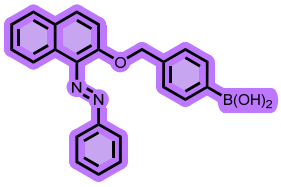

Commercial boronic acids

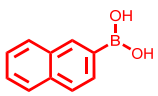

2-naphthylboronic acid (**BA**)

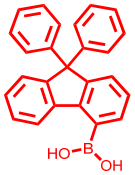

(9,9-Diphenyl-9H-fluoren-4-yl)
-boronic acid (**BA18**)

Figure 8. Structures of synthesised fluorescent arylboronic acid dyes were included in this study. The characteristic chromophore cores of the structures are highlighted in different colours.

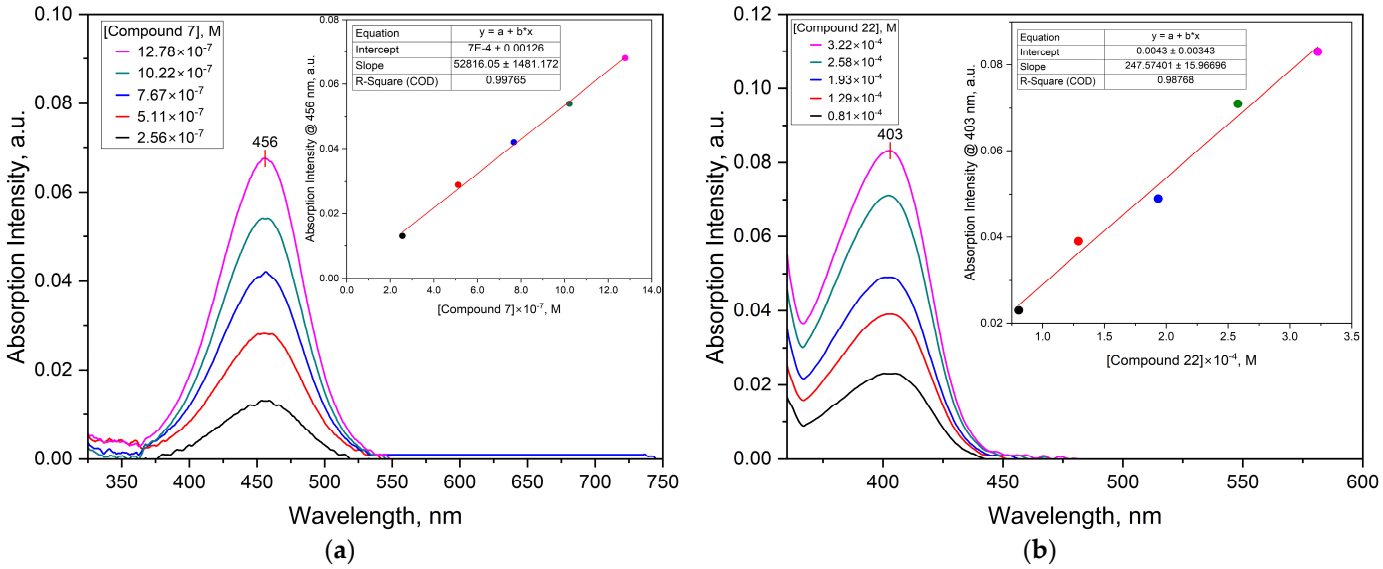

Figure 9. Absorbance spectra of various dyes in different organic solvents; insets: respective linearity plots for the evaluation of molar extinction coefficients (ε) for the dyes at the absorption maxima: (**a**) compound **7**; (**b**) compound **22**.

Additionally, the fluorescence emission curves were obtained by exciting the compounds at their respective absorption maxima. The normalised fluorescence emission spectra of the synthesised compounds are shown in Figure 10 and Figure S90. The maximum emission bands are as follows: **37** (λ_{em} = 525 nm at λ_{ex} = 480 nm), **7** (λ_{em} = 590 nm at λ_{ex} = 456 nm), **29** (λ_{em} = 405 nm at λ_{ex} = 318 nm), **36** (λ_{em} = 347 nm at λ_{ex} = 301 nm), **22** (λ_{em} = 448 nm at λ_{ex} = 403 nm), **39** (λ_{em} = 569 nm at λ_{ex} = 540 nm), and **45** (λ_{em} = 508 nm at λ_{ex} = 496 nm). The Stokes shift (Δλ)—defined as the difference between absorption maxima (λ_{abs}^{max}) and emission maxima (λ_{em}^{max})—was calculated for the various compounds. Fluorescence spectra of the varying concentrations of unknown samples and references with the absorbance values and integrated intensities (area under curve) of both samples and corresponding references are shown in Table 2**.** The relative fluorescence quantum yield (Φ_F) was determined relative to Rhodamine B in ethanol and Quinine sulphate in 0.1 M H_2SO_4 from fluorescence measurements. Quantum yield measurements require low absorbance (optical density), typically below 0.1 at the longest wavelength absorption maxima. Therefore, all solutions of all synthesised arylboronic dyes were prepared at low concentrations to limit the absorbance values to less than 0.1 in order to avoid any complications with dimer or aggregate formation [132], reduce or minimise possible non-linear effects arising from the inner filter (reabsorption effects) [64,132], and eliminate concentration-quenching effects, internal filter effects, and errors arising from uneven distribution of the excited species in the detected volume [65], which altogether may otherwise skew the resulting quantum yield.

Finally, the brightness of each of the synthesised dyes was calculated from the molar absorption coefficient at the excitation wavelength and the fluorescence quantum yield values. Brightness is defined as the product of ε and Φ_F ($B = \Phi_F \times \varepsilon$). The brightness values allow for more practically meaningful comparisons between different dyes and, as a result, can be used to determine the analytical sensitivity from the fluorophore side [52,133,134]. From the data obtained, the fluorescence emissions of most of the compounds occurred at longer wavelengths in the visible region of the electromagnetic spectrum as compared to the absorption spectra. This can be explained by the general principle that there are usually energy losses associated with absorption and emission spectra, thus shifting the fluorescence spectra to longer wavelengths [135]. The fluorescence observed can be attributed to n→π*

or π→π* transition states [136]. The Δλ values ranged from the least for **45** (Δλ = 12 nm) to sufficiently large Stokes shift values (Δλ > 80 nm) for **29**, **7**, and **24** with Δλ values of 87, 134, and 180.5 nm respectively. The BODIPY analogue **45** showed an intense absorption band with a maximum at 496 nm assigned at spin-allowed π-π* transitions, high molar extinction coefficient (ε = 29,259 ± 450 $M^{-1}cm^{-1}$ at 496 nm), emission maximum at 508 nm with the lowest calculated Δλ value of 12 nm. These properties are characteristic of the BODIPY chromophore subunits and consistent with reported data [115,137]. On the other hand, **7** with a high Δλ value of 134 nm has the coumarin core moiety.

Table 2. Absorbance and integrated fluorescence intensities (areas) for various samples and references.

	Integrated Fluorescence Intensity	
Absorbance @ 499 nm	**7**	Rhodamine B
0.020	2619195.0	2549829.2
0.016	2158588.5	2121340.3
0.012	1682211.2	1495319.2
0.009	1204913.3	1066673.4
0.004	591676.7	415287.3
Slope	128197000.0	115445000.0
Absorbance @ 358 nm	**22**	Quinine sulphate
0.072	2384944.0	9169983.2
0.058	2080661.1	7757302.9
0.051	1560798.8	6858240.1
0.038	1032764.1	5131493.2
0.028	510273.4	3945263.9
Slope	43905200.0	120830000.0
Absorbance @ 332 nm	**29**	Quinine sulphate
0.080	406256.1	10254500.0
0.066	331390.9	8717544.0
0.053	269142.8	7633669.7
0.040	195980.9	5868201.1
0.030	134100.4	4435606.5
Slope	5383876.6	114494000.0
Absorbance @ 502.5 nm	**37**	Rhodamine B
0.023	2014294.3	2863728.4
0.020	1785124.7	2380927.6
0.014	1300128.5	1745938.7
0.010	942578.1	1216051.1
0.005	455519.6	489246.6
Slope	861649000.0	128111000.0
Absorbance @ 544.5 nm	**39**	Rhodamine B
0.078	6696547.2	8871962.3
0.064	6251111.1	7476185.8
0.048	4931408.8	5593976.4
0.032	3405442.5	3872951.0
0.017	1858555.0	1555633.8
Slope	81524200.0	118451000.0
Absorbance @ 502.5 nm	**45**	Rhodamine B
0.023	3049627.7	2863728.4
0.019	2613267.2	2380927.6
0.014	1973366.8	1745938.7
0.010	1360672.8	1216051.1
0.005	731821.0	489246.6
Slope	127606000.0	128111000.0

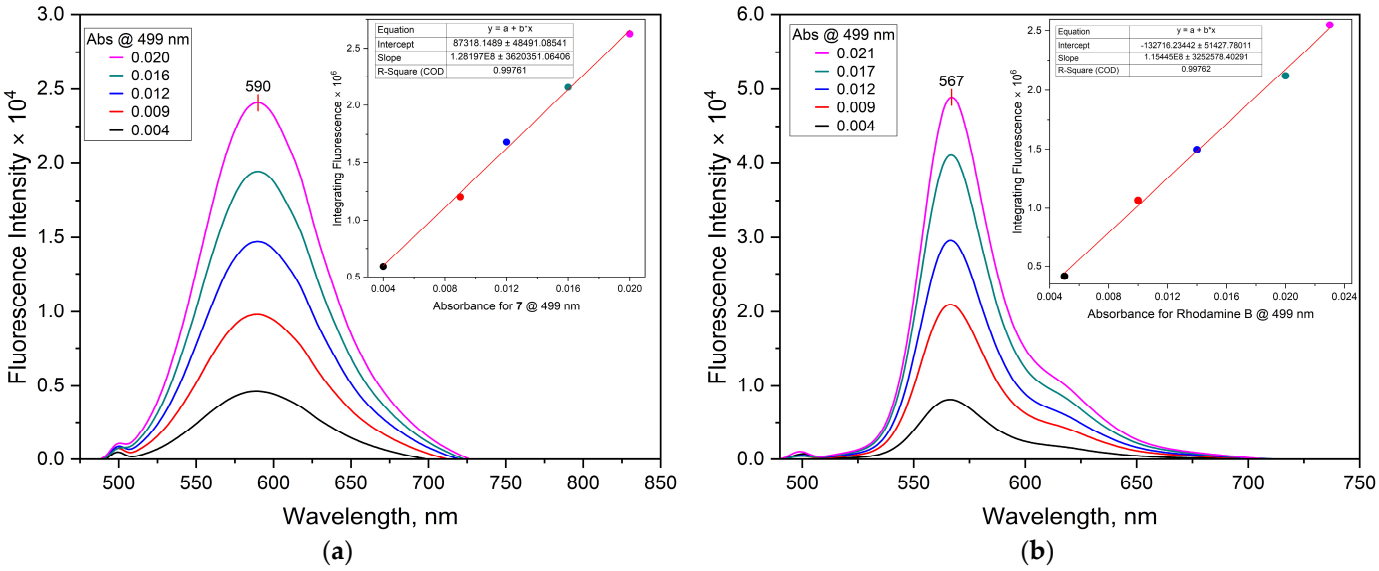

Figure 10. Fluorescence emission spectra of synthesised compounds (left) and reference compounds (Rhodamine B or Quinine sulphate (right)) with varying absorbance. Inset: calibration curves of integrated fluorescence intensity (area under curve) against absorbance for the following samples, respectively: (**a**) compound **7**; (**b**) Rhodamine B at 499 nm.

Some of the synthesised compounds such as **47a**–**47c** did not show fluorescence. Incidentally, all three compounds are azo dyes and this was not surprising because as a general rule, these categories of dyes do not fluoresce [138]. Here, the absorbed energy is dissipated by the medium or emitted as phosphorescence, which has a longer lifetime for the excited state [136]. However, all three synthesised azo dyes were characterised by high molar extinction coefficient values for example **47a** (ε = 21,696 ± 1997 $M^{-1}cm^{-1}$ at 464 nm), **47b** (ε = 20,551 ± 360 $M^{-1}cm^{-1}$ at 416 nm), and **47c** (ε = 27,245 ± 467 $M^{-1}cm^{-1}$ at 398 nm). The quantum yields for these dyes were not determined due to a lack of significant fluorescence emissions at their respective absorption maxima values and also because very small quantum yield values have been acquired for other azo dyes [139,140]. Unlike the azo dyes **47a**–**47c**, this was not the case for **48**, a Sudan I boronic acid derivative which is also an azo dye. Fluorescence was observed with **48**, giving an emission maximum at 384 nm and a $\Delta\lambda$ value of 49 nm. As a general principle, small-molecule fluorophores require a high degree of aromaticity to have absorptions in the visible region of the spectrum [4,135]. The compound with the largest molar extinction coefficient (ε = 52,816 ± 1481 $M^{-1}cm^{-1}$ at 456 nm), a $\Delta\lambda$ value of 134 nm, Φ_F = 0.78, and brightness value (41,196.6 $M^{-1}cm^{-1}$) was **7**, a coumarin derivative. This is typical of coumarin derivatives, which are usually characterised by high molar extinction coefficients in the near-UV and visible range and high fluorescence emission, and, as a result, have found many uses as fluorescent chromophores for several applications [141,142].

Based on the excellent photophysical properties of **7**, its fluorescent properties toward mycolactone were investigated. Sensitive detection of mycolactone was achieved through fluorescence spectroscopy as shown in Figure 11**.** For instance, free **7** (2.5×10^{-3} mg/mL) exhibited weaker fluorescence intensity at the emission maximum of 581 nm. However, the fluorescence intensity gradually increased as the concentration of mycolactone increased from 0 to 8.0×10^{-3} mg/mL (0–1.6 equiv.). The enhanced fluorescence of **7** was also visually observed on f-TLC plates when coupled with mycolactone and under a 365 nm UV lamp, as shown in Figure 12.

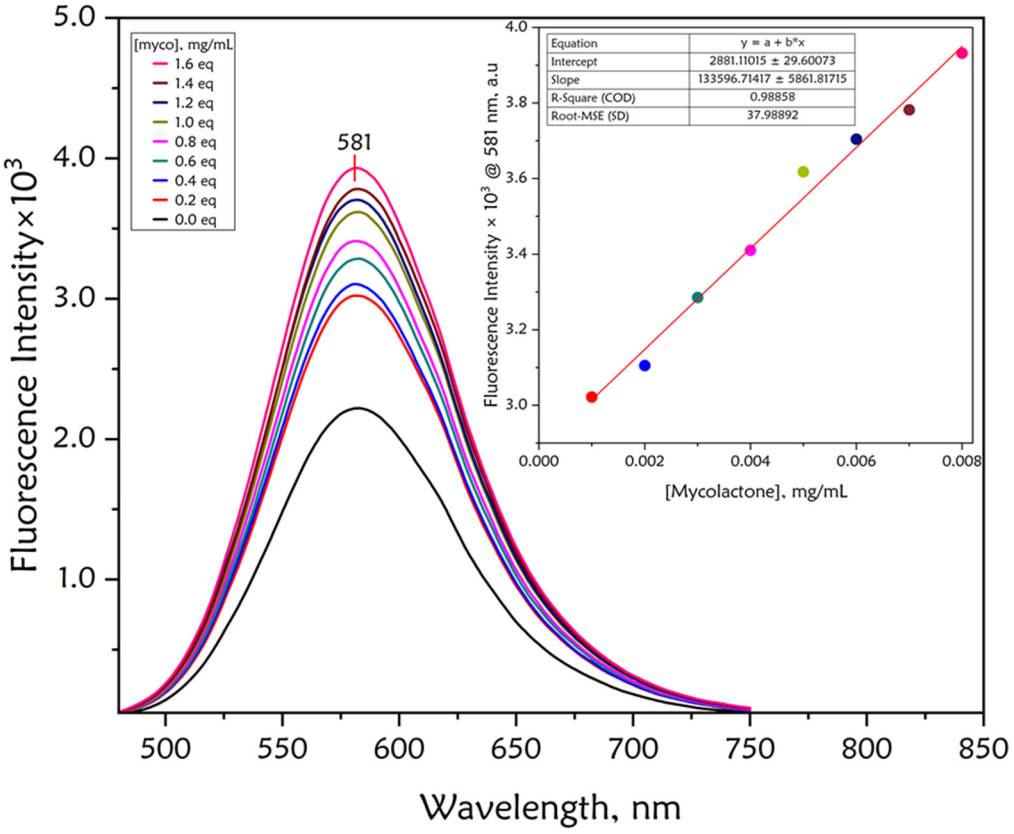

Figure 11. Fluorescence spectra of coumarin dye **7** (0.0025 mg/mL) upon gradual addition of serial concentrations of mycolactone (from bottom to top, 0–0.008 mg/mL) in ethanol. Inset: plot of the linear relationship between the fluorescence intensity and varying concentrations of mycolactone.

This can be explained by the coupling of the boronic acid moiety in the structure of **7** with the 1,3-diol moieties of mycolactone to form six-membered cyclic boronate esters, as has been established in the previous section on the proof-of-concept studies. The formation of the boronate coupled with the chromophore of the mycolactone resulted in the enhanced fluorescence. A calibration curve was obtained between the concentration of mycolactone and fluorescence intensity at 581 nm with good linearity (R^2 = 0.9886) (inset, Figure 11). The limit of detection (LOD) and limit of quantification (LOQ) were estimated to be 0.85 ng/µL (signal-to-noise ratio (S/N) × 3) and 2.84 ng/µL (signal-to-noise ratio (S/N) × 10), respectively; where *N* is the standard deviation (SD) of the peak area (n = 8), taken as a measure of the noise, and *B* is the slope of the corresponding calibration curve. This reveals that the **7** could detect a nanomolar-level concentration of mycolactone.

3.3. Detection of Mycolactone by the f-TLC Method Using the Synthesised Dyes

Boronic acids form reversible cyclic boronate complexes with 1,2- or 1,3-diols and this property. Neutral boronic acids are electrophilic because of the vacant *p*-orbital on the boron, and thus are highly reactive toward nucleophiles, such as diols [143]. The interaction between a boronic acid and a diol is one of the most powerful functional group interactions [144]. This unique property makes boronic acids useful selective and sensitive detection reagents for diols in TLC. For instance, boronic acids have been employed in the detection of mycolactone on thin-layer chromatography (TLC) [44,46]. Here, the synthesised aryl boronic acids coupled to mycolactone and the resulting fluorescent boronate complexes were visualised under a benchtop UV lamp (365 nm). The detection of mycolactone spots on TLC plates was optimised by using different concentrations of the synthesised boronic acids. Figure 12 shows the images of the fluorescence response of 5 µL/spot of

synthetic mycolactone after dipping in 0.1 mM and 0.01 mM acetone concentrations of various synthesised fluorescent aryl boronic acid chemosensors, together with the two boronic acids previously reported for use in the f-TLC method which were obtained commercially (BA and BA18) [44,45,48].

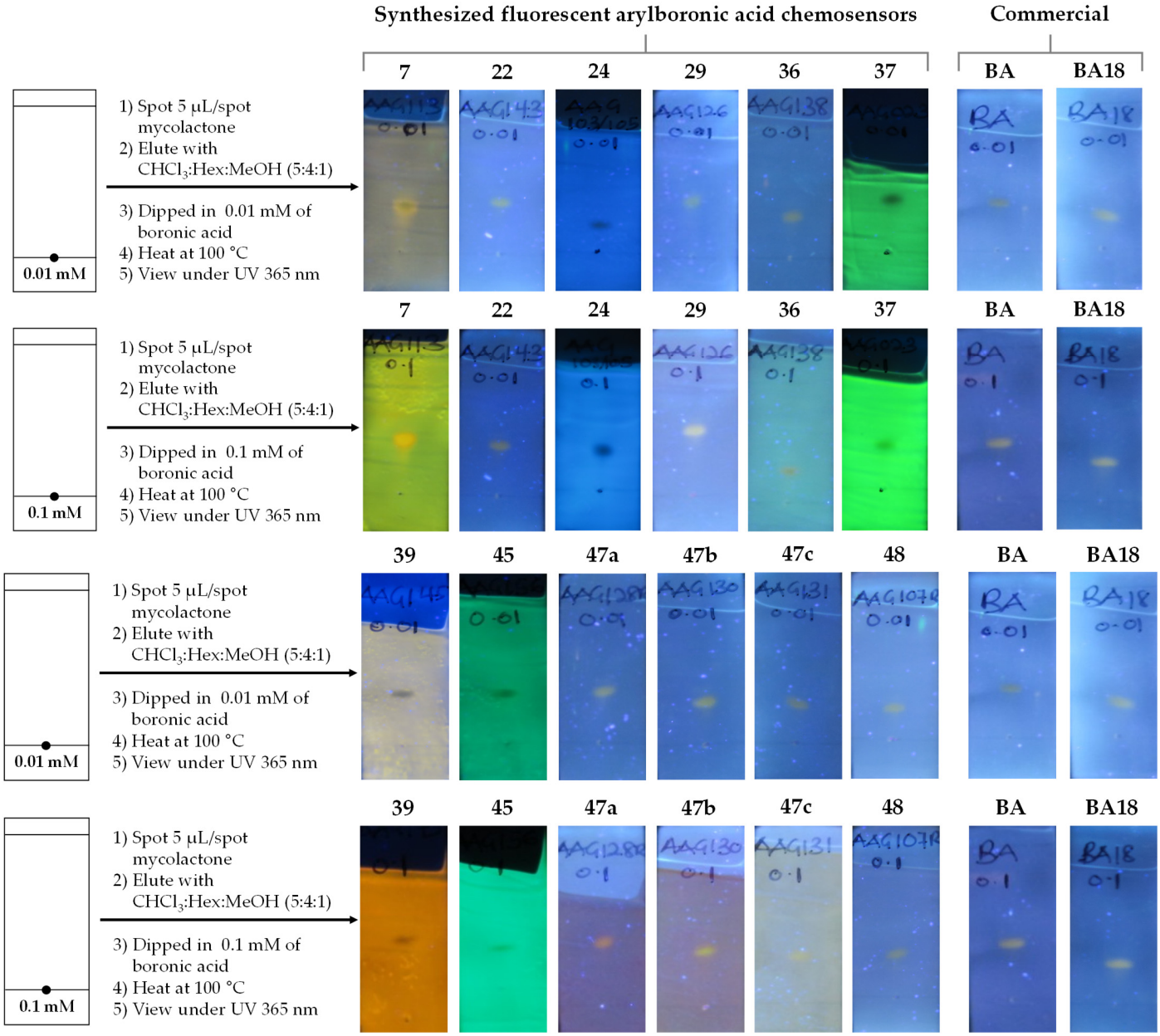

Figure 12. Images of the fluorescence response of 5 µL/spot of synthetic mycolactone after dipping in 0.1- and 0.01-mM acetone concentrations of various synthesised fluorescent aryl boronic acid chemosensors compared to two commercial boronic acids under 365 nm UV light.

First, a remarkable enhancement of fluorescence intensity of mycolactone was generally observed after dipping in either 0.01 mM or 0.1 mM solutions of the various boronic acids, particularly after heating. In this study, glass-backed TLC plates are used for the purpose of heating. Heating the plates to approximately 100 °C for just 60 s was sufficient to ensure the complete formation of the cyclic boronate esters of the various boronic acid sensors with the 1,3-diols motifs of the mycolactone. The boronic acid motif that is incorporated into various dyes has an empty sp^2 hybridised *p*-orbital on the boron centre with O−B−O bond angle of ~120°. It therefore readily binds covalently to 1,3-diols moieties

of mycolactone and adopts sp^3 hybridisation in the cyclic boronate ester product, with the boron adopting a tetrahedral configuration with O−B−O ~109.5°, like those in the literature [143]. This then triggers a change in the spectroscopic properties of the adduct because of significant perturbation of the π system. Secondly, the enhanced fluorescence after coupling was also attributed to the various signalling moieties—minoacridine, aminoquinoline, azo, BODIPY, coumarin, fluorescein, and rhodamine variants. They act as excellent fluorescent enhancers by stimulating the polarisation of the C–B bond due to extended π-conjugation systems. This induced the production of a rapid signal because of the highly polar C–B bond along with the corresponding boronate unit.

Generally, it was observed that the fluorescence band intensities of mycolactone adducts on TLC plates dipped in 0.1 mM acetone solutions of the synthesised chemosensors appeared more intense than those dipped in the same concentration of the commercially available BA and BA18 solutions, except for **37**, **48**, **47c**, **39**, and **45**. This observation was similar when 0.01 mM solutions of the boronic acids were used. Unlike other spots, it was observed that the mycolactone adduct spots appeared black on different backgrounds in solutions of **37**, **24, 39**, and **45**. Compound **37** produced the most intense black spot in the 0.01 mM solution while the **24** plate had the most intense black spot in the 0.1 mM solution.

Fluorescence is observable only if the absorbed energy is not fully dissipated during internal conversion. Typically, compounds that come into contact with the stationary phase lose some of their energy through transfer to the layer, which lowers the intensity of their fluorescence. When adsorbed onto silica gel, compounds that glow weakly in solution may either exhibit no fluorescence at all or fluorescence at wavelengths that are significantly longer than those observed in solution. An excited molecule in TLC quickly releases its vibrational energy as heat into the surrounding medium; in other words, the activated molecules transfer their excess photons to the TLC layer or to nearby molecules. Higher sample concentrations raise the likelihood of an excited and unexcited molecule colliding in a TLC layer [136]. Compounds **7**, **29**, **47a**, and **47b** had outstanding fluorescent bands on TLC, especially in 0.1 mM solutions. In the case of **37**, **47c**, **36**, **39**, and **45** the mycolactone adduct of TLC plates dipped in 0.1 mM solutions showed weak fluorescent band intensities in comparison to the band intensities of plates that were dipped in the 10-fold lower concentrations of the same boronic acids. This could partly be a result of fluorescence quenching leading to the reduced fluorescence bands on TLC [136]. Should this be the case, then, this concentration range might be unsuitable for evaluating these boronic acids because of the dramatic concentration quenching of fluorescence.

Compounds **36** and **37** are both fluorescein-based chemosensors. However, whereas **37** was fluorescent, **36** was weakly fluorescent. Generally, fluorescein dyes possess a unique spirolactam ring structure that exhibits a specific close-and-open feature with a 'turn-on' fluorescence response. However, when compound **36** was reacted with mycolactone, there was a fluorescence turn-on effect on TLC. This could be attributed the fact that the analyte, upon binding, was able induce the opening of the spirolactam ring which led to the enhancement in the fluorescence spot that was observed [145]. The fluorescence of compound **37** was strongly quenched when the adduct was formed on TLC in contrast to that of **36**. Unlike compound 36, the fluorescence of compound **37** adduct was significantly quenched on TLC. It is thought that a photoinduced electron-transfer mechanism causes compound **37** adduct fluorescence to be quenched. Compound **37** is a derivative of fluorescein isothiocyanate isomer I (FITC), and FITC fluorescence frequently exhibits self-quenching. Self-quenching usually happens at high concentrations due to increased energy transfer between interacting dye molecules as their concentration increases. Thus, it is possible that the high concentrations may be the cause of the quenching seen in **37** [146,147].

Compounds **7** and **22** both have a coumarin core; however, **7** was fluorescent, whereas 22 was non-fluorescent. In the design of compound **7,** the π-conjugation was extended at 3-position on the coumarin ring. The extended π-electron moiety leads to a red shift in the absorption and emission spectra. This means that the emitted light had a longer wavelength, and can also enhance fluorescence intensity [148]. Secondly, the enhanced fluorescence intensity observed in compound **7** could also be attributed to the presence of the electron-donating diethylamino moiety at the 7-position which influences the overall electronic structure of the molecule. This makes compound **7** a more efficient emitter of light, in which the emitted light had a longer wavelength [149]. On the other hand, compound **22** is a 7-hydroxycoumarin (unbelliferone) derivative and its fluorescence is entirely dependent on the excitation of the phenolic form only. Thus, it is non-fluorescent in its neutral form, but becomes strongly fluorescent as the phenolate anion in alkaline medium due to the blue emission of the phenolate anion [150]. Therefore, the non-fluorescence that was observed in **22** could possibly be explained by the derivation of the 7-hydroxy group to an ether linker to the methylphenylboronic acid recognition unit. In addition to the coumarin substitution, the fluorescence intensities in 7 and 22 could also be influenced by the solvent and solution pH [151,152]. The intensity of the fluorescence increases with increasing solution pH [152], and the absorbance of coumarin derivatives is red-shifted with increasing solvent polarity, while the emission of the coumarin moieties is broadened and shifted to higher wavelengths because of reinforced hydrogen bonding [148].

Solvent effect could also be attributed to the fluorescence intensity patterns that were observed in the aminoacridine adduct **24** and the 8-aminoquinoline adduct **29.** Hence, we observed that, whereas fluorescence enhancement was seen in the case of the adduct of compound **29**, that of **24** adduct was substantially quenched. As with the earlier sensors that contained the 8-aminoquinoline moiety, we proposed that the complexation between mycolactone and compounds **24** and **29** provided the "off-on" response via an internal charge transfer effect [153,154].

There was a turn-on effect in the fluorescence of the adducts of the azo derivatives **47a–c** and **48**. The boronic-acid-appended azo dyes are by themselves coloured in nature because of their unique chromophoric properties and can produce colour change in the presence of diols due to the enhancement of the Lewis acidity of boron upon binding. One possible explanation for the colorimetric turn-on response of these derivatives upon binding with mycolactone would be the combination of chromophoric characteristics and the Lewis acidity of boron in the complex. The azo chromophores have the capacity to transition into a donor-π-acceptor compound when Lewis bases such as the diols moiety on mycolactone coordinate at the Lewis acidic boron centre of the dyes, and this is accompanied by an increase in intramolecular charge-transfer interactions leading to the turn-on effect [155,156].

Under 365 nm UV irradiation, BODIPY compound **45** exhibited intense fluorescence and produced an intense bright green colour. However, the mycolactone adduct that was formed on TLC was effectively quenched. The significant quenching can be attributed to photoinduced electron transfer between mycolactone, lying in close proximity to boronic acid moiety of the BODIPY dye. In the case of compound **45** where the BODIPY is appended to boronic acid moiety as a recognition unit, boron assumes sp^2 hybridisation and hence is strongly fluorescent upon UV irradiation. However, the fluorescence is almost completely quenched in the adduct where boron, upon binding to the diol moieties of mycolactone, assumes sp^3-hybridised status [157–159]. Similarly, the rhodamine-based derivative **39,** which had a maximum absorption at 540 nm, was colourless in solution and turned pink when viewed with the naked eye. Under 365 light, it fluoresced orange at a maximum of 569 nm because of the spirolactam ring opening [99]. On TLC, however, quenching was

noted following the binding of the diol moieties of mycolactone to the boronic acid unit of compound **39.** This could be attributed to the inability of the complexation to facilitate the opening of the spirolactam unit of the rhodamine moiety of **39.** This shows that the energy transfer mechanism did not take place, resulting in the quenching of the fluorescence. Additionally, it is commonly known that other environmental factors including solvent polarity, viscosity, and temperature can impact the fluorescence properties of rhodamine dyes [160,161]. For instance, the rate of collisions increases with temperature, resulting in a greater amount of collisional quenching. The high temperature (~100 °C) used in the adduct formation of compound **39** could possibly promote the non-radiative process of its diethylamino groups and results in a condition that resembles a non-emissive TICT (twisted intramolecular charge transfer), resulting in the quenching in fluorescence intensity as was observed [162,163].

4. Conclusions

This paper has demonstrated synthetic approaches for the synthesis of a library of fluorescent arylboronic acid chemosensors by exploiting a range of dyes (fluorophores) of interest with beneficial photophysical characteristics. All the synthesised molecules have a boronic acid motif (recognition moiety) linked to a fluorescent dye which serves as a signalling moiety for possible complexation with the 1,3-diol moieties of mycolactone. All the synthesised dyes have been completely characterised using a set of complementary spectrometric and spectroscopic techniques such as NMR, LC-MS, FT-IR, and in some cases, X-ray crystallography. Following the successful characterisation of the synthesised dyes, their photophysical properties were determined. Likewise, their performance on TLC was also investigated in comparison to **BA** and **BA18**. The findings of the study indicated that the synthesised boronic acids were able to detect mycolactone both in solution and on TLC plates selectively and sensitively. Dye **7** had a better detection limit than **BA** and **BA18**. However, the diagnostic performance of the synthesised dye 7 is yet to be evaluated using real clinical samples of suspected BU cases. From the results, it can be concluded that all the synthesised arylboronic acids are selective for the detection of mycolactone and **7** gave the best outcomes in terms of fluorescence on TLC plates. It returned $\lambda_{abs}{}^{max}$ = 456 nm, $\lambda_{em}{}^{max}$ = 590 nm, $\Delta\lambda$ = 134 nm, ε = 52,816 $M^{-1}cm^{-1}$, Φ_F = 0.78, and brightness = 41,197 $M^{-1}cm^{-1}$.

Supplementary Materials: The following supporting information can be downloaded at: https://www.mdpi.com/article/10.3390/chemosensors13070244/s1, Figure S1–S87: 1H NMR, 13C NMR, 11B NMR, ESI-QTOF HRMS, and FTIR spectra of synthesized compounds; Figure S88: ORTEP representation of the molecular structure of BODIPY dye 45; Figure S89: Absorbance spectra of various dyes in different organic solvents; Figure S90: Fluorescence emission spectra of synthesized compounds; Table S1: Crystal data and refinement details for the X-ray structure determinations of **34** and **45**.

Author Contributions: Conceptualisation, G.A.A., B.M.P., T.D.C. and R.K.A.; methodology, G.A.A., B.M.P., T.D.C. and R.K.A.; validation, G.A.A., B.M.P., T.D.C., K.B.A. and R.K.A.; formal analysis, G.A.A., B.M.P. and R.K.A.; investigation, G.A.A., B.M.P., T.D.C. and R.K.A.; resources, B.M.P., K.B.A. and R.K.A.; data curation, G.A.A., B.M.P. and R.K.A.; writing—original draft preparation, G.A.A.; writing—review and editing, G.A.A., B.M.P., T.D.C. and R.K.A.; visualisation, G.A.A.; supervision, B.M.P., T.D.C. and R.K.A.; project administration, R.K.A. All authors have read and agreed to the published version of the manuscript.

Funding: This research was not funded by any organisation. Mass spectrometric and X-ray crystallography analysis was performed at the University of Sheffield.

Institutional Review Board Statement: Not applicable.

Informed Consent Statement: Not applicable.

Data Availability Statement: Data are contained within the article and supplementary materials.

Acknowledgments: The authors are grateful to the late Kishi Yoshito for generously donating synthetic mycolactone A/B through the World Health Organization for the study and to the Erasmus+ mobility grant between University of Ghana and University of Sheffield and Ghana National Petroleum Company (GNPC) for funding Gideon Atinga Akolgo's Doctoral research.

Conflicts of Interest: Author Kingsley Bampoe Asiedu was employed by the World Health Organization. The remaining authors declare that the research was conducted in the absence of any commercial or financial relationships that could be construed as a potential conflict of interest.

References

1. Whyte, G.F.; Vilar, R.; Woscholski, R. Molecular recognition with boronic acids—Applications in chemical biology. *J. Chem. Biol.* **2013**, *6*, 161–174. [CrossRef] [PubMed]
2. Czarnik, A.W. *Chemosensors of Ion and Molecule Recognition*; Springer Science & Business Media: Berlin, Germany, 2012; Volume 492.
3. Wu, J.-S.; Liu, W.-M.; Zhuang, X.-Q.; Wang, F.; Wang, P.-F.; Tao, S.-L.; Zhang, X.-H.; Wu, S.-K.; Lee, S.-T. Fluorescence Turn On of Coumarin Derivatives by Metal Cations: A New Signaling Mechanism Based on C=N Isomerization. *Org. Lett.* **2007**, *9*, 33–36. [CrossRef]
4. Valeur, B.; Berberan-Santos, M.N. *Molecular Fluorescence: Principles and Applications*; John Wiley & Sons: Hoboken, NJ, USA, 2012.
5. Tharmaraj, V.; Pitchumani, K. d-Glucose sensing by (E)-(4-((pyren-1-ylmethylene)amino)phenyl) boronic acid via a photoinduced electron transfer (PET) mechanism. *RSC Adv.* **2013**, *3*, 11566–11570. [CrossRef]
6. Curtius, H.; Kaiser, G.; Müller, E.; Bosbach, D. Radionuclide release from research reactor spent fuel. *J. Nucl. Mater.* **2011**, *416*, 211–215. [CrossRef]
7. Wu, X.; Chen, X.-X.; Jiang, Y.-B. Recent advances in boronic acid-based optical chemosensors. *Analyst* **2017**, *142*, 1403–1414. [CrossRef]
8. Hall, D.G. *Boronic Acids*; John Wiley & Sons: Hoboken, NJ, USA, 2011. [CrossRef]
9. Springsteen, G.; Wang, B. A detailed examination of boronic acid–diol complexation. *Tetrahedron* **2002**, *58*, 5291–5300. [CrossRef]
10. Springsteen, G.; Wang, B. Alizarin Red S. as a general optical reporter for studying the binding of boronic acids with carbohydrates. *Chem. Commun.* **2001**, *32*, 1608–1609. [CrossRef]
11. Lorand, J.P.; Edwards, J.O. Polyol complexes and structure of the benzeneboronate ion. *J. Org. Chem.* **1959**, *24*, 769–774. [CrossRef]
12. Yoon, J.; Czarnik, A.W. Fluorescent chemosensors of carbohydrates. A means of chemically communicating the binding of polyols in water based on chelation-enhanced quenching. *J. Am. Chem. Soc.* **1992**, *114*, 5874–5875. [CrossRef]
13. Guo, Z.; Shin, I.; Yoon, J. Recognition and sensing of various species using boronic acid derivatives. *Chem. Commun.* **2012**, *48*, 5956–5967. [CrossRef]
14. Lacina, K.; Skládal, P.; James, T.D. Boronic acids for sensing and other applications—a mini-review of papers published in 2013. *Chem. Cent. J.* **2014**, *8*, 60. [CrossRef] [PubMed]
15. Chaicham, A.; Sahasithiwat, S.; Tuntulani, T.; Tomapatanaget, B. Highly effective discrimination of catecholamine derivatives via FRET-on/off processes induced by the intermolecular assembly with two fluorescence sensors. *Chem. Commun.* **2013**, *49*, 9287–9289. [CrossRef]
16. Kaur, G.; Fang, H.; Gao, X.; Li, H.; Wang, B. Substituent effect on anthracene-based bisboronic acid glucose sensors. *Tetrahedron* **2006**, *62*, 2583–2589. [CrossRef]
17. Wu, W.; Mitra, N.; Yan, E.C.; Zhou, S. Multifunctional hybrid nanogel for integration of optical glucose sensing and self-regulated insulin release at physiological pH. *ACS Nano* **2010**, *4*, 4831–4839. [CrossRef]
18. Wu, W.; Zhou, T.; Berliner, A.; Banerjee, P.; Zhou, S. Glucose-Mediated Assembly of Phenylboronic Acid Modified CdTe/ZnTe/ZnS Quantum Dots for Intracellular Glucose Probing. *Angew. Chem. Int. Ed.* **2010**, *49*, 6554–6558. [CrossRef]
19. Huang, Y.-J.; Ouyang, W.-J.; Wu, X.; Li, Z.; Fossey, J.S.; James, T.D.; Jiang, Y.-B. Glucose sensing via aggregation and the use of "knock-out" binding to improve selectivity. *J. Am. Chem. Soc.* **2013**, *135*, 1700–1703. [CrossRef]
20. Zhai, W.; Male, L.; Fossey, J.S. Glucose selective bis-boronic acid click-fluor. *Chem. Commun.* **2017**, *53*, 2218–2221. [CrossRef] [PubMed]
21. Pohanka, M. Glycated Hemoglobin and Methods for Its Point of Care Testing. *Biosensors* **2021**, *11*, 70. [CrossRef]
22. Zhu, X.; Zhou, X.; Xing, D. Ultrasensitive and selective detection of mercury (II) in aqueous solution by polymerase assisted fluorescence amplification. *Biosens. Bioelectron.* **2011**, *26*, 2666–2669. [CrossRef]
23. Guan, R.; Chen, H.; Cao, F.; Cao, D.; Deng, Y. Two fluorescence turn-on chemosensors for cyanide anions based on pyridine cation and the boronic acid moiety. *Inorg. Chem. Commun.* **2013**, *38*, 112–114. [CrossRef]

24. Lee, S.A.; You, G.R.; Choi, Y.W.; Jo, H.Y.; Kim, A.R.; Noh, I.; Kim, S.-J.; Kim, Y.; Kim, C. A new multifunctional Schiff base as a fluorescence sensor for Al^{3+} and a colorimetric sensor for CN^{-} in aqueous media: An application to bioimaging. *Dalton Trans.* **2014**, *43*, 6650–6659. [CrossRef] [PubMed]
25. Pizer, R.; Tihal, C. Equilibria and reaction mechanism of the complexation of methylboronic acid with polyols. *Inorg. Chem.* **1992**, *31*, 3243–3247. [CrossRef]
26. Pizer, R.D.; Tihal, C.A. Mechanism of boron acid/polyol complex formation. comments on the trigonal/tetrahedral interconversion on boron. *Polyhedron* **1996**, *15*, 3411–3416. [CrossRef]
27. DeFrancesco, H.; Dudley, J.; Coca, A. Boron chemistry: An overview. In *Boron Reagents in Synthesis*; American Chemical Society: Washington, DC, USA, 2016; pp. 1–25.
28. Ooyama, Y.; Furue, K.; Uenaka, K.; Ohshita, J. Development of highly-sensitive fluorescence PET (photo-induced electron transfer) sensor for water: Anthracene–boronic acid ester. *RSC Adv.* **2014**, *4*, 25330–25333. [CrossRef]
29. Ooyama, Y.; Matsugasako, A.; Oka, K.; Nagano, T.; Sumomogi, M.; Komaguchi, K.; Imae, I.; Harima, Y. Fluorescence PET (photo-induced electron transfer) sensors for water based on anthracene–boronic acid ester. *Chem. Commun.* **2011**, *47*, 4448–4450. [CrossRef] [PubMed]
30. Chung, C.; Srikun, D.; Lim, C.S.; Chang, C.J.; Cho, B.R. A two-photon fluorescent probe for ratiometric imaging of hydrogen peroxide in live tissue. *Chem. Commun.* **2011**, *47*, 9618–9620. [CrossRef]
31. Nonaka, H.; An, Q.; Sugihara, F.; Doura, T.; Tsuchiya, A.; Yoshioka, Y.; Sando, S. Phenylboronic Acid-based 19F MRI Probe for the Detection and Imaging of Hydrogen Peroxide Utilizing Its Large Chemical-Shift Change. *Anal. Sci.* **2015**, *31*, 331–335. [CrossRef]
32. Fu, H.; Fang, H.; Sun, J.; Wang, H.; Liu, A.; Sun, J.; Wu, Z. Boronic acid-based enzyme inhibitors: A review of recent progress. *Curr. Med. Chem.* **2014**, *21*, 3271–3280. [CrossRef]
33. Cai, B.; Luo, Y.; Guo, Q.; Zhang, X.; Wu, Z. A glucose-sensitive block glycopolymer hydrogel based on dynamic boronic ester bonds for insulin delivery. *Carbohydr. Res.* **2017**, *445*, 32–39. [CrossRef]
34. Fang, H.; Kaur, G.; Wang, B. Progress in boronic acid-based fluorescent glucose sensors. *J. Fluoresc.* **2004**, *14*, 481–489. [CrossRef]
35. Chang, M.-H.; Chang, C.-N. Synthesis of three fluorescent boronic acid sensors for tumor marker Sialyl Lewis X in cancer diagnosis. *Tetrahedron Lett.* **2014**, *55*, 4437–4441. [CrossRef]
36. Chu, Y.; Wang, D.; Wang, K.; Liu, Z.L.; Weston, B.; Wang, B. Fluorescent conjugate of sLex-selective bisboronic acid for imaging application. *Bioorganic Med. Chem. Lett.* **2013**, *23*, 6307–6309. [CrossRef] [PubMed]
37. George, K.M.; Chatterjee, D.; Gunawardana, G.; Welty, D.; Hayman, J.; Lee, R.; Small, P.L. Mycolactone: A polyketide toxin from Mycobacterium ulcerans required for virulence. *Science* **1999**, *283*, 854–857. [CrossRef] [PubMed]
38. Demangel, C.; Stinear, T.P.; Cole, S.T. Buruli ulcer: Reductive evolution enhances pathogenicity of Mycobacterium ulcerans. *Nat. Rev. Microbiol.* **2009**, *7*, 50–60. [CrossRef]
39. George, K.M.; Pascopella, L.; Welty, D.M.; Small, P.L. A Mycobacterium ulcerans toxin, mycolactone, causes apoptosis in guinea pig ulcers and tissue culture cells. *Infect. Immun.* **2000**, *68*, 877–883. [CrossRef]
40. Scherr, N.; Gersbach, P.; Dangy, J.P.; Bomio, C.; Li, J.; Altmann, K.H.; Pluschke, G. Structure-activity relationship studies on the macrolide exotoxin mycolactone of Mycobacterium ulcerans. *PLoS Neglected Trop. Dis.* **2013**, *7*, e2143. [CrossRef]
41. Saint-Auret, S.; Chany, A.C.; Casarotto, V.; Tresse, C.; Parmentier, L.; Abdelkafi, H.; Blanchard, N. Total Syntheses of Mycolactone A/B and its Analogues for the Exploration of the Biology of Buruli Ulcer. *Chimia* **2017**, *71*, 836–840. [CrossRef] [PubMed]
42. Spangenberg, T.; Kishi, Y. Highly sensitive, operationally simple, cost/time effective detection of the mycolactones from the human pathogen Mycobacterium ulcerans. *Chem. Commun.* **2010**, *46*, 1410–1412. [CrossRef]
43. Hong, H.; Coutanceau, E.; Leclerc, M.; Caleechurn, L.; Leadlay, P.F.; Demangel, C. Mycolactone diffuses from Mycobacterium ulcerans–infected tissues and targets mononuclear cells in peripheral blood and lymphoid organs. *PLoS Neglected Trop. Dis.* **2008**, *2*, e325. [CrossRef]
44. Sarfo, F.S.; Phillips, R.O.; Rangers, B.; Mahrous, E.A.; Lee, R.E.; Tarelli, E.; Asiedu, K.B.; Small, P.L.; Wansbrough-Jones, M.H. Detection of Mycolactone A/B in Mycobacterium ulcerans-Infected Human Tissue. *PLoS Neglected Trop. Dis.* **2010**, *4*, e577. [CrossRef]
45. Akolgo, G.A.; Partridge, B.M.; Craggs, T.D.; Amewu, R.K. Alternative boronic acids in the detection of Mycolactone A/B using the thin layer chromatography (f-TLC) method for diagnosis of Buruli ulcer. *BMC Infect. Dis.* **2023**, *23*, 495. [CrossRef] [PubMed]
46. Kishi, Y. Chemistry of mycolactones, the causative toxins of Buruli ulcer. *Proc. Natl. Acad. Sci. USA* **2011**, *108*, 6703–6708. [CrossRef] [PubMed]
47. Converse, P.J.; Xing, Y.; Kim, K.H.; Tyagi, S.; Li, S.Y.; Almeida, D.V.; Nuermberger, E.L.; Grosset, J.H.; Kishi, Y. Accelerated detection of mycolactone production and response to antibiotic treatment in a mouse model of Mycobacterium ulcerans disease. *PLoS Neglected Trop. Dis.* **2014**, *8*, e2618. [CrossRef] [PubMed]
48. Amewu, R.K.; Akolgo, G.A.; Asare, M.E.; Abdulai, Z.; Ablordey, A.S.; Asiedu, K. Evaluation of the fluorescent-thin layer chromatography (f-TLC) for the diagnosis of Buruli ulcer disease in Ghana. *PLoS ONE* **2022**, *17*, e0270235. [CrossRef]

49. Wadagni, A.; Frimpong, M.; Phanzu, D.M. Simple, rapid Mycobacterium ulcerans disease diagnosis from clinical samples by fluorescence of mycolactone on thin layer chromatography. *PLoS Neglected Trop. Dis.* **2015**, *9*, e0004247. [CrossRef]
50. Yuan, L.; Lin, W.; Yang, Y.; Chen, H. A unique class of near-infrared functional fluorescent dyes with carboxylic-acid-modulated fluorescence ON/OFF switching: Rational design, synthesis, optical properties, theoretical calculations, and applications for fluorescence imaging in living animals. *J. Am. Chem. Soc.* **2012**, *134*, 1200–1211. [CrossRef]
51. Yang, X.-F.; Guo, X.-Q.; Zhao, Y.-B. Development of a novel rhodamine-type fluorescent probe to determine peroxynitrite. *Talanta* **2002**, *57*, 883–890. [CrossRef]
52. Lavis, L.D.; Raines, R.T. Bright building blocks for chemical biology. *ACS Chem. Biol.* **2014**, *9*, 855–866. [CrossRef] [PubMed]
53. Sheldrick, G.M. *Program for Empirical Absorption Correction of Area Detector Data. SADABS*; University of Göttingen: Göttingen, Germany, 1996.
54. Krause, L.; Herbst-Irmer, R.; Sheldrick, G.M.; Stalke, D. Comparison of silver and molybdenum microfocus X-ray sources for single-crystal structure determination. *J. Appl. Crystallogr.* **2015**, *48*, 3–10. [CrossRef]
55. Blessing, R.H. An empirical correction for absorption anisotropy. *Acta Crystallogr. Sect. A Found. Crystallogr.* **1995**, *51*, 33–38. [CrossRef]
56. Sheldrick, G. SHELXT—Integrated space-group and crystal-structure determination. *Acta Crystallogr. Sect. A* **2015**, *71*, 3–8. [CrossRef]
57. Sheldrick, G. Crystal structure refinement with SHELXL. *Acta Crystallogr. Sect. C* **2015**, *71*, 3–8. [CrossRef] [PubMed]
58. Dolomanov, O.; Bourhis, L.; Gildea, R.; Howard, J.; Puschmann, H. Johnkoivulaite, $Cs(Be_2B)Mg_2Si_6O_{18}$, A new mineral of the beryl group from the gem deposits of Mogok, Myanmar. *Am. Miner.* **2021**, *106*, 1844–1851. [CrossRef]
59. Ishiyama, T.; Murata, M.; Miyaura, N. Palladium(0)-Catalyzed Cross-Coupling Reaction of Alkoxydiboron with Haloarenes: A Direct Procedure for Arylboronic Esters. *J. Org. Chem.* **1995**, *60*, 7508–7510. [CrossRef]
60. Akgun, B. Boronic Esters as Bioorthogonal Probes in Site-Selective Labeling of Proteins. Ph.D. Thesis, University of Alberta, Edmonton, AB, Canada, 2018.
61. Ear, A.; Amand, S.; Blanchard, F.; Blond, A.; Dubost, L.; Buisson, D.; Nay, B. Direct biosynthetic cyclization of a distorted paracyclophane highlighted by double isotopic labelling of l-tyrosine. *Org. Biomol. Chem.* **2015**, *13*, 3662–3666. [CrossRef]
62. Promchat, A.; Wongravee, K.; Sukwattanasinitt, M.; Praneenararat, T. Rapid Discovery and Structure-Property Relationships of Metal-Ion Fluorescent Sensors via Macroarray Synthesis. *Sci. Rep.* **2019**, *9*, 10390. [CrossRef]
63. Lawson-Wood, K.; Upstone, S.; Evans, K. Determination of Relative Fluorescence Quantum Yields using the FL6500 Fluorescence Spectrometer. *Fluoresc. Spectrosc* **2018**, *4*, 1–5.
64. Würth, C.; Grabolle, M.; Pauli, J.; Spieles, M.; Resch-Genger, U. Relative and absolute determination of fluorescence quantum yields of transparent samples. *Nat. Protoc.* **2013**, *8*, 1535–1550. [CrossRef]
65. Brouwer, A.M. Standards for photoluminescence quantum yield measurements in solution (IUPAC Technical Report). *Pure Appl. Chem.* **2011**, *83*, 2213–2228. [CrossRef]
66. Velapoldi, R.A.; Mielenz, K. *A Fluorescence Standard Reference Material, Quinine Sulfate Dihydrate*; US Department of Commerce: Washington, DC, USA; National Bureau of Standards: Gaithersburg, MD, USA, 1980.
67. Herráez, J.V.; Belda, R. Refractive Indices, Densities and Excess Molar Volumes of Monoalcohols + Water. *J. Solut. Chem.* **2006**, *35*, 1315–1328. [CrossRef]
68. Ishiyama, T.; Itoh, Y.; Kitano, T.; Miyaura, N. Synthesis of arylboronates via the palladium (0)-catalyzed cross-coupling reaction of tetra (alkoxo) diborons with aryl triflates. *Tetrahedron Lett.* **1997**, *38*, 3447–3450. [CrossRef]
69. Ishiyama, T.; Ishida, K.; Miyaura, N. Synthesis of pinacol arylboronates via cross-coupling reaction of bis (pinacolato) diboron with chloroarenes catalyzed by palladium (0)–tricyclohexylphosphine complexes. *Tetrahedron* **2001**, *57*, 9813–9816. [CrossRef]
70. Wu, C.; Wang, J.; Shen, J.; Bi, C.; Zhou, H. Coumarin-based Hg^{2+} fluorescent probe: Synthesis and turn-on fluorescence detection in neat aqueous solution. *Sens. Actuators B Chem.* **2017**, *243*, 678–683. [CrossRef]
71. Pang, B.-J.; Li, Q.; Li, C.-R.; Yang, Z.-Y. A highly selective and sensitive coumarin derived fluorescent probe for detecting Hg^{2+} in 100% aqueous solutions. *J. Lumin.* **2019**, *205*, 446–450. [CrossRef]
72. Ma, S.; Wang, K.-N.; Xing, M.; Feng, F.; Pan, Q.; Cao, D. A coumarin-boronic ester derivative as fluorescent chemosensor for detecting H2O2 in living cells. *Inorg. Chem. Commun.* **2021**, *124*, 108414. [CrossRef]
73. Lin, C.; Zhang, M.; Yan, X.; Zhang, R.; He, X.; Yuan, Y. A Coumarin-boronic Based Fluorescent "ON-OFF" Probe for Hg^{2+} in Aqueous Solution. *Z. Anorg. Und Allg. Chem.* **2020**, *646*, 1892–1899. [CrossRef]
74. Li, Q.; Hu, Y.; Hou, H.-N.; Yang, W.-N.; Hu, S.-L. A new coumarin-carbonothioate-based turn-on fluorescent chemodosimeter for selective detection of Hg^{2+}. *Inorganica Chim. Acta* **2018**, *471*, 705–708. [CrossRef]
75. Abdallah, M.; Hijazi, A.; Graff, B.; Fouassier, J.-P.; Rodeghiero, G.; Gualandi, A.; Dumur, F.; Cozzi, P.G.; Lalevée, J. Coumarin derivatives as versatile photoinitiators for 3D printing, polymerization in water and photocomposite synthesis. *Polym. Chem.* **2019**, *10*, 872–884. [CrossRef]

76. Wang, Y.; Li, Y.; Yu, T.; Su, W.; Ma, H.; Zhao, Y.; Li, X.; Zhang, H. Functionalized coumarin derivatives containing aromatic-imidazole unit as organic luminescent materials. *Dye. Pigment.* **2020**, *173*, 107958. [CrossRef]
77. Klinck, R.; Stothers, J. Nuclear Magnetic Resonance Studies: Part I. The Chemical Shift of the Formyl Proton in Aromatic Aldehydes. *Can. J. Chem.* **1962**, *40*, 1071–1081. [CrossRef]
78. Bai, H.; Sun, Q.; Tian, H.; Qian, J.; Zhang, L.; Zhang, W. A Long-Wavelength Fluorescent Probe for Saccharides Based on Boronic-Acid Receptor. *Chin. J. Chem.* **2013**, *31*, 1095–1101. [CrossRef]
79. Akgun, B.; Hall, D.G. Fast and Tight Boronate Formation for Click Bioorthogonal Conjugation. *Angew. Chem.* **2016**, *128*, 3977–3981. [CrossRef]
80. Moriya, T. Excited-state reactions of coumarins. VII. The solvent-dependent fluorescence of 7-hydroxycoumarins. *Bull. Chem. Soc. Jpn.* **1988**, *61*, 1873–1886. [CrossRef]
81. Aaron, J.-J.; Buna, M.; Parkanyi, C.; Antonious, M.S.; Tine, A.; Cisse, L. Quantitative treatment of the effect of solvent on the electronic absorption and fluorescence spectra of substituted coumarins: Evaluation of the first excited singlet-state dipole moments. *J. Fluoresc.* **1995**, *5*, 337–347. [CrossRef]
82. Palanisamy, S.; Wu, P.-Y.; Wu, S.-C.; Chen, Y.-J.; Tzou, S.-C.; Wang, C.-H.; Chen, C.-Y.; Wang, Y.-M. In vitro and in vivo imaging of peroxynitrite by a ratiometric boronate-based fluorescent probe. *Biosens. Bioelectron.* **2017**, *91*, 849–856. [CrossRef] [PubMed]
83. Wang, C.; Wang, P.; Liu, X.; Fu, J.; Xue, K.; Xu, K. Novel enantioselective fluorescent sensors for tartrate anion based on acridinezswsxa. *Luminescence* **2017**, *32*, 1313–1318. [CrossRef]
84. Dai, Y.; Xu, K.; Li, Q.; Wang, C.; Liu, X.; Wang, P. Acridine-based complex as amino acid anion fluorescent sensor in aqueous solution. *Spectrochim. Acta Part A Mol. Biomol. Spectrosc.* **2016**, *157*, 1–5. [CrossRef] [PubMed]
85. Wang, C.; Fu, J.; Yao, K.; Xue, K.; Xu, K.; Pang, X. Acridine-based fluorescence chemosensors for selective sensing of Fe^{3+} and Ni^{2+} ions. *Spectrochim. Acta Part A Mol. Biomol. Spectrosc.* **2018**, *199*, 403–411. [CrossRef]
86. Turan-Zitouni, G.; Kaplancikli, Z.; Uçucu, Ü.; Özdemir, A.; Chevallet, P.; Tunali, Y. Synthesis of some 2-[(benzazole-2-yl) thio]-diphenylmethylacetamide derivatives and their antimicrobial activity. *Phosphorus Sulfur Silicon* **2004**, *179*, 2183–2188. [CrossRef]
87. Kaplancikli, Z.A.; Turan-Zitouni, G.; Revial, G.; Guven, K. Synthesis and study of antibacterial and antifungal activities of novel 2-[[(benzoxazole/benzimidazole-2-yl) sulfanyl] acetylamino] thiazoles. *Arch. Pharmacal Res.* **2004**, *27*, 1081–1085. [CrossRef]
88. Demir Özkay, Ü.; Özkay, Y.; Can, Ö.D. Synthesis and analgesic effects of 2-(2-carboxyphenylsulfanyl)-N-(4-substitutedphenyl) acetamide derivatives. *Med. Chem. Res.* **2011**, *20*, 152–157. [CrossRef]
89. Olszewska, A.; Pohl, R.; Brázdová, M.; Fojta, M.; Hocek, M. Chloroacetamide-Linked Nucleotides and DNA for Cross-Linking with Peptides and Proteins. *Bioconjugate Chem.* **2016**, *27*, 2089–2094. [CrossRef] [PubMed]
90. Czaplinska, B.; Spaczynska, E.; Musiol, R. Quinoline fluorescent probes for zinc–from diagnostic to therapeutic molecules in treating neurodegenerative diseases. *Med. Chem.* **2018**, *14*, 19–33. [CrossRef]
91. Sousa, K.A.P.; Lima, F.M.R.; Monteiro, T.O.; Silva, S.M.; Goulart, M.O.F.; Damos, F.S.; Luz, R.d.C.S. Amperometric Photosensor Based on Acridine Orange/TiO_2 for Chlorogenic Acid Determination in Food Samples. *Food Anal. Methods* **2018**, *11*, 2731–2741. [CrossRef]
92. López-Soria, J.M.; Pérez, S.J.; Hernández, J.N.; Ramírez, M.A.; Martín, V.S.; Padrón, J.I. A practical, catalytic and selective deprotection of a Boc group in N,N′-diprotected amines using iron(iii)-catalysis. *RSC Adv.* **2015**, *5*, 6647–6651. [CrossRef]
93. Han, G.; Tamaki, M.; Hruby, V. Fast, efficient and selective deprotection of the tert-butoxycarbonyl (Boc) group using HCL/dioxane (4 M). *J. Pept. Res. Off. J. Am. Pept. Soc.* **2001**, *58*, 338–341. [CrossRef] [PubMed]
94. Abdel-Magid, A.F.; Carson, K.G.; Harris, B.D.; Maryanoff, C.A.; Shah, R.D. Reductive amination of aldehydes and ketones with sodium triacetoxyborohydride. studies on direct and indirect reductive amination procedures1. *J. Org. Chem.* **1996**, *61*, 3849–3862. [CrossRef]
95. Rahman, A.F.M.M.; Park, S.-E.; Kadi, A.A.; Kwon, Y. Fluorescein Hydrazones as Novel Nonintercalative Topoisomerase Catalytic Inhibitors with Low DNA Toxicity. *J. Med. Chem.* **2014**, *57*, 9139–9151. [CrossRef]
96. Kaschula, C.H.; Hunter, R. Synthesis and structure–activity relations in allylsulfide and isothiocyanate compounds from garlic and broccoli against in vitro cancer cell growth. *Stud. Nat. Prod. Chem.* **2016**, *50*, 1–43.
97. Podhradský, D.; Drobnica, Ľ.; Kristian, P. Reactions of cysteine, its derivatives, glutathione, coenzyme A, and dihydrolipoic acid with isothiocyanates. *Experientia* **1979**, *35*, 154–155. [CrossRef]
98. Beija, M.; Afonso, C.A.; Martinho, J.M. Synthesis and applications of Rhodamine derivatives as fluorescent probes. *Chem. Soc. Rev.* **2009**, *38*, 2410–2433. [CrossRef] [PubMed]
99. Kim, H.N.; Lee, M.H.; Kim, H.J.; Kim, J.S.; Yoon, J. A new trend in rhodamine-based chemosensors: Application of spirolactam ring-opening to sensing ions. *Chem. Soc. Rev.* **2008**, *37*, 1465–1472. [CrossRef] [PubMed]
100. Wu, D.; Huang, W.; Duan, C.; Lin, Z.; Meng, Q. Highly sensitive fluorescent probe for selective detection of Hg^{2+} in DMF aqueous media. *Inorg. Chem.* **2007**, *46*, 1538–1540. [CrossRef] [PubMed]

101. Yang, Y.-K.; Yook, K.-J.; Tae, J. A Rhodamine-Based Fluorescent and Colorimetric Chemodosimeter for the Rapid Detection of Hg2+ Ions in Aqueous Media. *J. Am. Chem. Soc.* **2005**, *127*, 16760–16761. [CrossRef]
102. Kim, S.K.; Swamy, K.; Chung, S.-Y.; Kim, H.N.; Kim, M.J.; Jeong, Y.; Yoon, J. New fluorescent and colorimetric chemosensors based on the rhodamine and boronic acid groups for the detection of Hg^{2+}. *Tetrahedron Lett.* **2010**, *51*, 3286–3289. [CrossRef]
103. Xiang, Y.; Tong, A.; Jin, P.; Ju, Y. New Fluorescent Rhodamine Hydrazone Chemosensor for Cu(II) with High Selectivity and Sensitivity. *Org. Lett.* **2006**, *8*, 2863–2866. [CrossRef]
104. Mao, J.; Wang, L.; Dou, W.; Tang, X.; Yan, Y.; Liu, W. Tuning the selectivity of two chemosensors to Fe (III) and Cr (III). *Org. Lett.* **2007**, *9*, 4567–4570. [CrossRef]
105. Bossi, M.; Belov, V.; Polyakova, S.; Hell, S.W. Reversible red fluorescent molecular switches. *Angew. Chem. Int. Ed.* **2006**, *45*, 7462–7465. [CrossRef]
106. Treibs, A.; Kreuzer, F.H. Difluorboryl-komplexe von di-und tripyrrylmethenen. *Justus Liebigs Ann. Chem.* **1968**, *718*, 208–223. [CrossRef]
107. Ojida, A.; Sakamoto, T.; Inoue, M.-A.; Fujishima, S.-H.; Lippens, G.; Hamachi, I. Fluorescent BODIPY-based Zn (II) complex as a molecular probe for selective detection of neurofibrillary tangles in the brains of Alzheimer's disease patients. *J. Am. Chem. Soc.* **2009**, *131*, 6543–6548. [CrossRef]
108. Smith, N.W.; Alonso, A.; Brown, C.M.; Dzyuba, S.V. Triazole-containing BODIPY dyes as novel fluorescent probes for soluble oligomers of amyloid Aβ1–42 peptide. *Biochem. Biophys. Res. Commun.* **2010**, *391*, 1455–1458. [CrossRef]
109. Beatty, K.E.; Szychowski, J.; Fisk, J.D.; Tirrell, D.A. A BODIPY-cyclooctyne for protein imaging in live cells. *ChemBioChem* **2011**, *12*, 2137–2139. [CrossRef] [PubMed]
110. Lin, H.-Y.; Huang, W.-C.; Chen, Y.-C.; Chou, H.-H.; Hsu, C.-Y.; Lin, J.T.; Lin, H.-W. BODIPY dyes with β-conjugation and their applications for high-efficiency inverted small molecule solar cells. *Chem. Commun.* **2012**, *48*, 8913–8915. [CrossRef] [PubMed]
111. Altan Bozdemir, O.; Erbas-Cakmak, S.; Ekiz, O.O.; Dana, A.; Akkaya, E.U. Towards unimolecular luminescent solar concentrators: BODIPY-based dendritic energy-transfer cascade with panchromatic absorption and monochromatized emission. *Angew. Chem.* **2011**, *123*, 11099–11104. [CrossRef]
112. Rousseau, T.; Cravino, A.; Ripaud, E.; Leriche, P.; Rihn, S.; De Nicola, A.; Ziessel, R.; Roncali, J. A tailored hybrid BODIPY–oligothiophene donor for molecular bulk heterojunction solar cells with improved performances. *Chem. Commun.* **2010**, *46*, 5082–5084. [CrossRef]
113. Karolin, J.; Johansson, L.B.-A.; Strandberg, L.; Ny, T. Fluorescence and absorption spectroscopic properties of dipyrrometheneboron difluoride (BODIPY) derivatives in liquids, lipid membranes, and proteins. *J. Am. Chem. Soc.* **1994**, *116*, 7801–7806. [CrossRef]
114. Kollmannsberger, M.; Gareis, T.; Heinl, S.; Daub, J.; Breu, J. Electrogenerated Chemiluminescence and Proton-Dependent Switching of Fluorescence: Functionalized Difluoroboradiaza-s-indacenes. *Angew. Chem. Int. Ed. Engl.* **1997**, *36*, 1333–1335. [CrossRef]
115. Loudet, A.; Burgess, K. BODIPY dyes and their derivatives: Syntheses and spectroscopic properties. *Chem. Rev.* **2007**, *107*, 4891–4932. [CrossRef]
116. Ulrich, G.; Ziessel, R.; Harriman, A. The chemistry of fluorescent bodipy dyes: Versatility unsurpassed. *Angew. Chem. Int. Ed.* **2008**, *47*, 1184–1201. [CrossRef]
117. Boens, N.; Leen, V.; Dehaen, W. Fluorescent indicators based on BODIPY. *Chem. Soc. Rev.* **2012**, *41*, 1130–1172. [CrossRef]
118. Biagiotti, G.; Purić, E.; Urbančič, I.; Krišelj, A.; Weiss, M.; Mravljak, J.; Gellini, C.; Lay, L.; Chiodo, F.; Anderluh, M. Combining cross-coupling reaction and Knoevenagel condensation in the synthesis of glyco-BODIPY probes for DC-SIGN super-resolution bioimaging. *Bioorganic Chem.* **2021**, *109*, 104730. [CrossRef] [PubMed]
119. Mahato, P.; Saha, S.; Das, P.; Agarwalla, H.; Das, A. An overview of the recent developments on Hg^{2+} recognition. *RSC Adv.* **2014**, *4*, 36140–36174. [CrossRef]
120. Bartelmess, J.; De Luca, E.; Signorelli, A.; Baldrighi, M.; Becce, M.; Brescia, R.; Nardone, V.; Parisini, E.; Echegoyen, L.; Pompa, P.P. Boron dipyrromethene (BODIPY) functionalized carbon nano-onions for high resolution cellular imaging. *Nanoscale* **2014**, *6*, 13761–13769. [CrossRef]
121. Brückner, C.; Karunaratne, V.; Rettig, S.J.; Dolphin, D. Synthesis of meso-phenyl-4, 6-dipyrrins, preparation of their Cu (II), Ni (II), and Zn (II) chelates, and structural characterization of bis [meso-phenyl-4, 6-dipyrrinato] Ni (II). *Can. J. Chem.* **1996**, *74*, 2182–2193. [CrossRef]
122. Shah, M.; Thangaraj, K.; Soong, M.L.; Wolford, L.T.; Boyer, J.H.; Politzer, I.R.; Pavlopoulos, T.G. Pyrromethene–BF2 complexes as laser dyes: 1. *Heteroat. Chem.* **1990**, *1*, 389–399. [CrossRef]
123. Jameson, L.P.; Dzyuba, S.V. Expeditious, mechanochemical synthesis of BODIPY dyes. *Beilstein J. Org. Chem.* **2013**, *9*, 786–790. [CrossRef]
124. Snyder, H.; Weaver, C. The preparation of some azo boronic acids. *J. Am. Chem. Soc.* **1948**, *70*, 232–234. [CrossRef]
125. Smoum, R.; Srebnik, M. Boronated saccharides: Potential applications. *Stud. Inorg. Chem.* **2005**, *22*, 391.

126. Egawa, Y.; Miki, R.; Seki, T. Colorimetric sugar sensing using boronic acid-substituted azobenzenes. *Materials* **2014**, *7*, 1201–1220. [CrossRef]
127. Hansen, J.S.; Christensen, J.B.; Petersen, J.F.; Hoeg-Jensen, T.; Norrild, J.C. Arylboronic acids: A diabetic eye on glucose sensing. *Sens. Actuators B Chem.* **2012**, *161*, 45–79. [CrossRef]
128. DiCesare, N.; Lakowicz, J.R. Spectral Properties of Fluorophores Combining the Boronic Acid Group with Electron Donor or Withdrawing Groups. Implication in the Development of Fluorescence Probes for Saccharides. *J. Phys. Chem. A* **2001**, *105*, 6834–6840. [CrossRef] [PubMed]
129. Beda, N.; Nedospasov, A. A spectrophotometric assay for nitrate in an excess of nitrite. *Nitric Oxide* **2005**, *13*, 93–97. [CrossRef]
130. Sinan, R.; Al-Uzri, W.A. Spectrophotometric Method for Determination of Sulfamethoxazole in Pharmaceutical Preparations by Diazotization-Coupling Reaction. *Al-Nahrain J. Sci.* **2011**, *14*, 9–16. [CrossRef]
131. Gordon, P.F.; Gregory, P. *Organic Chemistry in Colour*; Springer Science & Business Media: Berlin, Germany, 2012.
132. Dhami, S.; de Mello, A.; Rumbles, G.; Bishop, S.; Phillips, D.; Beeby, A. Phthalocyanine fluorescence at high concentration: Dimers or reabsorption effect? *Photochem. Photobiol.* **1995**, *61*, 341–346. [CrossRef]
133. Resch-Genger, U.; Grabolle, M.; Cavaliere-Jaricot, S.; Nitschke, R.; Nann, T. Quantum dots versus organic dyes as fluorescent labels. *Nat. Methods* **2008**, *5*, 763–775. [CrossRef]
134. Cavazos-Elizondo, D.; Aguirre-Soto, A. Photophysical Properties of Fluorescent Labels: A Meta-Analysis to Guide Probe Selection Amidst Challenges with Available Data. *Anal. Sens.* **2022**, *2*, e202200004.
135. Lakowicz, J.R. *Principles of Fluorescence Spectroscopy*; Springer: Berlin/Heidelberg, Germany, 2006.
136. Spangenberg, B.; Poole, C.F.; Weins, C. *Quantitative Thin-Layer Chromatography: A Practical Survey*; Springer Science & Business Media: Berlin, Germany, 2011.
137. Giacomazzo, G.E.; Palladino, P.; Gellini, C.; Salerno, G.; Baldoneschi, V.; Feis, A.; Scarano, S.; Minunni, M.; Richichi, B. A straightforward synthesis of phenyl boronic acid (PBA) containing BODIPY dyes: New functional and modular fluorescent tools for the tethering of the glycan domain of antibodies. *RSC Adv.* **2019**, *9*, 30773–30777. [CrossRef] [PubMed]
138. Isak, S.J.; Eyring, E.M.; Spikes, J.D.; Meekins, P.A. Direct blue dye solutions: Photo properties. *J. Photochem. Photobiol. A Chem.* **2000**, *134*, 77–85. [CrossRef]
139. Dinçalp, H.; Toker, F.; Durucasu, İ.; Avcıbaşı, N.; Icli, S. New thiophene-based azo ligands containing azo methine group in the main chain for the determination of copper(II) ions. *Dye. Pigment.* **2007**, *75*, 11–24. [CrossRef]
140. Joshi, H.; Kamounah, F.S.; Gooijer, C.; van der Zwan, G.; Antonov, L. Excited state intramolecular proton transfer in some tautomeric azo dyes and schiff bases containing an intramolecular hydrogen bond. *J. Photochem. Photobiol. A Chem.* **2002**, *152*, 183–191. [CrossRef]
141. Rahal, M.; Mokbel, H.; Graff, B.; Toufaily, J.; Hamieh, T.; Dumur, F.; Lalevée, J. Mono vs. difunctional coumarin as photoinitiators in photocomposite synthesis and 3D printing. *Catalysts* **2020**, *10*, 1202. [CrossRef]
142. Rahal, M.; Graff, B.; Toufaily, J.; Hamieh, T.; Noirbent, G.; Gigmes, D.; Dumur, F.; Lalevée, J. 3-Carboxylic Acid and Formyl-Derived Coumarins as Photoinitiators in Photo-Oxidation or Photo-Reduction Processes for Photopolymerization upon Visible Light: Photocomposite Synthesis and 3D Printing Applications. *Molecules* **2021**, *26*, 1753. [CrossRef] [PubMed]
143. Marco-Dufort, B.; Iten, R.; Tibbitt, M.W. Linking molecular behavior to macroscopic properties in ideal dynamic covalent networks. *J. Am. Chem. Soc.* **2020**, *142*, 15371–15385. [CrossRef]
144. Yan, J.; Fang, H.; Wang, B. Boronolectins and fluorescent boronolectins: An examination of the detailed chemistry issues important for the design. *Med. Res. Rev.* **2005**, *25*, 490–520. [CrossRef] [PubMed]
145. Aruna; Verma, V.P.; Singh, A.P.; Shrivastava, R. Recent advancement in development of fluorescein based molecular probes for analytes sensing. *J. Mol. Struct.* **2024**, *1295*, 136549. [CrossRef]
146. Lakowicz, J.R.; Malicka, J.; D'Auria, S.; Gryczynski, I. Release of the self-quenching of fluorescence near silver metallic surfaces. *Anal. Biochem.* **2003**, *320*, 13–20. [CrossRef]
147. Imhof, A.; Megens, M.; Engelberts, J.J.; de Lang, D.T.N.; Sprik, R.; Vos, W.L. Spectroscopy of Fluorescein (FITC) Dyed Colloidal Silica Spheres. *J. Phys. Chem. B* **1999**, *103*, 1408–1415. [CrossRef]
148. Cazin, I.; Rossegger, E.; de la Guedes Cruz, G.; Griesser, T.; Schlögl, S. Recent Advances in Functional Polymers Containing Coumarin Chromophores. *Polymers* **2021**, *13*, 56. [CrossRef]
149. Al-Kindy, S.M.Z.; Al-Sharji, N.; Al-Harasi, A.F.; Suliman, F.O.; Al-Lawati, H.J.; Schulman, S. Synthesis and spectroscopic study of 2,7-diethylamino-2-oxo-2H-chromen-3-yl benzothiazole-6-sulfonyl chlorides and its derivatives. *Arab. J. Chem.* **2017**, *10*, S114–S120. [CrossRef]
150. Christopoulos, T.K.; Diamandis, E.P. 14—Fluorescence Immunoassays. In *Immunoassay*; Diamandis, E.P., Christopoulos, T.K., Eds.; Academic Press: San Diego, CA, USA, 1996; pp. 309–335.
151. Jones, G.; Jackson, W.R.; Choi, C.Y.; Bergmark, W.R. Solvent effects on emission yield and lifetime for coumarin laser dyes. Requirements for a rotatory decay mechanism. *J. Phys. Chem.* **1985**, *89*, 294–300. [CrossRef]

152. Hoshiyama, M.; Kubo, K.; Igarashi, T.; Sakurai, T. Complexation and proton dissociation behavior of 7-hydroxy-4-methylcoumarin and related compounds in the presence of β-cyclodextrin. *J. Photochem. Photobiol. A Chem.* **2001**, *138*, 227–233. [CrossRef]
153. Ma, Y.; Chen, H.; Wang, F.; Kambam, S.; Wang, Y.; Mao, C.; Chen, X. A highly sensitive and selective ratiometric fluorescent sensor for Zn^{2+} ion based on ICT and FRET. *Dye. Pigment.* **2014**, *102*, 301–307. [CrossRef]
154. Du, J.; Fan, J.; Peng, X.; Li, H.; Sun, S. The quinoline derivative of ratiometric and sensitive fluorescent zinc probe based on deprotonation. *Sens. Actuators B Chem.* **2010**, *144*, 337–341. [CrossRef]
155. Ward, C.J.; Patel, P.; James, T.D. Boronic acid appended azo dyes–colour sensors for saccharides. *J. Chem. Soc. Perkin Trans. 1* **2002**, *4*, 462–470. [CrossRef]
156. Oehlke, A.; Auer, A.A.; Schreiter, K.; Friebe, N.; Spange, S. Highly Lewis Acidic Arylboronate Esters Capable of Colorimetric Turn-On Response. *Chem. A Eur. J.* **2015**, *21*, 17890–17896. [CrossRef]
157. Hansen, J.S.; Petersen, J.F.; Hoeg-Jensen, T.; Christensen, J.B. Buffer and sugar concentration dependent fluorescence response of a BODIPY-based aryl monoboronic acid sensor. *Tetrahedron Lett.* **2012**, *53*, 5852–5855. [CrossRef]
158. Corminboeuf, C.; Prlj, A.; Fabrizio, A. Rationalizing Fluorescence Quenching in meso-BODIPY Dyes. *Phys. Chem. Chem. Phys.* **2016**, *18*, 32668–32672. [CrossRef]
159. Prlj, A.; Vannay, L.; Corminboeuf, C. Fluorescence Quenching in BODIPY Dyes: The Role of Intramolecular Interactions and Charge Transfer. *Helv. Chim. Acta* **2017**, *100*, e1700093. [CrossRef]
160. Snare, M.; Treloar, F.; Ghiggino, K.; Thistlethwaite, P. The photophysics of rhodamine B. *J. Photochem.* **1982**, *18*, 335–346. [CrossRef]
161. Casey, K.G.; Quitevis, E.L. Effect of solvent polarity on nonradiative processes in xanthene dyes: Rhodamine B in normal alcohols. *J. Phys. Chem.* **1988**, *92*, 6590–6594. [CrossRef]
162. Vogel, M.; Rettig, W.; Sens, R.; Drexhage, K.H. Structural relaxation of rhodamine dyes with different N-substitution patterns: A study of fluorescence decay times and quantum yields. *Chem. Phys. Lett.* **1988**, *147*, 452–460. [CrossRef]
163. Feng, Y.; Liu, W.; Mercadé-Prieto, R.; Chen, X.D. Dye-protein interactions between Rhodamine B and whey proteins that affect the photoproperties of the dye. *J. Photochem. Photobiol. A Chem.* **2021**, *408*, 113092. [CrossRef]